UNIVERSIDAD NACIONAL AUTÓNOMA DE MÉXICO
PROGRAMA DE MAESTRÍA Y DOCTORADO EN INGENIERÍA
INGENIERÍA MECÁNICA – INGENIERÍA MECATRÓNICA

FAULT-TOLERANT DATA ACQUISITION SYSTEM FOR MONITORING THERMODYNAMIC PROPERTIES IN A STEAM GENERATION UNIT OF A FLASH EVAPORATION BINARY CYCLE

TESIS
QUE PARA OPTAR POR EL GRADO DE:
MAESTRO EN INGENIERÍA

PRESENTA:
MIGUEL ÁNGEL BENÍTEZ TORREBLANCA

TUTOR PRINCIPAL
DR. GABRIEL ASCANIO GASCA
CENTRO DE CIENCIAS APLICADAS Y DESARROLLO TECNOLÓGICO

CIUDAD DE MÉXICO, NOVIEMBRE 2017

JURADO ASIGNADO:

Presidente:	Dr. Rogelio González Oropeza
Secretario:	Dr. Héctor Miguel Aviña Jiménez
Vocal:	Dr. Gabriel Ascanio Gasca
1er Suplente:	M.I. Serafín Castañeda Cedeño
2do Suplente:	M.I. Álvaro Núñez Flores

Lugar donde se realizó la tesis: Ciudad Universitaria, Ciudad de México, México

TUTOR DE TESIS:

Dr. Gabriel Ascanio Gasca

____

FIRMA

Fault-tolerant Data Acquisition System for Monitoring Thermodynamic Properties in a Steam Generation Unit of a Flash Evaporation Binary Cycle

by

Miguel Ángel Benítez Torreblanca

Submitted to the Graduate School of Engineering
in partial Fulfillment of the Requirements for the Degree of

Master of Engineering

at the

National Autonomous University of Mexico

Thesis supervisors

Dr. Gabriel Ascanio Gasca
Álvaro Núñez Flores, MEng

Mexico City, 2017

Fault-tolerant Data Acquisition System
for Monitoring Thermodynamic Properties
in a Steam Generation Unit
of a Flash Evaporation Binary Cycle

by

Miguel Ángel Benítez Torreblanca

Submitted to the Graduate School of Engineering
in partial Fulfillment of the Requirements for the Degree of
Master of Engineering

ABSTRACT

In this thesis the development of a fully functional fault-tolerant data acquisition system was conducted based on the Texas Instruments EK-TM4C1294XL evaluation board. The main objective was the visualization and recording of thermodynamic properties in an experimental steam generation unit part of a Flash Evaporation Binary Cycle. The developed platform included two power supply modules using cold standby redundancy, powering five pressure transducers and eight resistive temperature detectors. At the throttling process, enthalpy, entropy and steam fraction were computed using the industrial formulation of the International Association for the Properties of Water and Steam. Readouts were displayed in a stand-alone open-source graphical user interface. A reliability evaluation considering environmental and operational conditions for a mission time of ten years was calculated for each power supply module, achieving 99.978% for the 3.3 V module and 99.974% for the 5.0 V module. Moving average filters were applied on output signals, demonstrating their usefulness for smoothing signals. Although flash evaporation could not be assessed, experimental results were used to estimate required downstream pressures at the throttling process for different hypothetical values of downstream steam fraction.

Thesis Examination Committee

Rogelio González Oropeza, PhD
Héctor Miguel Aviña Jiménez, PhD
Gabriel Ascanio Gasca, PhD
Serafín Castañeda Cedeño, MEng
Álvaro Núñez Flores, MEng

Dedicated
to those I have met
along the way

I offer you whatever insight my books may hold

Jorge Luis Borges
Two English Poems (1934)

Contents

Acknowledgments

This section is usually used to thank all the people who supported the author in the process of writing a thesis. They are mostly used to praise those who were involved in both frustration and joy. I'm not an exception. I am enormously grateful to my family, friends and colleagues for their support throughout this process. However, I feel like this should be a brief statement about everything that has happened over the last years. In the end I am most grateful and proud about the people I have met, the places I have been and everything I have done besides the thesis itself. It has been an amazing adventure.

I would like to express my deepest gratitude to the following individuals that contributed to my professional and personal enlightenment:

Alice. Sometimes a single conversation changes everything. I was lucky enough to have an entire city. You are still making changes. Thank you.

Casey Brokaw. Thank you for your hospitality and generosity while I was learning how to be on my own in a new city.

Jeanne Lissot. Thank you for unexpectedly sharing your exciting adventure. Truly inspirational.

Maria Richards. Your speech at the 2015 WINGS reception held at the GRC annual meeting made a profound impact on me. "Always say yes" was the key phrase. Thank you for your continuous support and the confidence you placed in us.

Robert Dell. I sincerely appreciate your advices and insights. "Keep doing it, as long as it is fun", you said. Trust me, I'm still looking for it.

My *sad* and *dreaming* friends. Thank you for sharing the laughter.

The amazing people I met at the following events:

2015 and 2016 GRC annual meetings
2015 and 2016 Power Plays conferences
2017 Mexico-UK Workshop on sustainability
2017 Student Energy Summit and Community Contribution Program
2017 Mexican International Renewable Energy Congress
2017 Seminar on Energy Conservation and Low-carbon Industry Development

Specially to Andrés Ruzo, Andrew Xie, Andrew ZP Smith, Axe Tron, Aysegul Turan, Benedict Holbein, Bodo von Duering, Braeden Peterson, Brian Kakembo Galabuzi, Burke Brunson, Caitlin Hartig, Celso Fernando Baspineiro, Chinedu Richard Ezenwukwa, Churchill Agutu, Dariel de León, Enrico Castro, Erin Camp, Evan Allan Hubbard, Graeme Beardsmore, Javier Ramos, Jayesh Ghatkar, Jeff Witter, John Scrimgeour, José Armando Gastelo-Roque, Joshua Lincoln Alston, Jungmin Cho, Kevin Joseph Dillman, Lawrence Joshua Flomo, Louis-Charles Codere, Marcus Magnus Michael Clifford Blake, Matt Uddenberg, Mehmet Zeki Erincik, Nadia Abdrabou, Nema Shawki, Niklas Agarwal, Nikola Lakic, Patrick Hanson, Pattarapon Klaykul, Pavan Elapavuluri, Rahmi Mert Bolat, Raka Ikrar, Roberto Javier Weiser, Ryan Dick, Sam Wheat, Shimon Joseph, Soroush Daneshi, Tamarah Georgi-Ann Campbell, Theophilus Mambu, Yolaisis Borrero and William Foley.

Amauri Sierra, Diana Nájera, Lorena Basurto, Mauricio M. Canto Romero and Osvaldo Méndez. Thank you for sharing with me an amazing opportunity to make a change.

Estefy Villavicencio, Stavros Eleftheriou and Thalia Avilés. I keep the memorable conversations we had.

Chuxin Liu, Daniel Esteban Fierro, Prof. Dehua Liu, Ernesto Luis Barrera, Evelyn Faife, Gustavo Cerqueira, Iván Bolaños, Jorge Luis Alba, Rayane de Lima, Rejane Silva, Richmond Santani, Sandra Graciela Vergara, Scarlett Wu, Úrsula Crisy Cárdenas, Yvonne Nyokabi and Wensy Zhang. You are definitely gentle souls. I am forever grateful.

Finally, I thank those with forgotten names, sometimes not even known, appearing in unsent letters and dispersed pieces of paper. Thank you.

I express my most sincere appreciation and gratitude to the following organizations:

CeMIE-Geo project 207032 CONACYT/SENER
China-Latin America Joint Laboratory for Clean Energy and Climate Change
Dongguan University of Technology
Engineering Institute, National Autonomous University of Mexico
iiDEA® Group
The National Development and Reform Commission of the People's Republic of China
Tsinghua University

Miguel Ángel Benítez Torreblanca

List of Figures

Page intentionally left blank

List of Tables

Acronyms

$\overline{EN}$	Enable Input
μDMA	Micro Direct Access Memory
ADC	Analog to Digital Converter
ASIC	Application-specific Integrated Circuitry
ASME	American Society of Mechanical Engineers
AWG	American Wire Gauge
BCE	Before Common Era
BMWi	Bundesministerium für Wirtschaft und Energie
BPP	Binary Power Plants
CAN	Controller Area Network
CBC	Conventional Binary Cycle
CCS	Code Composer Studio
CeMIE-Geo	Mexican Center for Innovation in Geothermal Energy
CFE	Comisión Federal de Electricidad
CICERO	Center for International Climate and Environmental Research
CLD	Current Limiting Diode
CPU	Central Processing Unit

CR	Circuit Resistance
CSV	Comma–separated Values
DC	Direct Current
DIN	Deutsches Institut für Normung
DMIPS	Dhrystone Millions Instructions per Second
DRE	Distributed Renewable Energy
DSP	Digital Signal Processing
EEPROM	Electrically Erasable Programmable Read-Only Memory
EGS	Enhanced Geothermal Systems
EMI	Electromagnetic Interference
FDD	Fault Detection and Diagnosis
FDI	Fault Detection and Isolation
FDU	Fault Detection Unit
FEBC	Flash Evaporation Binary Cycle
FIR	Finite Impulse Response
FIT	Failure in Time
FMEA	Failure Mode and Effect Analysis
FMECA	Failure, Modes, Effects and Criticality Analysis
FPU	Floating Point Unit
FSS	Full Scale Span
GDF	Geothermal Development Facility for Latin America
GEA	Geothermal Energy Association
GEODESA	Geotérmica para el Desarrollo S.A.P.I. de C.V.

GHP	Geothermal Heat Pumps
GPIO	General Purpose Input/Output
GPP	Geothermal Power Plant
GPTM	General Purpose Timer Module
GUI	Graphical User Interface
HMI	Human-Machine Interface
HSZG	Hochschule Zittau/Görlitz University of Applied Sciences
I&C	Instrumentation and Control
I2C	Inter-Integrated Circuit
IAPWS	International Association for the Properties of Water and Steam
IBM	International Business Machines
ICL	Internal Current Limiting
IDDP	Iceland Deep Drilling Project
IDE	Integrated Development Environment
IEA	International Energy Agency
IFAC	International Federation of Automatic Control
iiDEA®	Instituto de Ingeniería, Desalación y Energías Alternas
IIR	Infinite Impulse Response
ISR	Interrupt Service Rutine
KfW	KfW Entwicklungsbank
LCOE	Levelized Cost of Electricity
LDO	Low–dropout Voltage Regulator
LED	Light-Emitting Diode

MAC	Media Access Control
MAF	Moving Average Filter
MCUs	Microcontrollers
MHPS	Mitsubishi Hitachi Power Systems, LTD
MIL–STD	Military Standard
MIL–HDBK	Military Handbook
MIREC	Mexican International Renewable Energy Congress
MIT	Massachusetts Institute of Technology
MOC	Maximum Output Current
MPEI	Moscow Power Engineering Institute
MSPS	Million Samples per Second
MTTF	Mean Time To Failure
NASA	National Aeronautics and Space Administration
NCG	Non-Condensable Gases
NIST	National Institute of Standards and Technology
O&M	Operation and Maintanance
OECD	Organization for Economic Co-operation and Development
ORC	Organic Rankine Cycle
OTG	On-the-go
PCB	Printed Circuit Board
PG	Power–Good
PHY	Physical Layer
PIND	Particle Impact Noise Detection

PSM	Power Supply Module
PV	Photovoltaic
PWM	Pulse Width Modulator
QSSI	Quad Synchronous Serial Interface
R&D	Research and Development
RBD	Reliability Block Diagram
RCP	Reverse Voltage Protection
REFPROP	Reference Fluid Thermodynamic and Transport Properties Database
RoHS	Restriction of Hazardous Substances
RTD	Resistive Temperature Detectors
RUB	Ruhr-Universität Bochum
S&H	Sample and Hold
SRAM	Static Random Access Memory
SWM	Stadwerke München
TCR	Temperature Coefficient of Resistance
TI	Texas Instruments
UART	Universal Asynchronous Receiver/Transmitter
UN	United Nations
UNAM	National Autonomous University of Mexico
UNEP	United Nations Environmental Program
UNESCO	United Nations Educational, Scientific and Cultural Organization
UNFCCC	United Nations Framework Convention on Climate Change
UNU	United Nations University - Geothermal Trainee Program

US	United States
USB	Universal Series Bus
US–DoD	United States Department of Defense
USD	United States Dollars
US–DoE	United States Department of Energy
WDT	Watchdog Timer
WEC	World Energy Council
WW2	World War II

Nomenclature

$\gamma(\pi, \tau)$	Dimensionless Gibbs free energy, Equation (4.13)
λ	Failure rate
ρ	Density
π	Reduced pressure, Equation (4.14)
τ	Inverse reduced temperature, Equation (4.15)
θ	Reduced temperature, Equation (4.26)
β	Transformed pressure, Equation (4.28a)
ϑ	Transformed temperature, Equation (4.28b)
σ	Standard deviation
$\pi(\theta)$	Auxiliary equation for the boundary between Regions 2 and 3 (Equation B23), Equation (4.25)
$\bar{x}$	Mean
$\gamma^{\mathbf{o}}$	Ideal-gas part of specific Gibbs free energy
γ^{r}	Residual part of specific Gibbs free energy
λ_{33}	Basic overall failure rate of 3.3 V PSM
λ_{33}^{*}	Updated overall failure rate of 3.3 V PSM
λ_{50}	Basic overall failure rate of 5.0 V PSM
λ_{50}^{*}	Updated overall failure rate of 5.0 V PSM

π_C	Capacitance Factor
π_E	Environment Factor
π_P	Power Factor
π_Q	Quality Factor
π_S	Power Stress Factor
π_{SR}	Series Resistance Factor
π_T	Temperature Factor
π_V	Voltage Stress Factor
λ_b	Base Failure Rate
ρ_c	Critical density
λ_{cap}	Part Failure Rate of Capacitor
λ_{cc}	Failure rate of ceramic capacitor
λ_r	Failure rate of carbon resistor
λ_{res}	Part Failure Rate for Capacitor
λ_{tc}	Failure rate of tantalum capacitor
M	Number of points in MAF window
P	Pressure
P^*	Reducing pressure
P^t	Pressure of the triple point
P_{IF97}	Pressure provided by the IAPWS–IF97 at given temperature
P_c	Critical pressure
P_{cal}	Calculated pressure using IAPWS–IF97 at given temperature

P_d	Downstream pressure
P_{sat}	Saturation pressure
$P_{sat}(T)$	Saturation pressure as a function of temperature, Equation (4.29)
P_u	Upstream Pressure
R	Specific gas constant of water
$R(t)$	Reliability over time
$R(t)$	Exponential Failure Law, Equation (3.46)
R_{33}	Basic reliability of 3.3 V PSM
R_{50}	Basic reliability of 5.0 V PSM
$R_p(t)$	Reliability of parallel elements, Equation (3.47a)
$R_s(t)$	Reliability of series elements, Equation (3.47b)
S_P	Power Stress
S_V	Voltage Stress
T	Temperature
T^*	Reducing temperature
T^t	Temperature at the triple point
T_{IF97}	Pressure provided by the IAPWS–IF97 at given pressure
T_c	Critical temperature
T_{cal}	Calculated temperature using IAPWS–IF97 at given pressure
T_d	Downstream Temperature
T_{sat}	Saturation temperature
$T_{sat}@P_d$	Saturation temperature at downstream pressure

$T_{sat}@P_u$	Saturation temperature at upstream pressure
T_u	Upstream Temperature
a	Specific Helmholtz free energy, Equation (3.11a)
g	Specific Gibbs free energy, Equation (3.11b)
g^{IG}	Ideal gas value of specific Gibbs free energy
g^R	Residual specific Gibbs free energy
h	Specific Enthalpy
h_{IF97}	Specific enthalpy provided by the IAPWS–IF97 at given pressure and temperature
h_{cal}	Calculated specific enthalpy using IAPWS–IF97 at given pressure and temperature
h_d	Specific downstream enthalpy
$h_f@P_d, T_{sat}$	Specific entropy of saturated liquid at upstream pressure and saturation temperature
$h_f@P_u, T_{sat}$	Specific enthalpy of saturated liquid at upstream pressure and saturation temperature
$h_g@P_d, T_{sat}$	Specific enthalpy of saturated steam at downstream pressure and saturation temperature
$h_g@P_u, T_{sat}$	Specific entropy of saturated steam at upstream pressure and saturation temperature
h_{sat}^t	Specific enthalpy of saturated liquid at the triple point
h_u	Specific upstream enthalpy
k	Filter kernel
n	Number of elements

s	Specific Entropy
s_{IF97}	Specific entropy provided by the IAPWS–IF97 at given pressure and temperature
s_{cal}	Calculated specific entropy using IAPWS–IF97 at given pressure and temperature
s_d	Specific downstream entropy
s_{sat}^t	Specific internal entropy of saturated liquid at the triple point
s_u	Specific upstream entropy
t	Mission time
u_{sat}^t	Specific internal energy of saturated liquid at the triple point
v	Specific volume
$x[]$	Input
x_d	Downstream steam fraction
$y[]$	Output

Chapter 1

Introduction

The outline of this Chapter is based on a proposal usually followed in embedded systems [1], [2]. Its main purpose is to serve as a preface, compiling every major aspect of the dissertation.

1.1 Overview

This section reviews the basic features of the instrumentation system generated for an experimental subsystem of a Flash Evaporation Binary Cycle, developed by the iiDEA® Group, part of the Engineering Institute of the National Autonomous University of Mexico (UNAM).

1.1.1 Objectives

The main objective of this thesis is to develop a functional instrumentation system for an experimental steam generation unit with fault–tolerant and data–logging capabilities. A number of specific objectives accompany the preceding objective, included below:

1. Construct a hardware platform for monitoring and supervision.
2. Update the reliability of Power Supply Modules using operating correction factors.
3. Develop a Fault Detection and Isolation scheme for fault–tolerant Low–dropout Voltage Regulators through cold standby redundancy.
4. Demonstrate the application of Moving Average Filters for smoothing signals.
5. Compose embedded software based on industrial formulations of properties of steam and water.
6. Display and preserve record of thermodynamic properties (pressure, temperature, enthalpy, entropy, steam fraction) at specific states.

1.1.2 Significance of the problem

The iiDEA® Group is an applied research organization focusing on technological development using renewable energies. Its main geothermal projects include a low–power generation cycle, a desalination unit and a food dehydrator, providing alternative solutions for off-the-grid generation of electricity, scarcity of drinking water and food conservation.

Given the original nature of the prototypes involved, laboratory tests become a fundamental matter for validating and redesigning prototypes. The platform reviewed in this thesis addresses an alternative to commercial systems already available in the market.

1.1.3 Roles and responsibilities

The author led a group of undergraduate students, each one having the following specific roles during the process:

- Rodrigo Edgardo Armenta Santiago – Signal conditioning of RTDs and electrical wiring.
- Luis Gerardo Carballo González – Design of PCBs and LED indicators.
- Pablo García Cerón – Sensor wiring and assembly of PCBs.
- Luis Enrique Valverde Fortanel – Evaluation of current sources for RTDs.

Recommendations and support from the following colleagues was determinant in the mechanical assembly of the instrumentation platform:

- Victor Emmanuel Zenón Arroyo, Mechanical Engineer
- Misael Joshimar Mendoza Ramírez, Mechanical Engineer
- Roberto Ramírez Sánchez, Mechanical Engineer
- José Alfredo Sandoval Vallejo, Mechanical Engineer

1.1.4 Interactions with existing systems

The experimental steam generation unit first reviewed in Section 3.2.4 has been intensely modified and studied through a 3–year period by a considerable number of members of the iiDEA® Group. Some recent examples include a dissertation conducted in 2015 concerning the design and manufacturing of the cyclone separator [3]; the same year an experimental evaluation of the pressure drop in a gate valve was used to design a set of orifice plates [4]. Additionally, a pressure drop and pumps evaluation along pipelines was also published as an undergraduate thesis [5]. Other elements such as the plate heat exchanger, radiator, pump and mixer, were also selected by members of the group, approaching the thermal requirements of the experimental setup.

As a consequence of the existence of the actual setup before the instrumentation system, wiring and placement of sensors occurred afterwards, with some constrains in the availability of space for wires. Concerning the location of sensors, minor modifications were performed to the original tees used with Bourdon pressure gauges and thermometers. In the past years, one of the most remarkable changes in the experimental setup had to do with the replacement of two gas boilers — connected in series — for an electric boiler and a major overhaul of the copper pipes. For the latter change, the author was involved in the final stage of the reconstruction.

1.1.5 Security

Intellectual property of the platform is owned by the National Autonomous University of Mexico in its entirety. Needed specifications for the reproduction of the platform, including schematic diagrams, Printed Circuit Board (PCB) designs and embedded code is held by the iiDEA® Group.

1.2 Function description

Once the principles of the instrumentation platform have been settled, a basic description of its functionality is outlined in this Section.

1.2.1 Functionality

The instrumentation platform assembled for the experimental steam generation unit achieves the following functionalities:

Fault Detection and Isolation (FDI) In the event of a fault in a power supply, the system immediately identifies the faulty regulator, disabling it and allocating a new spare module. The spare modules, disposed in a cold standby redundant arrangement, are not powered until needed.

Monitoring and supervision A Graphical User Interface (GUI) displays the pressure at five states along with the temperature at eight states; in the case of a value trespassing a threshold previously set, a visual indicator arises. With regard to diagnostics of voltage regulators, a panel indicates the presence of faults and the specific set of regulators enabled. At the throttling process, thermodynamic properties are also shown, including enthalpy, entropy and steam fraction. A $T-s$ diagram helps to identify the presence of flash evaporation.

Data logging Retrieved data can be exported for subsequent analysis/processing.

Local indicators An LED attached to each sensor serves as an on-site visual indicator.

1.2.2 Constraints

As later explained in Subsection 4.2.1, Chapter 4, the platform is expected to have a serviceable life of ten years. In regard to its life cycle, a later prototype is expected to be finished in posterior stages of the project, regardless of the new platform keeping some of the features discussed in this dissertation or not. As a consequence, reusing the existing system for other prototypes is not advised since product specifications may change in later versions.

Quality is measured in terms of the reliability analysis found in Section 4.2, Chapter 4, based on a series of assumptions and considerations limiting its expandability. Constrains due to environmental issues are not reported since the semiconductors used are RoHS compliant. With regard to the formulation used for the computation of thermodynamic properties, the use of this platform with refrigerants is not possible.

Finally, even when Code Composer Studio®, — the IDE used for this project — is compatible with Linux and MacOS®, the entirety of the software platform was developed on Microsoft® Windows 10, exclusively guaranteeing its functionality in computers with this operating system.

1.2.3 Prototypes

According to the Technology Readiness Levels, developed by the National Aeronautics and Space Administration (NASA), the prototype produced by this dissertation satisfies Level 4, known as "Component and/or breadboard validation in a laboratory environment", with hardware and software descriptions shown below, as defined by NASA [6]:

Hardware Low fidelity system built and operated to demonstrate basic functionality.

Software Key software components are integrated and functionally validated.

1.2.4 Performance

Performance of the generated prototype is approached in Section 4.10 of Chapter 4. The evaluation includes an assessment of the commutation of cold standby redundant voltage regulators and code profiling, highlighting the most important processes.

1.2.5 Usability

A total of seven interfaces were designed for the GUI. Based on the development experience, the interfaces are considered to be user-friendly and the final version of the GUI can be easily shared with any computer satisfying the requirements already mentioned in Subsection 1.2.2.

A user's manual can be eventually published, although a comprehensive study on the design and layout is suggested to ensure its clarity and ease of use.

1.2.6 Maintainability

Subsection 4.1.6 in Chapter 4 details the procedure used to improve the maintainability of the hardware platform. With regard to software, modular programming was used thoroughly, enhancing readability.

1.2.7 Scenarios

The final platform is intended to be used under laboratory conditions, with access to electricity and occasional transportation. It is certainly not intended to be used in critical situations or when a failure could result in injuries to personnel. Basic safety measures must be taken when interacting with the equipment.

1.3 Deliverables

The final results of the dissertation, considering constraints and design specifications, are presented in this Section. An exhaustive discourse is settled in Chapter 4.

1.3.1 Reports

This dissertation acts as a final report on the subject, concluding with the additional documentation mentioned in Subsection 1.1.5.

1.3.2 Outcomes

The final instrumentation platform, and the generated documentation accomplish the full set of deliverables for this project.

1.4 Outline

As already mentioned, **Chapter 1** served as an introduction for the reader, summarizing the contents of this dissertation. **Chapter 2** reviews the fundamentals of geothermal energy, covering a worldwide overview and current trends on electricity generation, including a study on conventional power plants. **Chapter 3** establishes the needed theoretical concepts to discern the main contents of the thesis, covered in **Chapter 4**, where an exhaustive discussion of the instrumentation system and its main components is conducted. Latter sections **Results and discussion** and **Conclusions** summarize the thesis and present some final insights on the subject.

Page intentionally left blank

Chapter 2

Geothermal energy

Energy is a widely-used term in everyday life, including society, politics and others, but even when it can be considered as understood by the majority — maybe in its most intuitive way —, sometimes we need to broaden its meaning and understanding through a more detailed thinking.

Historically, three approaches to the philosophy of energy and its relationship with technology can be enunciated [7]:

1. Scrutiny of the natural phenomenon of energy.
2. Criticism of the role of energy in society.
3. Philosophy of technology.

It is known that energy *is* and what we can see and understand of it relies on its transformations and manifestations, however, when it comes to its role in society as an economic process, four main processes can be associated with its cycle: conversion, production, consumption and creation [8].

Based on today's use and relevance of energy, there are two known elements considered as threats: climate change and the eventual exhaustion of fossil fuels — the fuel that modern society is relying the most on [7]. As a consequence of this situation, the proposal of *energy transition* to renewables is also an extensively recognized term.

This Chapter deals with the elemental aspects of geothermal energy, including its classification, relevance and current scenario regarding power generation.

2.1 Fundamentals of geothermal energy

A difference between renewable and alternative energy must be made. In a traditional fashion, the latter is used to produce electricity by uncommon means, that is, every source excluding those used by fossil fuel power generation (e.g. coil, gas and oil). On the other hand, renewable energies are those considered to be unlimited and self-replenishing based on the human life span. Not every alternative energy is considered to be renewable, being nuclear a fundamental example. Even when nuclear plants produce null emissions of greenhouse gases, given their nature, fuel cannot be rapidly restored.

The word *geothermal* is comprised of two Greek words: *geo*, meaning Earth, and *therme*, meaning heat. Thus, geothermal energy in its most essential form is the energy contained inside the Earth as heat. When it comes to the exploitation of geothermal energy, it is commonly referenced as *geothermal*. Following the main uses of geothermal, two branches may be discussed, namely power generation and direct uses. While the former is immediately recognized, direct use refers to the usage of geothermal energy as pure heat, commonly used in aquaculture, district heating, food drying and heat pumps.

The current geothermal installed capacity is estimated to be 83.4 GW , where 70.2 GW_t correspond to direct uses and 13.2 MW_e correspond to power generation [9]. Globally, power generation using geothermal is still behind conventional power generation, making less than 1% of the electricity produced in the world.

Direct use of geothermal energy has been an inherent part of the history of mankind, with the earliest use of hot springs for religious purposes in Mesoamerican and Mediterranean areas dated back to year 10,000 Before Common Era (BCE) [10].

Even when geothermal is a promising, proven renewable source of energy, some advantages and disadvantages can be addressed, as shown below [11], [12]:

Advantages

- Despite its relatively reduced availability, it is still more widely available than oil.
- Regarding the cost of installation, a geothermal power plant is significantly less expensive than a nuclear power plant.
- An average Geothermal Power Plant (GPP) holds a high load factor, up to 95%.
- Geothermal waste water can still be used in a cascade fashion, specially for direct uses.

Disadvantages

- Some reservoirs are located in protected zones, making them unaccessible.
- If the reservoir is merely used for direct uses, the unit must be located close to the well.
- Unpleasant smell given the content of sulfur in geothermal spots.
- Negative visual impact.

As shown in Figure 2.1, the Earth is comprised of several layers which, in their simplest form, constitute three major layers. Table 2.1 shows the average density and temperature of Earth with respect to depth.

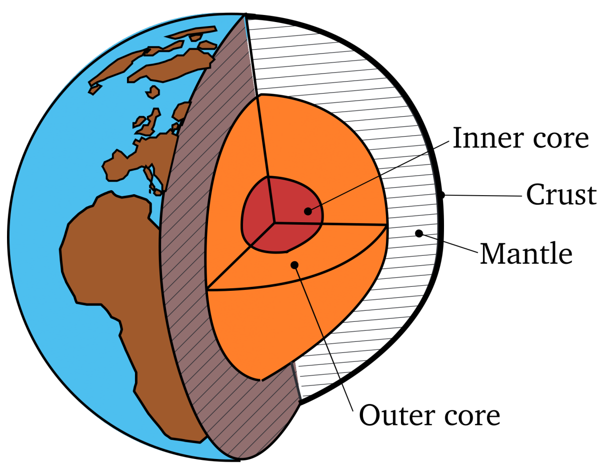

Figure 2.1: Basic internal structure of Earth. Adapted from [13].

Table 2.1: Physical properties of the Earth. Adapted from [14].

Layer	Depth km	Density $\frac{kg}{dm^3}$	Temperature °C
Earth's crust	0 – 30	2 – 3	up to 1,000
Earth's mantle	up to 3,000	3 – 5.5	1,000 – 3,000
Earth's core	up to 6,370	10 – 13	3,000 – 5,000

2.2 Classification of geothermal resources

The creation of a standard jargon has been encouraged by numerous publications, however, once a factual classification of geothermal resources was intended, various approaches have arisen contributing to a deep and meaningful set of categorizations according to different areas of interest.

In a simple definition, a geothermal system is constituted by three main elements [10], [15]:

1. Heat source due to heat flow from the center of the earth (10%) and radioactive decay (90%).

2. A constrained set of unpermeable layers.

3. A fluid to transfer the contained heat in the reservoir.

A second basic dissection of geothermal resources involves the actual resource produced by a well. Wells producing a greater fraction of steam are generally called *steam-dominated* reservoirs; when the wells produce the opposite, they are known as *liquid-dominated* or *hydrothermal* resources [16]. When the reservoir contains superheated steam, it is also known as a *dry-steam* field.

2.2.1 Classification by geothermal system

After the main discussion of geothermal reservoirs based on the type of resource they produce, one can add further types of geothermal resources, establishing the following definitive list of geothermal systems [17]–[19]:

Hydrothermal Briefly discussed in Section 2.2, it needs the following five elements to be commercially viable: 1) Heat source, 2) Permeable volume of rock, 3) Water, 4) An hermetic cap layer and 5) A reliable way to recharge the water reservoir (natural or artificial).

Steam-dominated Also reviewed in Section 2.2, these geothermal systems are common in some of the most representative geothermal fields around the globe, like Cerro Prieto (Mexico), Wairakei (New Zealand), Reykjavik (Iceland), Salton Sea (United States (US)) and Otake (Japan).

Hot Dry Rock (HDR) This type of geothermal system is characterized for: a) the lack of a fluid in the reservoir or b) low permeability in its upper layers. One way to take advantage of the heat stored and make it commercially suitable is through the injection of a working fluid, process known as *hydraulic fracturing*. Since this technique is essentially "enhancing" the reservoir because of the addition of a fluid, these systems are called Enhanced Geothermal Systems (EGS).

Geopressure Identified based on abnormal pressure in the reservoir, these systems are known to contain water at high pressures and temperatures along with dissolved methane, making them attractive to be used with hydraulic turbines, heat engines and combustion on site, taking advantage of these three forms of energy contained in the geothermal system.

Magma energy In some reservoirs, magma can be located at a shallow depth. If cold water is passed through it, magma would suddenly cool down, forming a solid glass-like substance still hot enough to transfer heat to water, now readily available to be used in a power cycle. In 2009, the Iceland Deep Drilling Project (IDDP) stumbled upon magma at a 2-km depth while drilling a new well in the Krafla geothermal field. Unfortunately, due to corrosion problems they had to shut it down, setting a milestone for the most powerful geothermal well, producing over 30 MW_e [20]. In late 2016, the same project began a new well, this time hoping to provide a long-term production well.

2.2.2 Classification by potential

When the term *geothermal potential* is used, sometimes the context in which it is used may be unclear. According to a current proposal, renewable energies can be classified based on a sequence of "progressively realizable" theoretical, technical, economic, sustainable and developable potential where the last stage signifies the best possible scenario in terms of its profitability [21]. The aforementioned stages, shown in Figure 2.2, are summarized below:

Theoretical potential Estimates the total energy contained in a specific region over a period of time. As a result of different constraints (technical, structural and administrative) it cannot be exploited in its full manner and only a fraction of it is finally utilized.

Technical potential Based on the current technology and legal restrictions, describes the geothermal resource that can be exploited.

Economic potential Given the time and localization of the resource than can be utilized, considers the economic feasibility of the project taking into account the needed investment along with maintenance and operational costs.

Sustainable potential Bearing in mind that the exploitation of the geothermal field involves profit, a sustainable use may involve lower production rates and a slower return of investment in exchange of a longer period of exploitation.

Developable potential Describes the fraction of the sustainable potential that can be developed considering realistic conditions such as regulations, policies and social constraints.

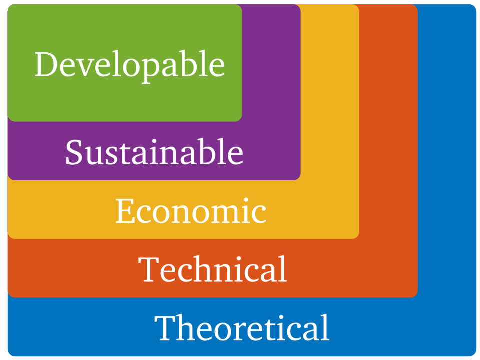

Figure 2.2: Classification of geothermal resources by potential. Adapted from [21].

2.2.3 Classification by accessibility and discovery status

Besides the assessment of geothermal resources by potential, as discussed in Subsection 2.2.2, another way to define them is through their specific place in terms of their economic feasibility and geological assurance [22]. These definitions, gathered in Figure 2.3, are discussed below:

Resource base Geothermal energy contained inside the Earth's crust, localized in a specific area.

Inaccessible resource base Geothermal energy contained between the inner layer of the Earth's crust and a given depth beneath the crust.

Accessible resource base Geothermal energy contained between the Earth's surface and a given depth beneath the crust.

Residual accessible resource base Portion of the accessible resource base that as a consequence of economic and legal issues is unlikely to be exploited.

Useful accessible resource base (RESOURCE) Portion of the accessible resource area that is likely to be exploited at some time in the future (near or not) based on its economic feasibility.

Subeconomic resource Portion of the geothermal resource that, on account of the existence of different energy sources (renewable or not), its exploitation is not commercially viable. The possibility of its eventual extraction still remains open.

Economic resource Portion of the geothermal resource whose profitability is cost-competitive with other commercially available sources of energy.

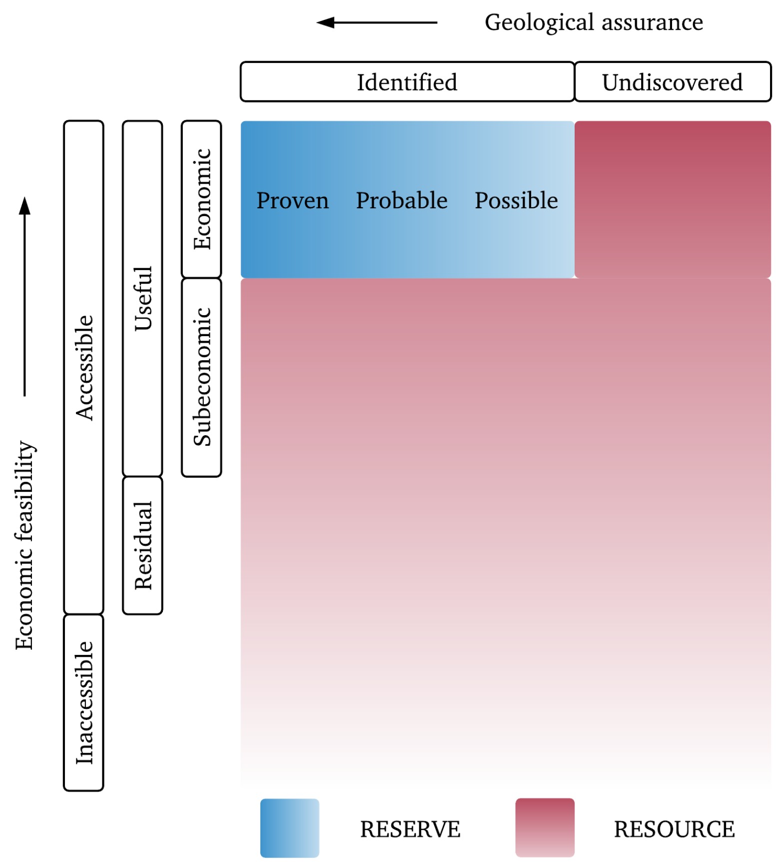

Figure 2.3: Categories of geothermal resources. Adapted from [22].

Undiscovered economic resource Regions where geothermal resources are not confirmed through exploration.

Identified economic resource (RESERVE) Portion of the economic resource characterized by drilling or exploration evidence (geochemical, geophysical or geological).

2.2.4 Classification by temperature

Even when classification of geothermal resources by temperature may be the widest and most generalized approach, its utilization is sometimes used as a synonym of *enthalpy*, which leads to a misuse of the concept. This weak link, along with other arguments, has been used to refute this manner to classify geothermal, as described in Subsection 2.2.5. Nevertheless, Table 2.2 brings together the most common classification with regard to the temperature of the geothermal reservoir.

Table 2.2: Classification of geothermal resources by temperature. Adapted from [10].

Category	Muffler [22] °C	Hochstein [23] °C	Benderitter [24] °C	Haenel [25] °C
Low temperature	< 90	< 125	< 100	< 150
Intermediate	90 – 150	125 – 225	100 – 200	–
High temperature	> 150	> 225	> 200	> 150

2.2.5 Classification by exergy

A relatively new approach to geothermal resources classification involves the use of exergy [26]. According to this concept, the inconsistencies related to the use of temperature alone as a way to characterize geothermal fluids are considerable. Besides that, the used ranges are primarily arbitrary and in most cases they do not provide meaningful data about their potential use. Classification solely based on temperature may be the easiest way to *understand* geothermal fluids but there are more elements to distinguish thermodynamically.

One of the primary arguments of this new framework deals with the fact that two thermodynamical properties are needed to define the state of a fluid, discarding the use of temperature — on its own and when misused as enthalpy — as a proper way to categorize the fluid. Following this premise, it proposes the use of exergy as an indicator of the ability of the reservoir to produce work.

2.2.6 Classification by attributes

One recent formulation attempts to cover technical aspects of the reservoir proposed for power generation besides its thermodynamic properties, classifying reservoirs into classes. Each class is analyzed according to the following elements [27]:

1. Temperature of the reservoir.
2. Phase of fluid in reservoir (liquid, biphasic, steam).
3. Driving mechanism (self-flowing, pumped).
4. Phase of fluid at wellhead (liquid, biphasic, steam).
5. Well productivity (output in MW_e).
6. Applicable conversion technology (direct uses for non-electrical grade; binary, flash, hybrid or steam for power plants).

7. Operational problems (Non-Condensable Gases (NCG), scaling, fouling, corrosion).

Although this scheme was commissioned by the United States Department of Energy (US–DoE) as a way to assess their geothermal resources and keep them in mind while conducting new projects, it is a meaningful way to allocate geothermal resources in a more generalized way.

2.3 Worldwide overview of geothermal

The decade between 2004 and 2014 established a milestone in the number of new policies concerning the promotion of renewables, expanding the number of countries with at least one policy from 48 to 144, making both developed and developing countries to change the way they were seeing renewables [28].

Several organizations have addressed the need to identify and recognize energy efficiency as a remarkable attribute not only exclusive to renewables, but also to heating, cooling and transportation. The International Energy Agency (IEA) is an autonomous non-profit organization having published annual reports about this topic for its members, including 29 countries, most of which are also part of the Organization for Economic Co-operation and Development (OECD).

In relation to climate change, the Paris Agreement, assembled by the United Nations Framework Convention on Climate Change (UNFCCC) in 2015, aims to bring together efforts to hold back its effects through the enhancement of technology development and transfer as well as the assistance to developing countries, willing to keep global warming below 2 °C [29].

Bringing another assessment to the conversation, in agreement to a survey conducted in 1999, based on the worldwide geothermal potential at the time and the available technology, there were 39 countries which could be powered in their entirety by geothermal means, being Central American, Asian and African Countries the ones with the highest potential [30]. Additionally, Chile is one of the few countries with such geothermal potential that could power half of the country's demand; in the case of Mexico, the estimated percentage is around 20 percent of the total demand.

2.3.1 Global potential

As of 2015, only 24 countries in the world were producing electricity using geothermal energy. When compared to the 72 countries taking advantage of geothermal energy (out of 90+ countries where geothermal resources had been identified) through direct use in 2009, the scenario may have seemed not so promising, however, in 2016 the market experienced a new wave of geothermal projects, investments and additions, with a planned capacity of 12.5 GW_e divided among 82 countries in the years to come [31], [32].

In the feasible long-term, the forecast for 2050 includes 70 GW_e from hydrothermal resources and up to 140 GW_e from EGS, establishing a breakthrough in geothermal development, representing 8.3% of the world electricity production, serving 17% of the global population [33]. Regarding the global geothermal potential for power generation, several computations have been published in the last 15 years, resulting in intricate efforts to bring a definitive figure. Still, as reported by the Geothermal Energy Association (GEA) in 2016, the total potential of conventional hydrothermal reservoirs is between 200 MW_e and 230 MW_e [31], representing 16 times the current capacity [34].

Furthermore, once EGS are fully developed, 100 GW_e could be added just to the US geothermal potential (representing 30+ times the current installed capacity), and if the forecasts of theoretical studies turn out to be feasible based on an improvement of current technology, the total global potential could reach up to 2 TW_e, magnifying the benefits of cost-competitive EGS [32], [35], [36].

2.3.2 Global installed capacity

As of 2016, geothermal power and heat have been increasing at a fairly constant rate, even when the previous year was characterized by low fossil-fuel prices and the constant costs associated with the development of geothermal projects. Likewise, there are other barriers that new investments in geothermal power have overcome, including the acquisition of power purchase agreements in the case of markets allowing them [31]. Figure 2.4 shows the global installed capacity for geothermal power generation.

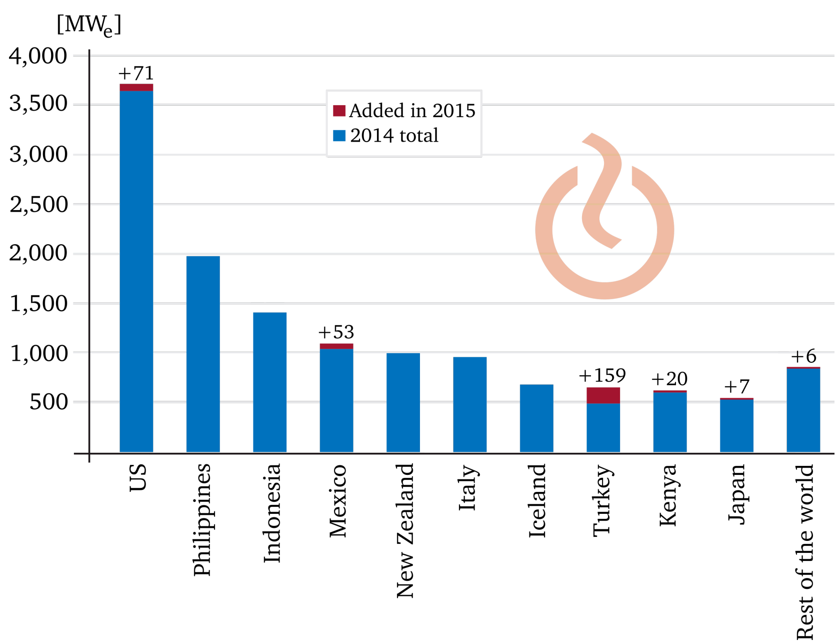

Figure 2.4: Geothermal power capacity and additions, 2015. Adapted from [37].

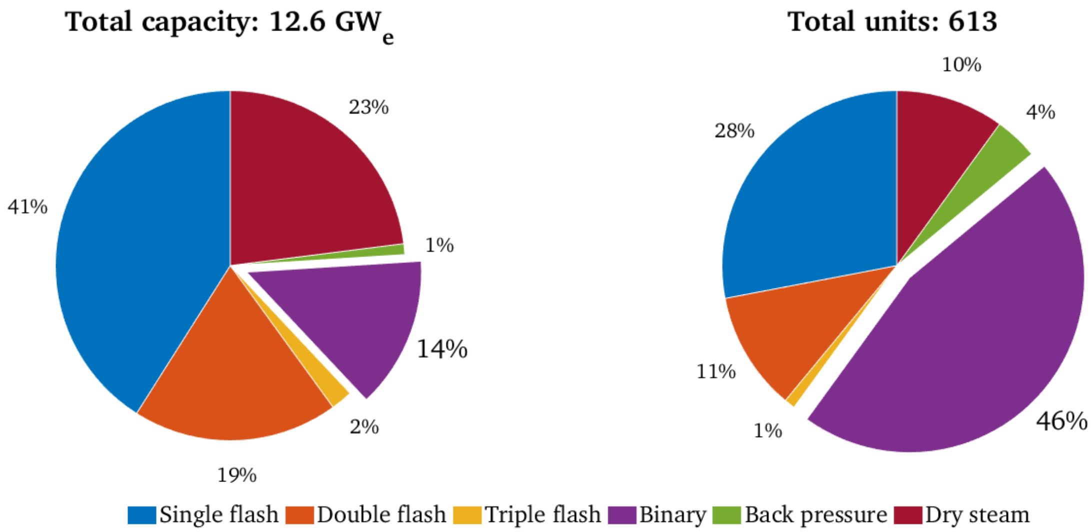

Figure 2.5: Distribution of geothermal power plants worldwide, 2015. Adapted from [33].

When analyzing the global allocation of GPPs and their net production, as shown in Figure 2.5, one can identify that even when the number of Binary Power Plants (BPP) is greater than that of any other kind of power plant, they do not produce the greatest share of the installed capacity. If the evidence that BPPs have much more less efficiency (2.8% – 5.5%) than steam power cycles (up to 15%) is added, the scenario may seem strange. The cause of this apparent inconsistency lies in the fact that steam-dominated reservoirs are not that abundant, whereas hydrothermal resources are available at a greater number of sites [38].

2.3.3 Geothermal energy in developing countries

According to the World Energy Council (WEC), a sustainable scenario for energy is dependent on the following elements: energy security, energy equity (access and affordability) and environmental sustainability [34]. This results contrasting when one analyzes the case of Latin America, where a 50 MW_e plant can cost as much as 250 million United States Dollars (USD) without taking into account the initial associated costs, adding up to USD 20 million to the project [39].

There are many developing countries using geothermal energy for both power generation and direct uses. Although not a general rule, while developed countries like the US — with the highest installed geothermal capacity — satisfy 0.4% of its electricity demand using geothermal energy, some developing countries like Costa Rica, El Salvador, Kenya, Nicaragua and the Philippines have relied on geothermal for the majority of their electricity generation, with values as high as 20% of the total production [40].

A remarkable issue about the countries previously shown in Figure 2.4 is that four of them, part of the top ten, are developing countries (Mexico, Indonesia, Turkey and Kenya). When discussing new approaches to the evolution of geothermal in developed countries, EGS play a prime role in the next wave of geothermal projects. In 2006 the Massachusetts Institute of Technology (MIT) published an assessment concerning the feasibility to provide electricity in the US by 2050 through EGS, an emerging, still under development technology [35]. As of August 2016, there are 216 geothermal-related Research and Development (R&D) projects in the US funded by federal grants [41].

After the 2015 Geothermal Congress for Latin America and the Caribbean, three central challenges for geothermal development were addressed [42]:

1. If governments support private investment in geothermal, resource risk is still an issue requiring funds from the same governments or public institutions.

2. The investment atmosphere must be enhanced by governments, developing clear policies and frameworks to assure financial and legal aid.

3. Governments need to engage developers with enough expertise to conduct geothermal projects.

Numerous organizations have devoted some efforts to the assistance and support of geothermal projects in developing countries. To name a remarkable example, Dewhurst Group, a US-based company primarily dedicated to geological exploration, along with KfW Entwicklungsbank (KfW), a German bank committed to the funding of developing countries, announced a 50 million euros grant to the initiative Geothermal Development Facility for Latin America (GDF) in 2016, promoting the advancement of geothermal energy in selected countries, excluding Mexico [43].

Besides the preceding example, the recognition of geothermal as a way to improve the status of developing countries is not new. In 2002, consultants from the United Nations (UN), in conjunction with the United Nations Educational, Scientific and Cultural Organization (UNESCO), the United Nations Environmental Program (UNEP), the Center for International Climate and Environmental Research (CICERO) and world-renowned academics gathered to publish what may be considered as an ultimate guide to the development of geothermal energy in developing countries, practically covering every aspect, from potential, sustainability and risk, to financing and feasibility; from drilling techniques to case studies and examples of direct uses [44].

Additional efforts put together by the UN were leaned towards the formation of the United Nations University - Geothermal Trainee Program (UNU) in 1978. Since its inauguration it has served 647 fellows from 60 countries, comprising below-ground topics such as Reservoir Engineering, Geophysics, Geology and Drilling Technology [45].

In spite of the above, when the estimated potential in developing countries is compared with the amount of fossil fuels they are purchasing from foreign countries, the fact that geothermal is underexploited is palpable [46].

Although 95% of inhabitants of Latin America and the Caribbean have access to electricity, it is tremendously uneven, with over 22 million people in Argentina, Bolivia, Colombia, Guatemala, Haití, Nicaragua and Peru without a connection to the electrical grid [37]. Another example of this situation is the Middle East and North Africa, where 92% of the population are part of the grid even when 54% of Yemen's inhabitants lack access to electricity [47]. In a worldwide perspective, 16% of the global population (around 1,200 million people) is excluded from the accessibility to the grid [48]. Countries located in the sub-Saharan Africa and developing Asia make 95% of this figure; at the same time, 80% are located in rural areas.

2.3.4 Geothermal energy in Mexico

Ever since the promotion of Mexico's Energy Reform back in 2013, a lot of questions were raised pointing towards the upcoming changes in the regulatory framework. Since the open auctions of 2016, Mexico has awarded over 4.9 GW_e in contracts for private investors setting the ground for an outlook of USD 6.6 billion invested by the end of 2018, almost surpassing twice the average annual investment in power generation since 2010 [49].

One of the main antecedents of this change is the Energy Transition Act, decreed in 2013 and updated in 2015, aiming to increase the total contribution of renewables to the country's electricity generation up to 35% by year 2024 [50]. After this leading change in legislation and the added policies and measures taken by Mexico, the IEA named this scheme of foreseen welfare Mexico's New Policies Scenario.

According to the UN, even when global fertility has diminished over the last years, population growth for the next 33 years is imminent. In the case of Mexico, specifically, an annual growth rate of 0.9% is expected, doubling the OECD average rate. As of 2015, Mexico's population was estimated in 127 million inhabitants, with the not so promising forecasts of 148 million and 163 million by years 2030 and 2050, respectively [51].

This expected demographic growth becomes a remarkable matter when analyzing the consequences it has in energy demand. Between 2014 and 2040, following Mexico's New Policies Scenario, an anticipated annual rate of 2.4% in electricity demand eclipses the OECD rate up to three times [49]. Changes in the demand are also followed by changes in the sector requesting it, as shown in Figure 2.6, where it can be seen that the two areas predominantly increasing their demand are Agriculture and Transport, followed by Industry as the largest electricity user.

As stated in Section 2.3, Mexico is one of the top ranked countries with geothermal power operating capacity, occupying the 4th place with over 1,069 MW_e, lying behind the US (3,567 MW_e), Philippines (1,939 MW_e) and Indonesia (1,375 MW_e) [31], [37]. On the contrary, while in a worldwide scenario Geothermal Heat Pumps (GHP) and space heating (with 70.95% and 10.74% of the worldwide capacity) are the two most utilized forms of exploitation of geothermal heat, in Mexico is still essentially dedicated for bathing and swimming purposes [52].

AlbeitM1qu1mau there has been a shift from the use of oil towards the use of natural gas, fossil fuels still make up 90% of the energy demand in Mexico, as shown in Figure 2.7. In relation to the sectoral demand, transportation holds the largest consumption, with over 40% [49].

After the energy outlook for Mexico conducted by the IEA, it is clear that Mexico must commit to double its economy by year 2040, keeping the increase in energy demand around 20%. This outlook continues the optimistic path previously discussed, increasing the geothermal power generation capacity to 980 MW_e by the same year [49].

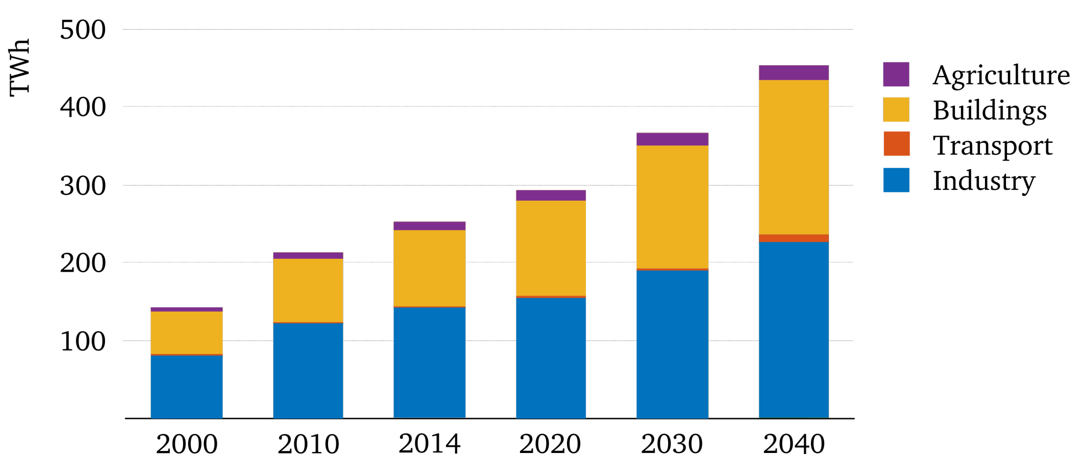

Figure 2.6: Electricity demand in Mexico. Adapted from [49].

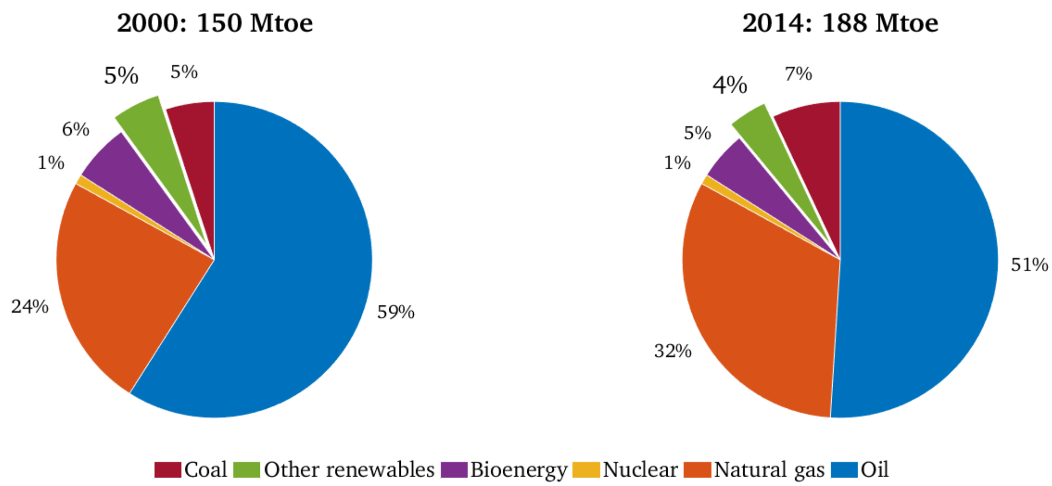

Figure 2.7: Energy demand by fuel in Mexico. Adapted from [49].

Out of the expected 21,000 MW_e to be installed in 2020, Mexico ranks fifth worldwide with a forecast of 1,400 MW_e, representing 6.6% of the total [33]. One of the reasons behind the high expectations for Mexico's geothermal development is the establishment of the Mexican Center for Innovation in Geothermal Energy (CeMIE-Geo) and the accompanying changes in the regulatory framework, proclaimed the same year, opening geothermal fields for private investors [53], [54].

The CeMIE-Geo, a consortium founded in 2014 reuniting academia, government and private companies to conduct 30 R&D projects, aims for the evaluation, exploration and exploitation of geothermal energy for power generation and direct uses, with an initial budget of USD 87 million [55].

In 2015, an update of the Los Azufres III Phase I turbine was commissioned by Comisión Federal de Electricidad (CFE), also assigning the design, manufacturing, civil work and installation to Mitsubishi Hitachi Power Systems, LTD (MHPS). The aforementioned improvements to Mexico's installed capacity represented 17% of the global additions to geothermal power capacity in that year [37], as already shown in Figure 2.4.

The same year, MHPS installed two 5 MW_e plants in the Domo San Pedro field, owned by Geotérmica para el Desarrollo S.A.P.I. de C.V. (GEODESA), the first private company operating a geothermal power plant; in early 2016, upon a second request from GEODESA, MHPS finished the installation of a new 27 MW_e turbine in the Domo San Pedro field to replace the two previous units [56], [57]. Table 2.3 shows an update of the geothermal fields in Mexico and their corresponding additions throughout the years.

Additionally, as part of the 2015 Mexican International Renewable Energy Congress (MIREC), Green Power considered Mexico as one of the most anticipated emerging markets for private investors, forecasting several regions for geothermal developments including both power generation and direct uses, as shown in Figure 2.8.

After this new scenario, electricity generation using renewables is going towards a surprisingly positive direction; at the same time, an overwhelming reduction in the use of oil and coal for electricity generation is contemplated, as shown in Figure 2.9.

Table 2.3: Geothermal fields in Mexico. Adapted from [57]–[59].

Geothermal field	Operator	Year	Installed capacity MW_e 2014	2015	2016	Running capacity MW_e 2014	2015	2016
Cerro Prieto	CFE	1973	720	720	720	570	570	570
Los Azufres	CFE	1982	191.4	227.4	227.4	191.4	224.4	224.4
Los Humeros	CFE	1991	93.6	93.6	93.6	68.6	68.6	68.6
Las Tres Vírgenes	CFE	2001	10	10	10	10	10	10
Domo San Pedro	GEODESA	2015	0	10	27	0	10	25.5

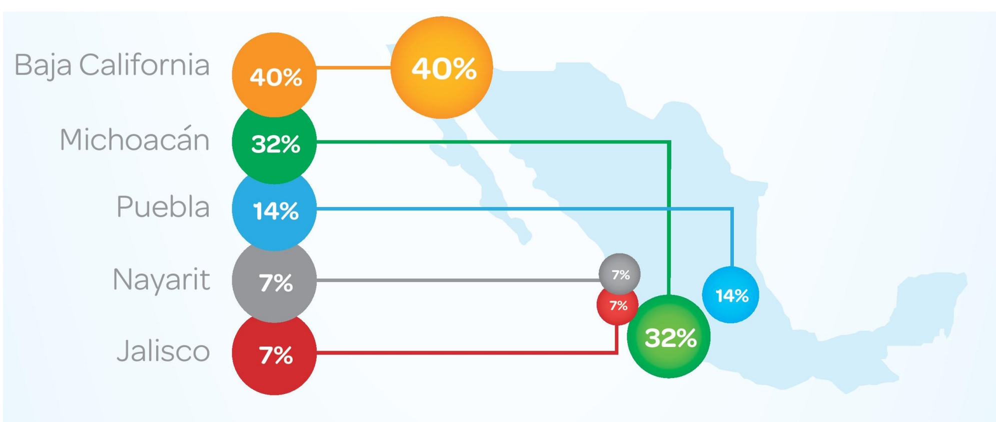

Figure 2.8: Forecast of regions with future geothermal developments in Mexico [60]

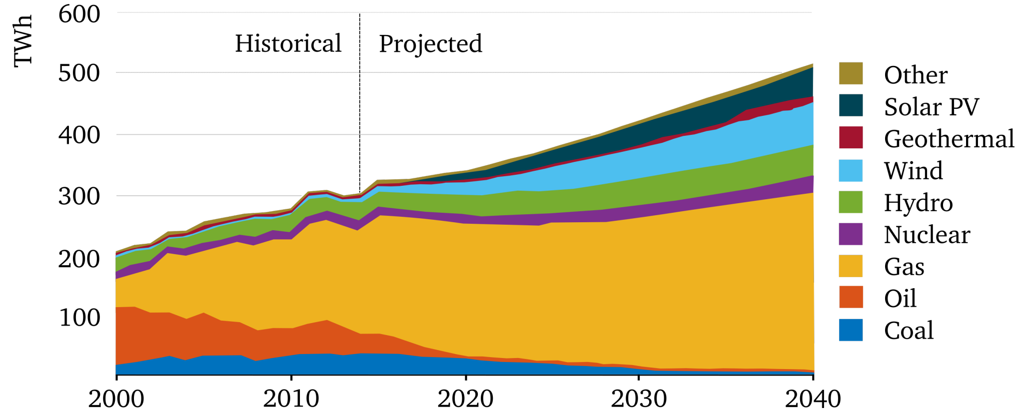

Figure 2.9: Projected electricity generation in Mexico by source. Adapted from [49].

2.4 Low-scale geothermal projects

When talking about low-scale geothermal power projects, many criteria have appeared, showing that a formal definition of what a *small* project is remains ambiguous. A basic distinction between the scale of the project taking into consideration the electrical load can be made. For example, some authors have proposed narrow ranges not exceeding 100 kW_e to be small, others have broaden the range, up to 1 MW_e [61], [62]. In the end, characteristics besides the output power, such as a remote location and rural electrification as main goal may be added when defining a project as *small*.

One relevant topic in the discussion is the cost associated with the Operation and Maintanance (O&M) of the plant. Sometimes, a small BPP may be installed next to a large GPP to make use of the still-hot brine, augmenting the efficiency of the overall cycles. The associated costs to these secondary cycles are reduced because of the previous technical expertise in the same area. This situation is completely different when the same BPP is installed at a remote, isolated location, where financial security is still in risk. Thus, the success of a small geothermal project may be compromised, making it more risky at first glance [44].

2.4.1 Worldwide

There are plenty of examples depicting the enthusiasm towards low-scale GPPs. Out of the projects that have gained notoriety one can list the rural electrification program proposed for Indonesia back in 1995; in late 2016, Indonesia announced the addition of 4,013 MW_e, ranking first in the list of capacity under development that year [31], [63] and exceeding the forecast expedited in 2015 of 1,340 MW_e by 2020 [33].

Another example of a country encouraging these projects is Germany, who has managed to stimulate the use of power generation even with the lack of high-enthalpy geothermal energy through the use of a Kalina or an Organic Rankine Cycle (ORC) [33]. Regarding direct uses, the city of Munich has attracted a lot of attention since the announcement of the Stadwerke München (SWM), stating that, by 2040, the district heating of Munich will be the first in Europe fully supplied from geothermal sources [64]. With the addition of the annually average of 15.32 million euros spent by the Bundesministerium für Wirtschaft und Energie (BMWi) for geothermal R&D between 2004 and 2013, the German government keeps supporting renewables with the objective of supplying 80% of the demand in electricity with renewable sources by 2050 [65], [66].

There are other not so fortunate examples of countries having low-enthalpy geothermal energy and using it for power generation. One major example is Greece, installing and operating a 2 MW_e geothermal power plant between 1985 and 1989 before shutting it down as a consequence of the social pressure put in the project and reported technical issues [67].

2.4.2 Mexico

Since 2000, many hot spots have been identified in Baja California Peninsula, a place also known for its water scarcity, making it a remarkable site for the installation of desalination units using geothermal energy [68].

Back in the 1990s, CFE paid for two 1.5 MW_e BPPs (using isopentane) developed by ORMAT Technologies — a US-based provider of technology in the renewables market — with the objective of having them installed in the Los Azufres field with waste brine as primary heat source.

The next decade, CFE also acquired four 300 kW_e BPPs from ORMAT. After drilling a 300 m–depth well with temperatures exceeding 120 °C and a mass flow rate of 32 tons of water per hour, one of these units turned into a pilot for rural electrification in Maguarichic, Chihuahua, providing off-the-grid electricity to 380 inhabitants. Table 2.4 shows the most relevant information about the aforementioned projects.

Table 2.4: Low-temperature binary power plants in Mexico. Based on data from [69].

Year	Location	Net output kW_e	Number of units	Temperature °C	Years in operation
1997	Los Azufres, Michoacán	1,500	2	175	17
2001	Maguarichic, Chihuahua	300	1	120 – 170	7

2.5 Electricity generation using geothermal energy

By the end of 2015, 23.7% of the world's electricity generation was provided by some kind of renewable energy, geothermal contributing with less than 0.4%, as shown in Figure 2.10. Concerning the installed capacity of renewables in the same year, 28.9% was the total share, making an increment of 9% with respect to the previous year [37].

Even when geothermal makes up a small percentage of the global share of renewables, one must bear in mind that GPPs operate 24/7, having high load factors and as a consequence, leading to more electricity generated per installed MW_e when compared to other renewable sources of energy [70].

The use of geothermal energy to produce electricity has unique aspects differentiating it from conventional power generation (i.e. fossil-fuel power plants), being the most relevant the ones shown below [11], [13], [38], [71]:

1. Pollution is extremely reduced due to the absence of combustion and the reinjection of brine.
2. GPPs have, generally, lower efficiencies (around 15% for steam and flash power cycles, 5% for BPPs) when compared to fossil-fuel power plants as a consequence of lower steam temperature and the presence of NCG.
3. GPPs are usually more convenient when used as base-load units (constant power supplied to the grid, as opposed to peak-load power, used when there is an increase in consumption).
4. As a way to avoid heat losses, geothermal units are frequently located close to the well. Still, geothermal power generation can be controlled based on the extraction rate of the geothermal fluid.
5. As a result of the demand of steam (an average of 80 tons of steam per hour for a 100 MW_e power plant), sometimes multiple wells serve a single unit.
6. Geothermal steam contains minerals that, when used directly in a power plant, cause corrosion.

A typical method to measure the competitiveness of a power generation technology is the Levelized Cost of Electricity (LCOE). Fundamentally, this criterion is based on the actual cost per unit of produced energy taking into consideration the associated expenditures of building and operating a power plant, including capital, fuel, fixed and variable costs over a finite financial and operational period [72].

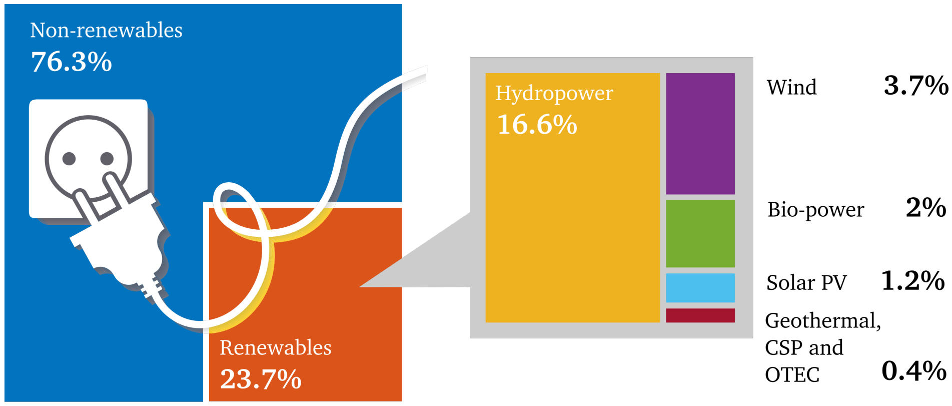

Figure 2.10: Renewable energy share of global electricity production in 2015. Due to rounding, percentages do not add up. Adapted from [37].

Based on a recent survey, conducted in late 2016, wind and solar[1] are still considered the most cost-competitive sources (46 USD/MWh to 56 USD/MWh for the former, 32 USD/MWh to 62 USD/MWh for the latter) closely followed by natural gas reciprocating engines, biomass and geothermal [73]. Still, according to a short-term forecast, this scenario may change by year 2022 in the US, where the average LCOE for upcoming geothermal plants is expected to be the lowest compared to any other source, renewable or not, reaching 39.5 USD/MWh [72].

2.5.1 Distributed Renewable Energy

As discussed in Section 2.3.3, one can realize that most of the global population without access to electricity is in a rural environment. Three main alternatives to energy access can be enunciated to provide a solution [37]:

1. The use of off-the-grid power generation systems.
2. Creation of a mini or micro-grid for certain community.
3. Extension of the electrical grid beyond regular urban areas.

Projections made in 1994, discussing the relevance of geothermal units for off-the-grid powering considered that, depending on the development of the area, the demand for electricity per person would range between 0.2 kWh and 1 kWh [13], [61]. Even when geothermal potential is highly asserted and well-known in a large scale, low scale power generation in isolated areas is still trying to reach its maturity, mainly due to market issues and profitability. Still, one can highlight the benefits of installing off-the-grid power plants as follows [74]:

[1] Solar Photovoltaic (PV) - Thin film utility scale

1. Local power plants may be an option to the expansion of grids, which is an expensive option.
2. Small geothermal plants can avoid the use of diesel generators, reducing costs associated to fuels and transportation.
3. Local power plants improve the development of poor areas.

A survey conducted in 2008 demonstrated that 95% of the world's inhabitants were located in 10% of the total Earth's surface. Another interesting fact is that only the tenth part of this surface was considered to be *remote* (i.e. a region more than 48 hours away from a major city) [75]. These remote (also known as rural) regions have at least one of the following elements: long distance to the nearest electrical grid, challenging routes of access or harsh climatic conditions [74].

In addition to the arguments later reviewed in Subsection 2.6.4, the use of binary cycles for remote powering includes the following distinctive highlights [13], [61]:

1. Given the fact that BPPs are usually designed in a modular fashion (hundreds of kW_e to tens of MW_e), they can be easily transported.
2. They are versatile enough to fit a wide range of low-temperature reservoirs (100 $^{\circ}$C – 150 $^{\circ}$C). If the temperature is higher, another kind of GPP may be more suitable in terms of the cost, however, independent binary units can be installed together to obtain greater capacities.
3. Considering the overall size of a binary plant and the number of wellheads serving it, piping costs are generally low.
4. Geothermal waste water can be used in secondary direct uses.
5. Even when geothermal power plants have large load factors (as mentioned in Sections 2.1 and 2.5), if the application is critical, the need of a backup source is prevailing.

When it comes to the economically viable use of Distributed Renewable Energy (DRE), Electratherm suggests the following requisites [76]:

1. Accessible hot source of water surrounding 150 $^{\circ}$C.
2. A potential electrical demand between 25 kW_e and 110 kW_e.
3. To avoid potential losses, the electrical load (on or off-the-grid) must be close to the power unit.
4. The regular cost of electricity expanding the current available electrical grid is greater than 10 cents per kWh.

In regard to the current market of modular, low-scale power generation units, one can mention the following engineering firms:

Infinity turbine, LLC As one of the first companies to start mass-producing low power ORCs (with designs covering from 1 kW_e to 50 kW_e), their main market is the installation of modular units using waste heat to provide supplementary energy. According to the information provided by the company, the standard efficiency of their units ranges between 5% and 15%, making them a good option when the heat source is already available [77].

Electratherm One of the singular aspects of the Power+Generator, the series of ORCs designed and built by Electratherm, is the use of screw expanders in the expansion stage — contrary to the more common use of turbines — focusing on the exploitation of waste heat and low-temperature geothermal resources (below 122 °C) [78].

The two previous examples of companies using both waste heat and low-temperature geothermal energy concentrate on modularity, scalability and unattended operation, turning them into well-known competitors in the low-power, low-temperature market, which is about 20 years old [31].

2.6 Geothermal power plants

One major element sometimes easily overlooked is the fact that power generation, no matter what the source of energy is, needs water, being this sector responsible for one tenth of the global water usage [79]. This close relationship between production of electricity and water is a known subject because of the eventual increase in the demand of both water and energy, mainly due to an expected increment in global population.

The use of water in power plants can be divided in two categories, described below [80]:

1. Water withdrawn: Volume of water removed from its main source, then returned partially, keeping its availability.
2. Water consumed: Volume of water removed and depleted, without recovery.

Although conventional power plants demand water as the primary working fluid, sometimes the use of refrigerants is encouraged (e.g. ORC). As a consequence, power generation relies on water for cooling purposes. The actual amount of water needed in GPPs depends on the actual type of power plant, however, the use of both consumption and withdrawal water ranges between $1-100,000$ liters per MWh [81]. Moreover, waste water coming out of GPPs is sometimes an issue. For example, Yangbajin, a geothermal facility in China is causing the pollution of local water beyond regional standards [80].

Focusing on the feasibility of power generation, the following essential parameters must be well-studied [82]:

Determination of fluid flow rate and temperature These two properties are determinant when assessing a geothermal reservoir. Given their values it will not only validate the previous geologic, geophysical and geochemical studies, but also will bring the project one more step towards its realization.

Type of power plant and working fluid Once the primary properties of the geothermal fluid are known, the next step is the design of the power cycle and the selection of the working fluid. This step is crucial since it will be the stage where the dimensioning and selection of equipment will be conducted.

2.6.1 Exploration and drilling

As previously stated in Subsection 2.3.3 and Section 2.4, one of the downsides related with power generation using geothermal energy is the fact that it needs previous studies to minimize the financial risk. The associated cost per installed megawatt ranges between 4,500,000 USD and 5,500,000 USD, where 50% of it is spent during the drilling stage [83]. As a way to ensure and minimize this risk, the main necessary preliminary stages to assess the feasibility of a reservoir through exploration are briefly described below [17]:

1. **Literature survey** Based on public or governmental databases, information about the specific region of interest can be obtained.

2. **Airborne survey** Based on aerial exploration and photography, the existence of faults is appraised.

3. **Geologic survey** This survey is known to be the first performed on-site, gathering data to create geologic maps and conceptual models of the reservoir.

4. **Hydrologic survey** Its main relevance relies on the compilation of meteorological data, including temperature and flow rates of superficial manifestations, like hot springs.

5. **Geochemical survey** Identifies the nature of the reservoir (liquid or steam dominated) along with its temperature and properties; additionally, estimates the mechanisms for recharge.

6. **Geophysical survey** Based on several tests (measurement of heat flux, temperature gradient, electrical resistivity) this survey identifies the best locations to drill the first deep wells.

2.6.2 Flash steam power plants

As reviewed in Subsection 2.3.2, BPPs comprise the majority of the worldwide installed capacity, making them the first and relatively simplest choice of GPP for biphasic, liquid-dominated reservoirs. Once the geothermal fluid is extracted from the production well, liquid (brine) and steam are separated through the use of a cyclone separator. While the generated steam is led to a single-pressure turbine, the separated saturated liquid is reinjected to the reservoir. Once the steam comes out of the turbine, it is condensed in a heat exchanger, using water from a cooling tower. One main issue arisen from using geothermal fluid as working fluid is the handling of NCGs which generally contain flammable compounds like H_2S, H_2 and CH_4. On the other hand, unlike conventional power plants, flash steam power plants do use saturated steam, instead of superheated steam, which requires an additional amount of energy [17].

As the name suggests, these power plants involve a *flashing* process where the geothermal fluid is transformed into a biphasic mixture as a consequence of a sudden pressure drop, taking the fluid from its original condition (pressure and temperature) to a new one below the saturation pressure. This process can take place in the reservoir, the production well or an orifice plate before the cyclone separator, however, even when the specific location has a vital relevance in the actual process in terms of the operation and selection of equipment, thermodynamically, the spot is negligible [17]. In the case of having a biphasic fluid at the wellhead, the orifice plate can be omitted, as shown in Figure 2.11, where a simplified single-flash steam plant is shown.

The relevance of the separator in the second stage is crucial. Outlet steam of the separator, now being the inlet turbine steam, is expected to be at least 99.995% dry [17]. If liquid passes through the turbine, it will eventually lead to corrosion and scaling in the piping and, in a worst-case scenario will also affect the turbine. A rule of thumb commonly known as the *Baumann rule* states that for every 1% of moisture in the steam entering the turbine, a corresponding decrease of 1% in the efficiency of the turbine will be experienced [84]. It should be noticed that after the separation a moisture removal process may be needed, depending on the efficiency of the separator and the distance from the separator to the turbine.

Flash steam power plants can include additional, consecutive separation stages, where each steam outlet is redirected to a multi-stage turbine, as shown in Figure 2.12. This is usually pursued when an increase in the overall efficiency of the plant is desired, nonetheless, one must take into consideration the eventual need to drill supplementary wells to satisfy the new requirements of the cycle [85] as well as the need to install further orifice plates and separators to acquire the needed pressure drops.

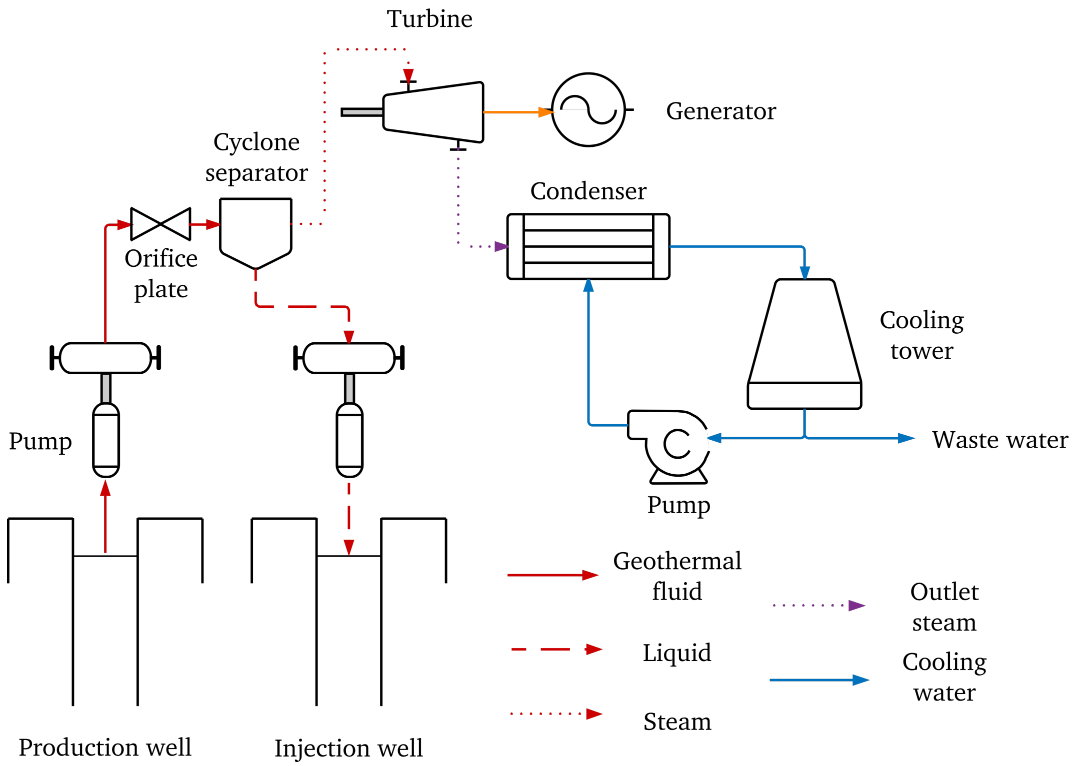

Figure 2.11: Schematic diagram of a single-flash steam cycle. Adapted from [17], [58], [86].

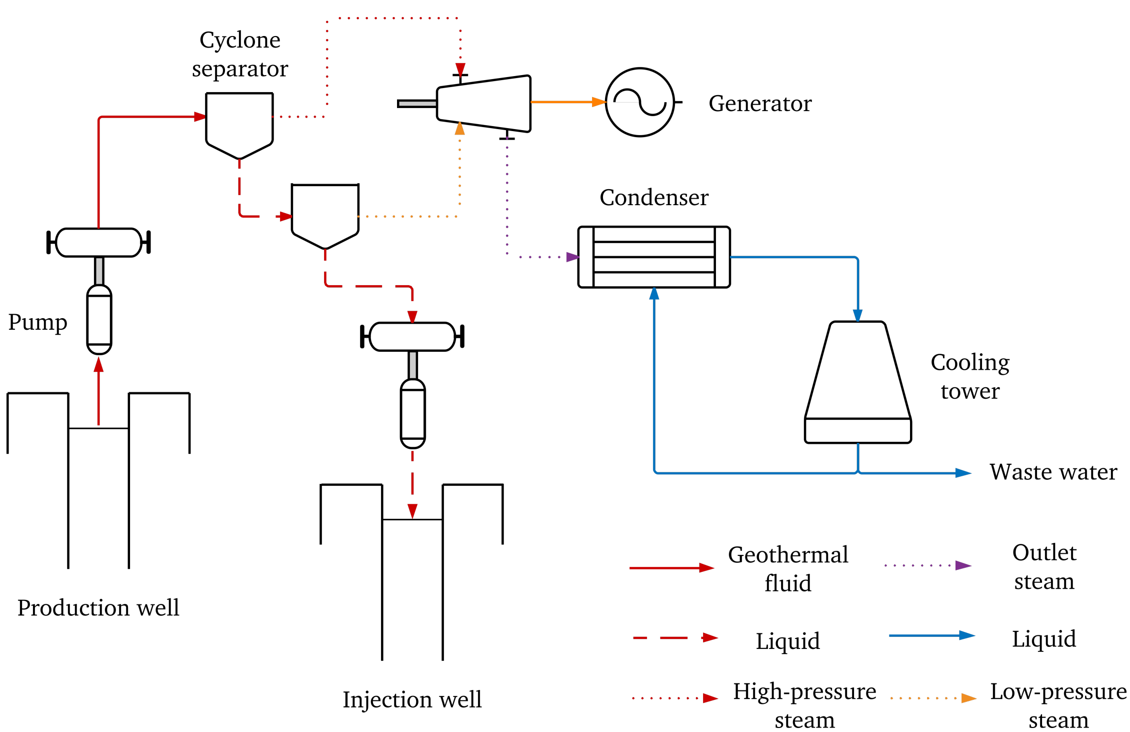

Figure 2.12: Schematic diagram of a double-flash steam cycle. Adapted from [17], [58], [86].

2.6.3 Dry steam power plants

Historically, the first demonstrative prototype using geothermal energy for power generation was completed in 1904, commissioned by Prince Piero Ginori, who used the dry-steam from a reservoir to produce 15 kW_e and power light bulbs. Out of the steam-dominated reservoirs, Larderello and The Geysers are the only two major dry-steam geothermal fields in the world, being part of the 5% of all hydrothermal systems producing saturated or superheated steam [87].

One particularity of using dry-steam as main source lies in the outlet steam of the turbine. Given the nature of the reservoir a back-pressure turbine is usually used, discharging the outlet steam to the atmosphere, as shown in Figure 2.13, making it not only the simplest but also the cheapest power cycle for geothermal power generation [88].

Steam pre-treatment is also needed even if the field is steam-dominated. As in the case of the flash steam power cycle, a cyclone separator, particulate remover, baffled demister or *scrubber* can be added to the powerhouse, just before the inlet of the turbine. Additionally, even if the reservoir contains superheated steam, one common pretreatment includes the addition of clean water to it in order to desuperheat it and turn it to saturated steam. Although this may seem controversial, the contained compounds in the steam causing scaling issues concentrate in the added liquid so when the added moisture is finally removed before the turbine inlet, they are left out [89].

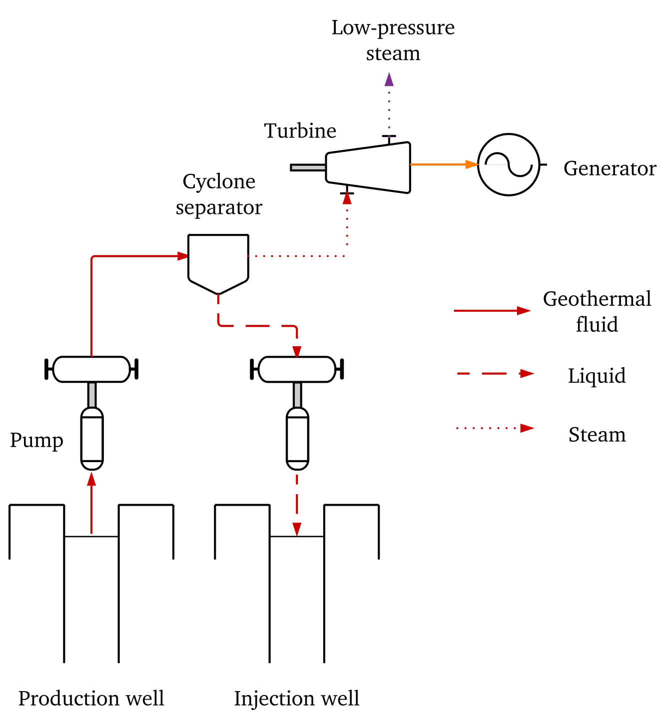

Figure 2.13: Schematic diagram of a dry-steam power cycle. Adapted from [17], [58], [86].

2.6.4 Binary power plants

There is documentation showing that the first BPP operated in the island of Ischia, Italy, during World War II (WW2) with an installed capacity of 300 kW_e [90]. Due to the period in which it was installed and operated, information about it is not widely accessible. In 1967, 24 years after its shutdown, the second BPP was installed in Paratunka, Russia. Regardless of the apparent slow development of BPPs, their current distribution is greater than that of any other kind of power plant due to the availability and allocation of low-temperature reservoirs, as recalled in Section 2.3.

Even when BPPs can generate power with resources at relatively low temperatures (up to 73 °C), ordinarily they are meant to be used with hydrothermal reservoirs around 150 °C, with power outputs reaching 10 MW_e [82], [91].

Unlike the preceding power cycles, where the geothermal fluid is used as working fluid in an "open" circuit passing over auxiliary equipment including the turbine, it goes through a heat exchanger, ceding part of its thermal energy to a closed secondary circuit, containing a working fluid with a higher molecular mass and a lower boiling point when compared to those of water.

The working fluid, now turned into steam, is led to the turbine, generating power when expanded, then it is condensed to repeat the process. When the working fluid is organic, the plant is commonly known as an ORC, first demonstrated in 1961 [10]. The environmental impact of BPPs during operation is essentially due to thermal pollution, since the geothermal fluid is always contained and never discharged to the atmosphere or surrounding reservoirs of fresh water. A schematic diagram of a BPP is shown in Figure 2.14.

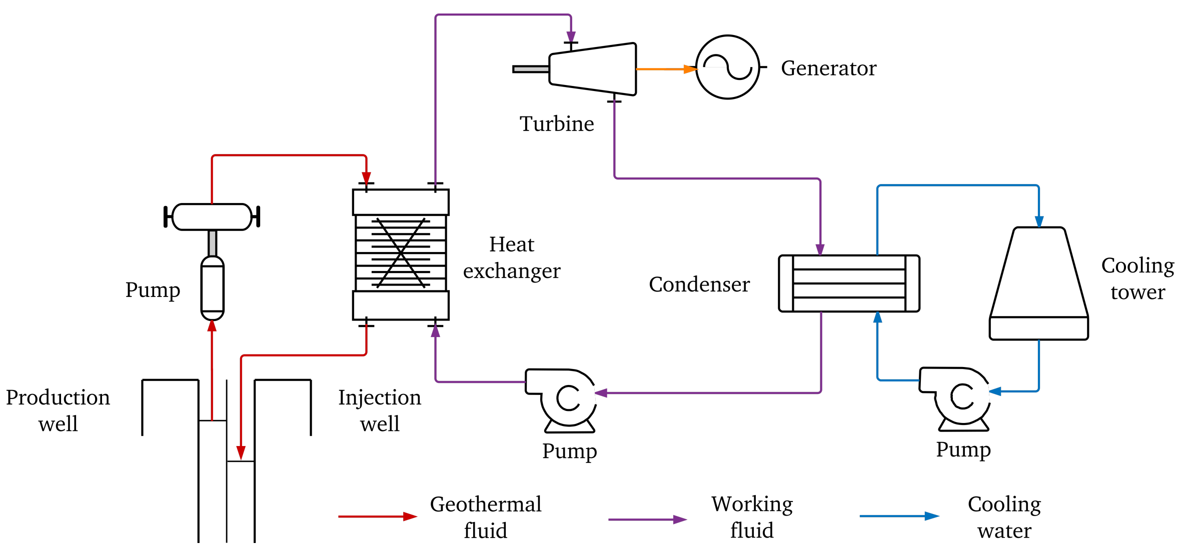

Figure 2.14: Schematic diagram of a binary cycle power plant. Adapted from [17], [58], [86].

Table 2.5: Comparison of geothermal power plants. Adapted from [17].

Type of plant	Reservoir temperature °C	Efficiency %	Cost and complexity	Current usage
Single-flash	200 – 360	30 – 35	Moderate	Widespread
Double-flash	240 – 320	35 – 45	Moderate → high	Widespread
Triple-flash	260 – 320	40 – 50	High	Selected sites
Dry-steam	180 – 300+	50 – 65	Low → moderate	Special sites
BPP	125 – 165	25 –45	Moderate → high	Widespread

2.6.5 Final remarks

As examined earlier in Subsection 2.6.2, the extraction and compression of NCGs is critical. Gas removal systems generally employ ejectors — devices without moving parts capable of generating high vacuum. Their principle of operation includes the use of a primary working fluid (also known as motive fluid) to drag a secondary fluid originally contained inside a chamber, generating vacuum in this reservoir. Depending on the availability and economics of the resource, steam or air may be used as primary fluid.

In relation to the overall characteristics of each cycle, Table 2.5 gathers a general overview of each cycle. One special BPP worth mentioning is the Kalina cycle. Its main modification relies on the use of an ammonia-water mixture as working fluid, passing through the turbine as superheated steam. One of the main advantages of this cycle over a BPP lies in the efficiency, being up to 40 percent more efficient [13]. The efficiency of a BPP is intrinsically linked to the temperature of the reservoir, decreasing at lower temperatures [61].

2.7 Conclusions

This Chapter introduced the reader to the fundamentals of geothermal energy. The basic elements regarding its nature, classification, potential and means of exploitation for power generation were summarized, exhibiting the enormous contributions that geothermal is making to the renewables sector. In addition to the above, a survey of current trends and local policies was conducted. Finally, this Chapter serves as a background for the exposition of the Flash Evaporation Binary Cycle, examined in later chapters.

Chapter 3

Theoretical framework

This chapter briefly reviews some of the needed foundations used for this dissertation. It covers the theory behind thermodynamic relations, putting special emphasis on the Gibbs free energy. Subsequently, the Flash Evaporation Binary Cycle is discussed, covering its thermodynamic states and basic operation. Additionally, the used experimental setup is also summarized. As support topics, an outline of instrumentation systems and Digital Signal Processing (DSP) are included. Finally, an outline of reliability analysis wraps up the chapter, preceeding the main discussion.

3.1 Thermodynamic relations

In engineering processes, properties such as pressure, temperature and flow rate are commonly directly measured, however, when it comes to other valuable – and sometimes essential — thermodynamic properties such as enthalpy or entropy, the use of generalized thermodynamic relations is a must. This section deals with this background.

3.1.1 TdS relations

Recall the mathematical definition of entropy of an internally reversible system, stated in the following equation:

$$dS = \left(\frac{\delta Q}{T}\right) \tag{3.1}$$

If one integrates Equation (3.1), the change in entropy can be found, as shown below:

$$\Delta S = \int_1^2 \left(\frac{\delta Q}{T}\right) \tag{3.2}$$

Equation (3.2) is distinctively relevant because it implies an isothermal process. This is not an unique case, hence the need to develop two auxiliary equations, known as the $T\,dS$ relations [92]. Conservation of energy for a closed system comprehending an incompressible substance in an internally reversible process can be expressed as:

$$\delta Q - \delta W = dU \tag{3.3}$$

Notice that Equation (3.3) includes differential work, which can be expressed in terms of pressure and the differential of volume, as follows:

$$\delta W = P\,dV \tag{3.4}$$

Thus, substituting Equation (3.1) into Equation (3.3) leads to the first $T\,dS$ relation:

$$T\,dS = dU + P\,dV \tag{3.5}$$

Or, in terms of specific properties:

$$T\,ds = du + P\,dv \tag{3.6}$$

Comparing Equations (3.5) and (3.6) one can notice that equations in terms of specific properties are self explanatory based on their notation (lowercase letters). This assumption will be used throughout the rest of the document without further clarification. If the reader needs additional assistance, the Nomenclature section may be consulted.

In order to find the second relation, one must recall the definition of specific enthalpy:

$$h = u + PV \tag{3.7}$$

Finding the differential, the following equation is obtained:

$$dh = du + P\,dv + v\,dP \tag{3.8}$$

Finally, substituting Equation (3.8) into Equation (3.6), the second relation is acquired:

$$T\,ds = dh - v\,dP \tag{3.9}$$

Equations (3.6) and (3.9), known as the $T\,dS$ relations, are usually written in terms of specific internal energy and specific enthalpy, in the following manner:

$$du = T\,ds - P\,dv \tag{3.10a}$$

$$dh = T\,ds + v\,dP \tag{3.10b}$$

3.1.2 The Gibbsian equations

Section 3.1.1 examined the first two fundamental relations of the set known as *Gibbsian equations*. This section will elaborate on the remaining two, introducing the specific Helmholtz free energy equation (a) and the specific free Gibbs energy equation (g), defined by the following equations [93]:

$$a = u - Ts \tag{3.11a}$$

$$g = h - Ts \tag{3.11b}$$

Essentially, the Helmholtz free energy is the "maximum amount of work a system can do at constant volume and temperature"; similarly, the Gibbs free energy is "the maximum amount of work a system can do at constant pressure and temperature"[94].

Differentiating Equation (3.11a):

$$da = du - T\,ds - s\,dT \tag{3.12}$$

Substituting Equation (3.10a) into Equation (3.12):

$$da = -P\,dv - s\,dT \tag{3.13}$$

Likewise, differentiating Equation (3.11b):

$$dg = dh - T\,ds - s\,dT \tag{3.14}$$

Substituting Equation (3.10b) into Equation (3.14) produces:

$$dg = v\,dP - s\,dT \tag{3.15}$$

Equations (3.10a), (3.10b), (3.13), (3.15) constitute the Gibbsian equations, summarized below:

$$du = T\,ds - P\,dv \tag{3.10a revisited}$$

$$dh = T\,ds + v\,dP \tag{3.10b revisited}$$

$$da = -P\,dv - s\,dT \tag{3.13 revisited}$$

$$dg = v\,dP - s\,dT \tag{3.15 revisited}$$

3.1.3 Maxwell relations

In pursuance of the review of Maxwell equations, one should consider a brief study on partial derivatives and exact differentials [92]. Let z be a function of one dependent variable z, and two independent variables x and y, such as:

$$z = z(x, y) \tag{3.17}$$

Then, the differential change of z with respect to changes in x and y is expressed as:

$$dz = \left(\frac{\partial z}{\partial x}\right)_y dx + \left(\frac{\partial z}{\partial y}\right)_x dy \tag{3.18}$$

Introducing auxiliary variables M and N, Equation (3.18) can be written as:

$$dz = M\,dx + N\,dy \tag{3.19}$$

Where:

$$M = \left(\frac{\partial z}{\partial x}\right)_y \tag{3.20a}$$

$$N = \left(\frac{\partial z}{\partial y}\right)_x \tag{3.20b}$$

Then, the partial derivative of Equation (3.20a) with respect to y yields:

$$\left(\frac{\partial M}{\partial y}\right)_x = \frac{\partial^2 z}{\partial x \partial y} \tag{3.21}$$

Equivalently, taking the partial derivative of Equation (3.20b) with respect to x generates:

$$\left(\frac{\partial N}{\partial x}\right)_y = \frac{\partial^2 z}{\partial y \partial x} \tag{3.22}$$

Given the thermodynamic context in which the discussion is based on, function z and variables x and y represent physical properties, which have exact differentials. Therefore, dismissing the order of differentiation, Equations (3.21) and (3.22) are equal:

$$\left(\frac{\partial M}{\partial y}\right)_x = \left(\frac{\partial N}{\partial x}\right)_y \tag{3.23}$$

Equation (3.23) is enormously important because it can be applied to the Gibbsian Equations (Eqs. (3.10a), (3.10b), (3.13), (3.15)) previously discussed in Section 3.1.2 and having the same structure as Equation (3.18), generating the set of Maxwell relations, shown below:

$$\left(\frac{\partial T}{\partial v}\right)_s = -\left(\frac{\partial P}{\partial s}\right)_v \tag{3.24a}$$

$$\left(\frac{\partial T}{\partial P}\right)_s = \left(\frac{\partial v}{\partial s}\right)_P \tag{3.24b}$$

$$\left(\frac{\partial s}{\partial v}\right)_T = \left(\frac{\partial P}{\partial T}\right)_v \tag{3.24c}$$

$$\left(\frac{\partial s}{\partial P}\right)_T = -\left(\frac{\partial v}{\partial T}\right)_P \tag{3.24d}$$

3.1.4 The Gibbs free energy function as a generating function

The specific Gibbs free energy as a function of pressure and temperature, $g(P, T)$, is a major relation because it allows finding every thermodynamic property [95] in terms of the two most commonly measured and controlled properties [96].

Going back to the differential specific Helmholtz equation and differential specific Gibbs equation (Eqs. (3.13) and (3.15)) and taking advantage of the property of partial derivatives explained in Equation (3.23), they can be rewritten in the following form:

$$da = \left(\frac{\partial a}{\partial v}\right)_T dv + \left(\frac{\partial a}{\partial T}\right)_v dT \tag{3.25}$$

$$dg = \left(\frac{\partial g}{\partial P}\right)_T dP + \left(\frac{\partial g}{\partial T}\right)_P dT \tag{3.26}$$

After analyzing Equations (3.13) and (3.25) along with Equations (3.15) and (3.26), the following additional expressions can be attained:

$$P = -\left(\frac{\partial a}{\partial v}\right)_T \tag{3.27}$$

$$s = -\left(\frac{\partial a}{\partial T}\right)_v = -\left(\frac{\partial g}{\partial T}\right)_P \tag{3.28}$$

$$v = \left(\frac{\partial g}{\partial P}\right)_T \tag{3.29}$$

Notice that Equation (3.29) shows that specific volume can be obtained as a partial derivative of the Gibbs function. At the same time, Equation (3.28) is expressly pertinent considering that it allows expressing specific entropy as a function of the partial derivative of $g(P,T)$, as follows:

$$s = -\left(\frac{\partial g}{\partial T}\right)_P \tag{3.30}$$

Lastly, Equation (3.30) can be substituted into the specific Gibbs function (Eq. (3.11b)), generating the following equation for specific enthalpy, also in terms of the function $g(P,T)$ and its derivative:

$$h = g(P,T) - T\left(\frac{\partial g}{\partial T}\right)_P \tag{3.31}$$

3.1.5 Dimensionless specific Gibbs free energy function

Notice that the Gibbs free energy function (Eq. (3.15)) was shown in its specific form, in terms of P, T, v and s; nonetheless, as discussed in Section 3.1.4, when it is presented solely as a function of P and T, its capabilities for finding thermodynamic properties are boosted. Additionally, it is usually written in a dimensionless form with the aid of the specific gas constant of water R, with the following value [97], [98]:

$$R = 0.461526\,\frac{kJ}{kg\,K} \tag{3.32}$$

Then, the dimensionless nature of the Gibbs free energy function is presented below:

$$\left[\frac{g(P,T)}{RT}\right]_u = \frac{\left[\frac{kJ}{kg}\right]}{\left[\frac{kJ}{kg\,K}\right][K]} = [1] \tag{3.33}$$

Let $\frac{g(P,T)}{RT}$ be the dimensionless Gibbs free energy function, its total differential is shown:

$$d\left(\frac{g(P,T)}{RT}\right) = \frac{1}{RT}\,dG - \frac{G}{RT^2}\,dT \tag{3.34}$$

Substituting Equations (3.11b) and (3.15) into Equation (3.34):

$$d\left(\frac{g(P,T)}{RT}\right) = \frac{v}{RT}\,dP - \frac{h}{RT^2}\,dT \tag{3.35}$$

The resulting equation, shown as Equation (3.35), follows the structure of exact differentials disserted in Section 3.1.3 (Eq. (3.18) and (3.19)), where:

$$\frac{v}{RT} = \left(\frac{\partial \left(\frac{G}{RT} \right)}{\partial P} \right)_T \tag{3.36a}$$

$$\frac{h}{RT} = -T \left(\frac{\partial \left(\frac{G}{RT} \right)}{\partial T} \right)_P \tag{3.36b}$$

This set of generated equations reveals that the dimensionless Gibbs function and its derivatives can also work as generating functions for thermodynamic properties. This is specially relevant for the next Chapter where the International Association for the Properties of Water and Steam (IAPWS) industrial formulations will be discussed.

3.1.6 Residual properties

The specific Gibbs free energy function and its dimensionless form provide thermodynamic information for liquids, solids and gases. When it comes to gases, a further analysis can be conducted considering the concept of residual properties.

The elementary definition states that a thermodynamic property of a real gas is not exact because of limitations of the ideal gas theory, therefore, a residual property is the difference between the value of the property as an ideal gas and the actual value. Then, for the specific Gibbs free energy:

$$g = g^R + g^{IG} \tag{3.37}$$

Where:

g Specific Gibbs free energy

g^R Residual specific Gibbs free energy

g^{IG} Ideal gas value of specific Gibbs free energy

3.2 Flash Evaporation Binary Cycle

As formerly reviewed in Sections 2.5 and 2.6, geothermal energy has been extensively used for power generation, even when its contribution to the world's electricity market is still reduced — compared to other renewables. When it comes to the side-benefits of power generation using geothermal for rural or isolated communities, distributed networks discussed in Subsection 2.5.1 proved to be feasible possible choices for the emerging market of local generation.

Regarding Mexico, as already examined in Subsections 2.3.4 and 2.4.2, its latent potential is well known. In addition to its installed capacity, an estimation of the viable potential of geothermal projects for power generation in Mexico, using small sized plants, predicted 200 MW_e based on hydrothermal manifestations [99]. Additionally, a series of surveys have demonstrated the occurrence of several geothermal prospects in the Baja California Peninsula [100], making it an attractive area for cascade projects.

Precisely, given the nature of the Baja California Peninsula — having both the thermal resources and scarcity of fresh water —, the iiDEA® Group, part of the Engineering Institute of the National Autonomous University of Mexico (UNAM), currently part of the CeMIE-Geo, is developing low-enthalpy geothermal projects for power generation, seawater desalination and food dehydration, aiming for the use of these prototypes in an isolated fashion (for use with geothermal resources or waste heat) or as part of a cascade project. The Flash Evaporation Binary Cycle (FEBC) is the proposed alternative for low-power, off-the-grid power generation using geothermal.

3.2.1 Introduction

The FEBC is a modified version of a binary cycle, which may be considered a hybrid between a Conventional Binary Cycle (CBC) and a single-flash steam cycle. It is versatile enough to use water or a refrigerant as working fluid, and low-to-medium enthalpy geothermal fluid or waste heat, depending on the operating conditions and availability of the resource. Furthermore, given its modular nature, it can be connected in series to achieve a greater output power. Among its advantages, one can mention the following [101]:

1. Change of phase does not occur in the heat exchanger. Instead, passive devices such as an orifice plate and a cyclone separator are used.

2. Minor footprint.

3. Numerous environmental benefits when using water as working fluid.

4. Short maintenance periods given the use of plate heat exchangers.

3.2.2 General overview

Figure 3.1 shows a schematic representation of the FEBC, depicting the main elements involved in the cycle. Notice the binary nature of the cycle in the plate heat exchanger, where the geothermal resource and the working fluid do not enter in contact with each other, avoiding corrosion and scaling in the turbine — the most critical component. Once the working fluid is heated and brought to saturated liquid conditions, it passes through an orifice plate, suddenly dropping its pressure and turning it into a biphasic mixture. This process is known as *flash evaporation*, hence the name of the cycle. The mixture is then taken to a cyclone separator, where the separated steam enters the turbine and the remaining liquid is mixed with the now condensed steam before restarting the process.

A comparison of the theoretical energetic performance of a CBC and a FEBC (CBC using isopentane as working fluid, FEBC using water) conducted by the iiDEA® Group demonstrated some facts about the viability of the FEBC for a 1.2 MW_e plant [101], shortly discussed below:

1. Given a geothermal resource below 146 °C, and an ambient temperature of 25 °C, the second-law-efficiency of the FEBC is greater than that of a CBC.
2. Mass flow rate of working fluid in a FEBC is significantly greater than the one needed for a CBC. On the other hand, necessary mass flow rate of geothermal fluid is slightly less in a FEBC for a fixed net output power.

3.2.3 Thermodynamic states

For the sake of clarity, a new schematic diagram with numbered thermodynamic states is shown in Figure 3.2. An accompanying $T-s$ diagram for water as a working fluid is also shown in Figure 3.3. As already mentioned in Subsection 3.2.2, the working fluid is heated up to saturation liquid state (6 – 7) before passing through the orifice plate. Flashing (7 – 8) is modeled as an isenthalpic process because it occurs spontaneously, adiabatically and does not comprise work [17]. Separated steam (1) enters the turbine, expanding to the condenser pressure (2, for real expansion; 2s, for isentropic one), while separated liquid (5) is brought to the mixer (5'), where it joins condensed steam (3) pumped up (4) to the mixer pressure.

Note that the flashing process in the orifice plate minimizes the energetic requirements of the cycle; additionally, a throttling valve can also be used, offering a variable pressure drop — and as a consequence, a variable steam fraction — as a function of its opening position. Finally, observe that thermodynamically, the working fluid is essentially going through the same process as the one carried out in a single-flash steam cycle, with the advantages previously discussed in Subsection 3.2.1.

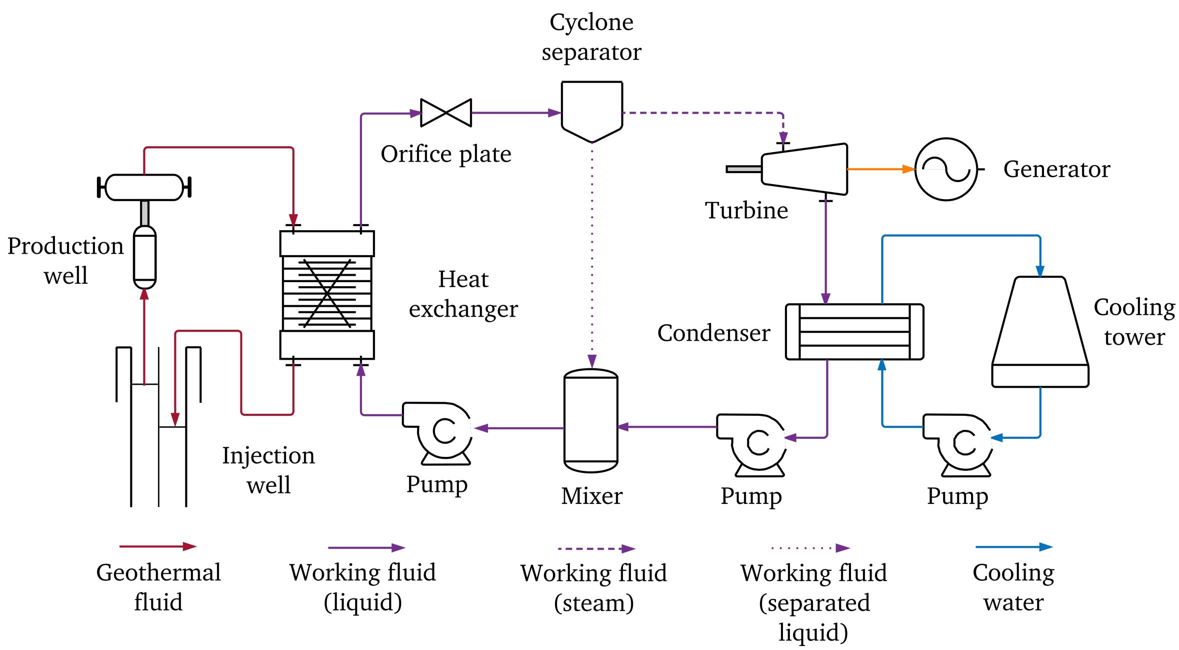

Figure 3.1: Flash Evaporation Binary Cycle

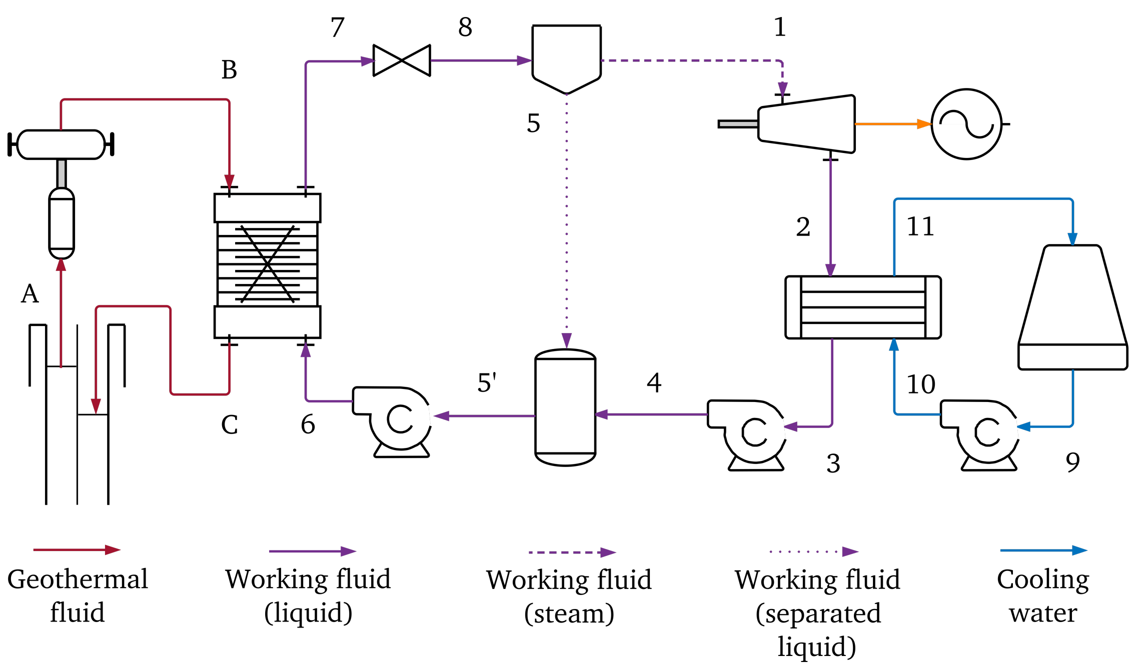

Figure 3.2: Thermodynamic states of Flash Evaporation Binary Cycle

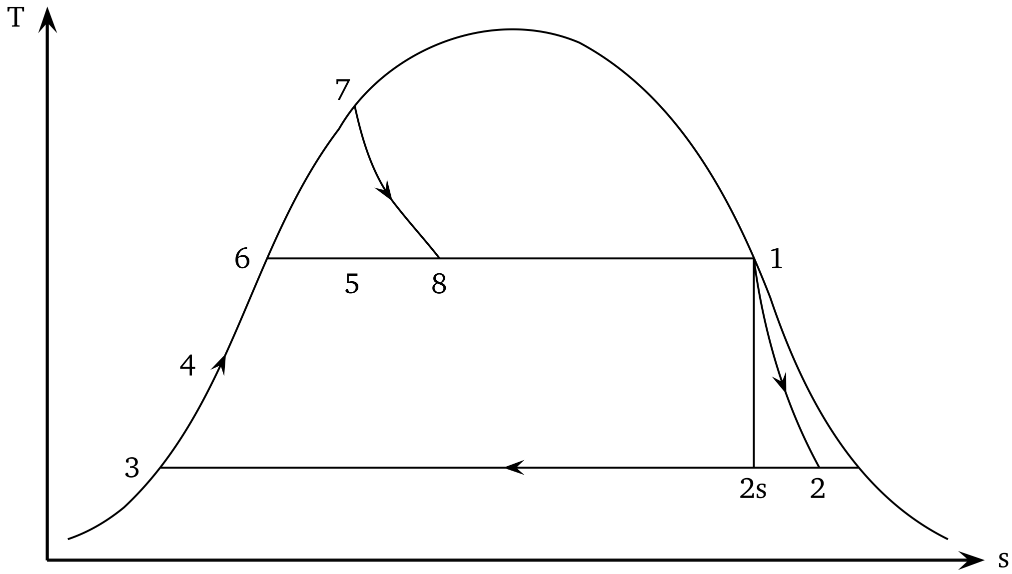

Figure 3.3: $T - s$ diagram of Flash Evaporation Binary Cycle. Adapted from [101].

3.2.4 Experimental setup

For testing purposes, an experimental steam generation unit was set up by the iiDEA® Group, thoroughly detailed in previous dissertations [3]–[5], [58]. Several modifications were conducted on the original theoretical cycle in order to produce a reduced version, capable of generating steam. Among the modifications, geothermal fluid was simulated using an electric boiler, and the inclusion of a radiator for cooling substituted the original wet cooling system. For a 1 kW_e output, Table 3.1 shows the theoretical data for the system. Finally, Figure 3.4 shows the elements of the experimental steam generation system, with the inclusion of states U and V.

Table 3.1: Theoretical conditions of steam generation system. Adapted from [5].

Device	State	Pressure kPa	Temperature °C
Heat exchanger	B	412	140
	C	362	106.7
	V	487	103.7
Orifice plate	7	332	137
Cyclone separator	5	130	107.1
	8	130	107.1

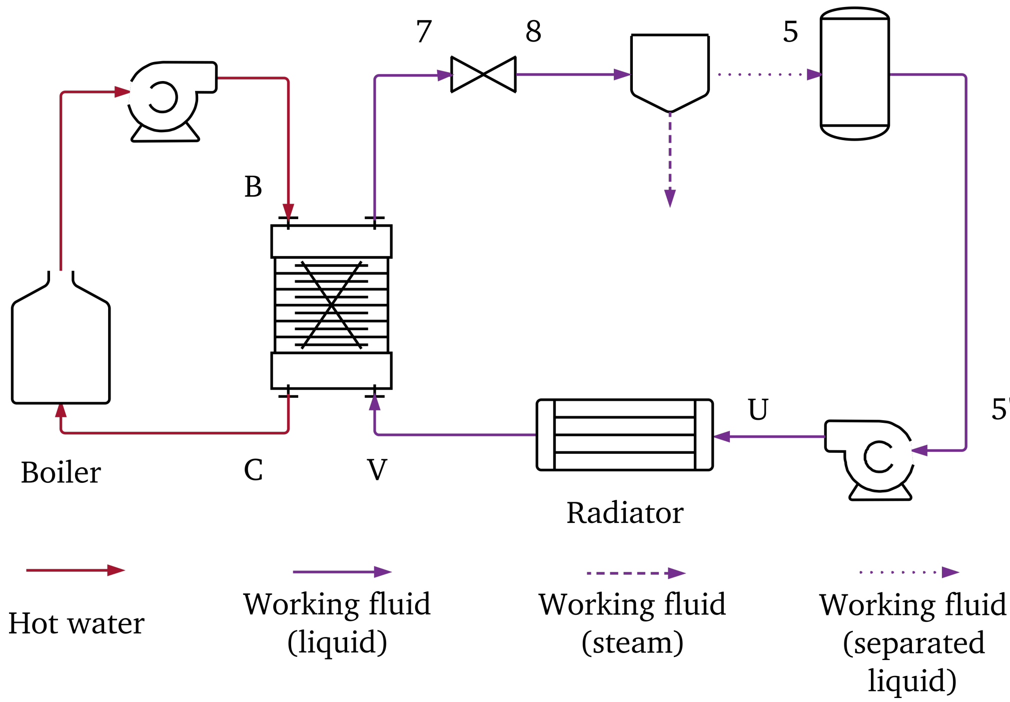

Figure 3.4: Steam generation experimental unit

3.3 Instrumentation

Instrumentation systems have become ubiquitous elements in industrial processes. Their inherent relevance extends throughout the whole specter of industries, providing valuable information which contributes to control, safety and quality consents. In its most basic form, instrumentation can be illustrated through Figure 3.5, where the three main elements of the process are present.

Simply put, once a physical variable of interest is measured through a device known as sensor, raw information about the physical media is now contained in its output signal. Later on, signal processing is conducted through digital or analog means and depending on the final application, it may be recorded, transmitted or visualized by the operator. In essence, instrumentation systems gather information about the world, which later can be used in a vast number of applications.

Figure 3.5: Basic instrumentation scheme. Adapted from [102].

3.3.1 Sensors

Sensors can be simply categorized as *active* or *passive*, depending on its interaction with the physical media. The former type adds energy to the environment in which the measurement is being conducted; on the other hand, the latter type of sensors do not add energy but may remove energy contained or stored in the media while in operation [103]. With reference to its output signal, it can be analog or digital, single-ended or differential. When it comes to quality, cost and application, numerous characteristics of a sensor come to mind, including accuracy, operating conditions, operating range, precision, reliability, resolution, sensitivity, specificity and uncertainty [104].

Accuracy is primarily affected by systematic errors (bias) and/or random error (regarding precision). While systematic errors have to do with a — sometimes known and constant – shift in the input–output response of the sensor, random errors are intrinsically present [103].

3.3.2 Signal processing

Signal processing refers to the process in which the raw output signal from the sensor is conditioned to satisfy the requirements of the receiver equipment [105]. Among the most common processes, one can include Digital-to-Analog conversion, amplification and filtering, being the last a quite interesting one since it may be conducted by analog or digital means.

3.3.3 Visualization / data logging

As previously mentioned in Section 3.3, the last stage of the instrumentation process may include recording, transmission or visualization of data gathered by the sensors. At an industrial level, several protocols are known for their reliability and extended use; additionally, a Human-Machine Interface (HMI) installed in several stages of a process has become common over the years.

3.4 Digital Signal Processing (DSP)

As the name implies, DSP focus on signal manipulation exclusively through digital means. Even with the significant amount of inner areas involved in it, ranging from electronics and numerical analysis to probability and statistics, DSP has demonstrated its usefulness in science and engineering.

Back in the 1960s DSP applications were concentrated in a few areas and still restricted to a minority; nowadays, the widespread use of DSP techniques is actively known in space, medical, commercial, military, industrial and scientific areas [106].

3.4.1 Analog-to-Digital conversion

In order to take an analog input to transform it into a digital input, one must review the digitization process, which is made out of two inner processes. Sampling refers to the process in which time is converted from a continuous variable to a discrete variable, in terms of the number of samples per second. On the other hand, quantization relates to that in which the dependent variable (commonly voltage) is turned into a discrete variable [106].

Sampling is ruled by the Sample and Hold (S&H) unit while quantization precision relates to the number of bits in the Analog to Digital Converter (ADC). In order to represent an analog input in the most representative way and avoid aliasing, the sampling theorem states that the sampling frequency must — at least — double the highest frequency of the signal. In practice, it is often recommended that sampling frequency must exceed ten times the largest frequency component of the original analog signal to be sampled [1].

3.4.2 Digital filters

One of the most well-known applications of DSP techniques is digital filtering. They usually serve one of the following two main purposes: separation and restoration of signals [106]. Given their nature, and in contrast to analog filters, they provide flexibility in design, mitigate costs and reduce electronic footprint.

Filter classification can be described in terms of the mathematical method of implementation (convolution or recursion) and their main objective (smoothing, Direct Current (DC) removal, separating frequencies and deconvolution). Furthermore, depending on the desired manipulation, time domain parameters like step response, overshoot and linear phase may be of interest. On the other hand, if frequency domain parameters are more relevant, low-pass, band pass, high-pass or band-reject responses should be taken into consideration [106]. Table 3.2 shows filter classification in terms of the two criteria previously outlined.

Table 3.2: Filter classification. Adapted from [106].

	Convolution	Recursion
	Finite Impulse Response (FIR)	Infinite Impulse Response (IIR)
Time domain	Moving average	Single pole
Frequency domain	Windowed-sinc	Chebyshev
Custom	FIR custom	Iterative design

3.4.3 Moving average filter

One of the most prevailing and advantageous DSP techniques for smoothing signals is the Moving Average Filter (MAF). As a consequence of having exceptional results in the time domain, it suffers from a poor frequency domain performance, however, given its main target, it does not represent a noticeable drawback. Moreover, it is the fastest digital filter available [106].

MAFs can be computed in their most basic form through recursion or in a more elegant way, using convolution. As the name suggests, arithmetically is an average of consecutive samples. When the consecutive numbers are taken in one *side*, it can be computed as follows [106]:

$$y[i] = \frac{1}{M} \sum_{j=0}^{M-1} x[i+j] \tag{3.38}$$

Where:

i, j Indexes

M Number of points in MAF window

$x[]$ Input

$y[]$ Output

If the filter takes points from the input signal symmetrically around the output signal, then Equation (3.38) can be rewritten in the following way, where M must be an odd number and $N = M - 1$:

$$y[i] = \frac{1}{M} \sum_{j=-N/2}^{N/2} x[i+j] \tag{3.39}$$

One disadvantage of the MAF is the presence of delays in its output. One–sided MAF with M number of points in its window have a delay of $M-1$ samples; on the other hand, every symmetric MAF will display a delay of $(M-1)/2$ samples [107].

In relation to the computation of the filter using convolution, one can notice from Equation (3.39) that the MAF is a convolution of the input signal $x[]$ with a kernel k with M number of elements, describing a rectangular pulse with unit area [106], defined by:

$$k = \left[\frac{1}{M}, \frac{1}{M}, \frac{1}{M}, \cdots, \frac{1}{M} \right] \tag{3.40}$$

Finally, Equation (3.39) can be rewritten using convolution sum, displayed below:

$$y[i] = \sum_{j=0}^{M-1} k[j]\, x[i-j] \tag{3.41}$$

3.5 Reliability

Reliability is defined as "the ability of certain element to perform a required function under given conditions, for a given interval" [108]. Reliability analysis extends to numerous areas besides engineering itself. Its applicability is broadly employed by many industries, including, but not limited to at least one of the following departments: customer service, environmental, financial, insurance, legal, quality, risk management, safety and security [109].

As with other areas of engineering, origins of reliability engineering date back to WW2, when the German army started to execute reliability concepts — previously applied to electric power generation by some researchers — on V1 and V2 rockets [110]. Afterwards, in 1952, the United States Department of Defense (US–DoD) created a dedicated area, responsible for publishing numerous military reliability handbooks (MIL–HDBK) and standards (MIL–STD).

3.5.1 Reliability fundamentals

Reliability deals with the performance of a system through time. A system is fault-tolerant when even in the presence of a fault, the system accomplishes its required function. When describing the difference between faults and failures, a standardized definition published by the International Federation of Automatic Control (IFAC) is reproduced [111]:

Fault An unpermitted deviation of at least one characteristic property (...) of the system from the acceptable/usual/standard condition.

Failure A permanent interruption of a system's ability to perform a required function under specified operating conditions.

Notice that the definition exhibited implies that a device may still perform after a fault, producing an error as a consequence, which is the mathematical difference between an ideal — or desired — value, and the actual value. Furthermore, a failure can lead to a catastrophic situation in which the process can be unrecoverable and may need a replace or major maintenance.

A failing system can be classified according to its failure mode, defined as the array of possibilities in which a system can fail [112]. A previous dissertation reviewed a popular methodology known as Failure Mode and Effect Analysis (FMEA) aimed at the mitigation of risks [58]. Table 3.3 portrays an overall view of primary faults prone to be found in different components.

Table 3.3: Primary faults for different components. Adapted from [113].

Type of faults		Components			
		Mechanical components	Electrical components	Electronic hardware	Software
Form	Systematic	✓		✓	✓
	Random		✓	✓	✓
Time behavior	Permanent			✓	✓
	Transient	✓	✓	✓	
	Noise		✓	✓	
	Drift	✓	✓	✓	
Extent	Local	✓	✓	✓	✓
	Global			✓	✓

3.5.2 Hardware faults

Numerous reliability and safety guides point at nuclear facilities as the best example where keeping a safe environment through Instrumentation and Control (I&C) is a serious matter, nevertheless, this is not exclusive of nuclear power plants. Every power generation system carries an extensive number of subsystems where I&C is not only necessary for monitoring and supervision of critical variables, but also for safety measures.

Regarding power systems, the relevance of redundancy as a way to improve reliability is known [114]. Additionally, there is evidence pointing at the added value of reliable power systems and how the added cost can be justified [115]. In preliminary stages of the design of the fault-tolerant instrumentation system, aimed at increasing the reliability of power supplies for sensors, an overall reliability of 99.77% was achieved with a 12.44% increase in the total cost [58].

Finally, as previously shown in Table 3.3, part of Subsection 3.5.1, electronic hardware is subject to every major known fault, subsequently, assuring the reliability of electronic hardware and associated electrical components is crucial. The aforementioned facts are an essential part of this dissertation, where fault-tolerant power supply modules are assembled, evaluated and tested. As a side note, Figures 3.6 and 3.7 show some common faults and failures attributable to actuators and sensors.

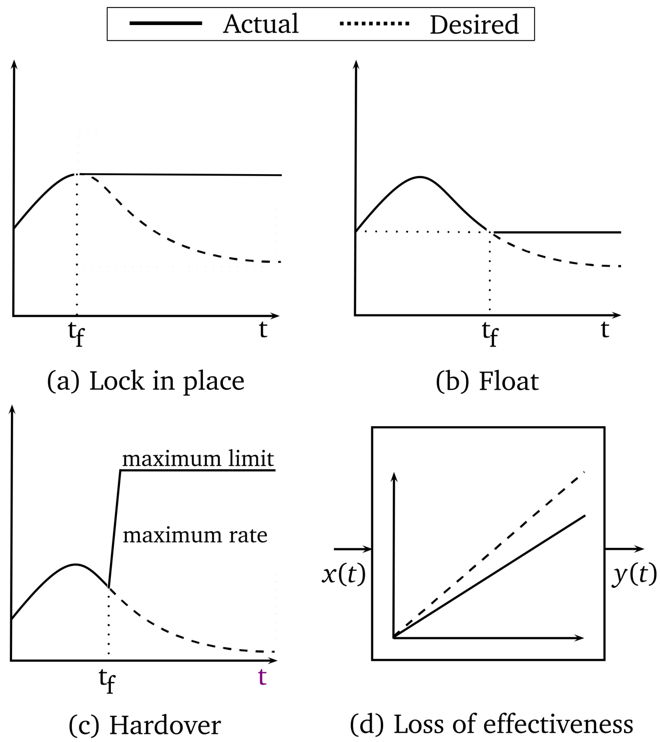

(a) Lock in place (b) Float

(c) Hardover (d) Loss of effectiveness

Figure 3.6: Fault and failures on actuators. Adapted from [116].

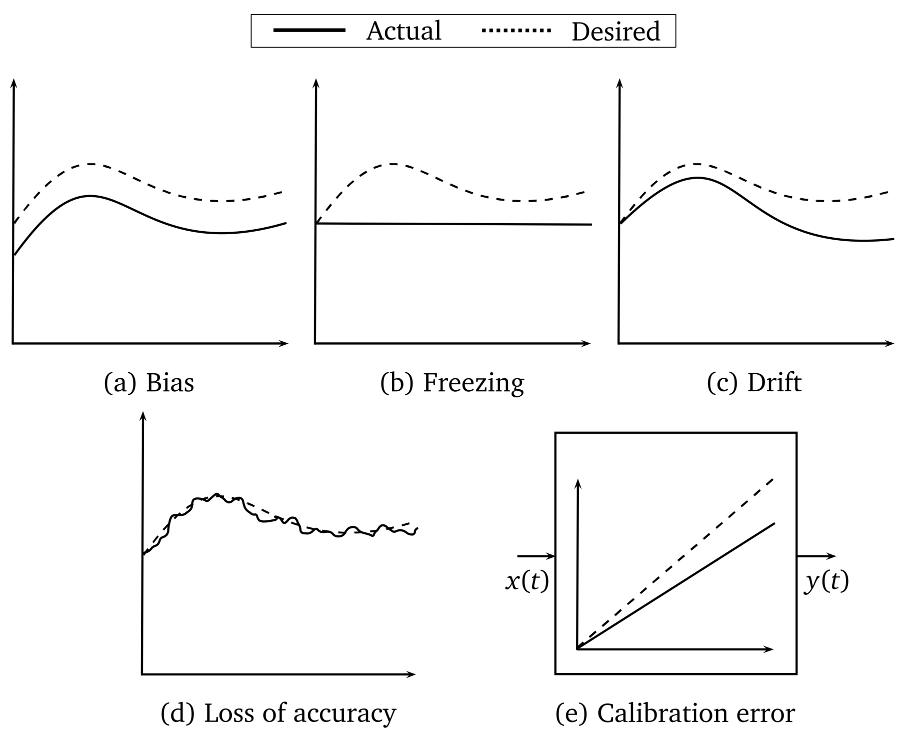

(a) Bias (b) Freezing (c) Drift

(d) Loss of accuracy (e) Calibration error

Figure 3.7: Fault and failures on sensors. Adapted from [116].

3.5.3 Screening methods

As reviewed in Subsections 3.5.1 and 3.5.2, electronic and electrical components are prone to faults. Manufacturers put special emphasis on testing their products through exhaustive assessments before being available on the market. Laboratory tests made by manufacturers mostly try to cover a wide set of scenarios where faults are caused by external factors, including — but not limited to — the following [117]:

- Electrical noise caused by power lines
- Electromagnetic Interference (EMI)
- Extreme environments
- Ionizing radiation
- Unstable power supplies
- Usage issues attributed to the end user
- Wearing out of components due to programming cycles

Table 3.4 demonstrates some typical screening methods for electronic devices; on the other hand, Table 3.5 displays the usual accelerated lifetime tests conducted on them.

Table 3.4: Typical screening methods for semiconductors. Adapted from [118].

Type	Screening method
Non-stress methods	Visual inspection before packaging Visual inspection after packaging X-ray inspection
Thermal stress methods	Temperature cycling Thermal shock Low-temperature testing
Mechanical stress methods	Drop testing Constant acceleration test Particle Impact Noise Detection (PIND)
Electrical stress methods	Burn in High-voltage application

Table 3.5: Representative accelerated lifetime tests. Adapted from [118]

Stress method	Accelerated test	Main stressor	Failure mechanism
Constant stress	High-temperature storage	Temperature	Junction degradation, impurities deposit, ohmic contact
	Operating lifetime	Current, temperature, voltage	Surface contamination, junction degradation, electromigration
	High humidity and temperature storage	Humidity, temperature	Corrosion, surface contamination, pinhole
	High humidity and temperature bias	Humidity, temperature, voltage	Corrosion, surface contamination, juntcion degradation
Cyclic stress	Temperature cycle	Duty cycle, temperature difference	Cracks, thermal fatigue, broken wires, metallization
	Power cycle		Insufficient adhesive strenght of ohmic contact
	Humidity-temperature cycle	Humidity and temperature difference	Corrosion, surface contamination, pinhole
Step stress	Operating test	Current, temperature, voltage	Surface contamination, junction degradation, electromigration
	High-temperature reverse bias	Temperature, voltage	

3.5.4 Software faults

Software faults should not be dismissed in embedded systems. Back in the late 1980s they were still making up to 60% of the faults in computational systems [119]. One special attribute of software faults is that they do not follow the usual behavior assumed in hardware reliability analysis since they are systematic faults caused by the design of the software itself [120].

Given the complex nature of the functions involved in the IAPWS–IF97 standard — as later examined in Subsection 4.5.3 —, quantitative evaluation of every function involved was conducted according to the numerical tests proposed by the standard itself. As an additional source of reference, the results obtained were compared with those generated by the X–Steam MATLAB® function, found on the MathWorks® database and developed by X–Engineering [121].

3.5.5 Reliability evaluation

It should be noticed, as a warning, that the terms *fault* and *failure* are sometimes used indistinctly in literature, as opposed to the definition given in Subsection 3.5.1, but one must be careful and discern based on the context if it has to do with one or another. This dissertation primarily deals with non-catastrophic unrepairable faults.

Dependability is considered the major goal of reliability engineering techniques. Its standardized definition states it as "the (...) state used to describe the availability performance and its influencing factors: reliability, maintainability and maintenance support performance" [108]. Reliability evaluation is a major area of reliability engineering and is determinant in the design stage to minimize the occurrence of faults and failures. In relation to reliability evaluation, three main approaches may be taken [58]:

Quantitative Probabilistic evaluation to estimate the attributes of dependability: reliability, availability, maintainability and safety. Common techniques include Markov Models, Transition Matrices and State Diagrams.

Qualitative Evaluation of possible consequences of faults and failures. FMEA, Failure, Modes, Effects and Criticality Analysis (FMECA) and Fault Tree Analysis are some well known techniques.

Other Axiomatic and experimental methods are sometimes used based on the availability of data and available time.

In regard to quantitative evaluation, failure rate λ is one of the most common dependability measures for repairable and unrepairable devices, defined as the number of failures over time:

$$\lambda = \frac{Failures}{Time} \tag{3.42}$$

A second measure for unrepairable systems is the Mean Time To Failure (MTTF), which express the time of the occurrence of a failure since its first time of continuous operation [112], defined in terms of the failure rate:

$$MTTF = \frac{1}{\lambda} \tag{3.43}$$

For electronic components, failure rates range between $10^{-10}\,\frac{failures}{hour}$ and $10^{-7}\,\frac{failures}{hour}$, generating an auxiliary measure to deal with failure rates for electronics easily [122], known as Failure in Time (FIT), defined below:

$$FIT = \frac{failures}{10^9 h} \tag{3.44}$$

To compute the reliability of a device over certain mission time t, the following expression is used [123]:

$$R(t) = e^{-\int_0^t \lambda(t)dt} \tag{3.45}$$

Where:

$R(t)$ Reliability over time

$\lambda(t)$ Failure rate as a function of time

In general, failure rate changes over time based on three main regions: early failure, useful life and wear out, commonly displayed in a *bathtub* curve. Nevertheless, during the useful life region, the failure rate remains constant [123], yielding the expression known as the exponential failure law, displayed below [112]:

$$R(t) = e^{-\lambda t} \tag{3.46}$$

Reliability of interconnected systems is computed based on the relationship between them — frequently displayed in a Reliability Block Diagram (RBD). Elements are connected in *series* when a single fault makes the whole system fail, and in *parallel* when the fault only disables the affected unit. Expressions for computing parallel ($R_p(t)$) and series ($R_s(t)$) reliability for n elements are introduced below [112]:

$$R_p(t) = 1 - \prod_{i=1}^{n}[1 - R_i(t)] \tag{3.47a}$$

$$R_s(t) = \prod_{i=1}^{n} R_i(t) \tag{3.47b}$$

3.5.6 Fault-tolerant systems

Dependability of a system can be reached – or enhanced — through the use of fault tolerance and a combination of the following additional means: fault forecasting, fault prevention and fault removal [112]. The essence of fault tolerance lies in redundancy, either in hardware, software, information or time.

Fault tolerance, in its most elemental definition, can be stated as a feature of a device or system in which its required function is performed even in the presence of faults. With the inherent addition of redundancy, a fault-tolerant system is prone to follow as many as the following eight stages, concisely reviewed below [124]:

1. **Fault confinement** Limitation of the spread of fault effects after a primary fault.

2. **Fault detection** Recognition of an unexpected state of a component or system. The time between the occurrence of the fault and its detection is known as *fault latency*. Detection of faults is *online* when it provides a real–time detection, contrary to *offline* detection, where the process must be stopped to perform a test on it.

3. **Diagnosis** If the previous stage did not provide the location or properties of the fault, an offline diagnostic must be conducted.

4. **Reconfiguration** In the presence of a fault, the system must keep its functional specifications, this is achieved replacing or isolating the faulty component.

5. **Recovery** After the manifestation of a fault, it is necessary to remove its effects. In computer science *fault-masking* and *rollback* are common techniques.

6. **Restart** After recovery, a *hot* restart resumes operations immediately after fault detection, a *warm* restart resumes part of the process and a *cold* one reloads the system from its starting point.

7. **Repair** Online or offline replacement of a faulty component takes place. If an element is instantly replaced by a backup spare, it is considered equivalent to a reconfiguration process.

8. **Reintegration** If the defective element is repaired, then it must be reinstalled.

Although Fault Detection and Isolation (FDI) is regularly found among fault-tolerant systems, the presence of FDI techniques does not imply fault–tolerance, and vice versa. On the other hand, fault diagnosis is a more general assignment due to the addition of analytic and heuristic procedures, most frequently described by Fault Detection and Diagnosis (FDD) [125], [126].

3.5.7 Cold-standby redundancy

As per the previous statement found in Subsection 3.5.6, redundancy is an inherent part of fault tolerance, however, in order to accomplish a complete fault-tolerant system, it must be both meaningful and useful to keep the system running. Hardware redundancy may be the most expensive type of redundancy due to its nature, still, it is one of the most used kinds of redundancy in systems that are not easily reachable and maintenance becomes a complex maneuver [112].

Active, passive and hybrid redundancy comprise the alternative techniques that a system may encompass. The first one involves the detection of a fault before being able to tolerate it; the second one deals with *masking* faults without external intervention. Lastly, the two previous techniques may be joint together to form a hybrid, sometimes called *warm* redundancy [112], [122].

Among active redundancy, standby redundancy holds a special place given its unique dynamic characteristics. In hot standby systems, a main module is powered with a set of spare modules — also powered up — ready to substitute the main module in case of failure [125]. Cold standby is similar in nature, with the main difference that spare modules are only powered and reconfigured once a failure in the main module has been detected. Figure 3.8 shows a schematic diagram of cold standby redundancy.

Notice that as a consequence of the detection–reconfiguration mechanism, downtime is an undesired attribute. Additionally, the technique relies in a *perfect* switching instrument. The expression used to find the reliability of a cold standby system of n identical spare elements and perfect switching is given by the following equation [127]:

$$R_s(t) = e^{-\lambda t} \sum_{j=0}^{n-1} \frac{(\lambda t)^j}{j!} \tag{3.48}$$

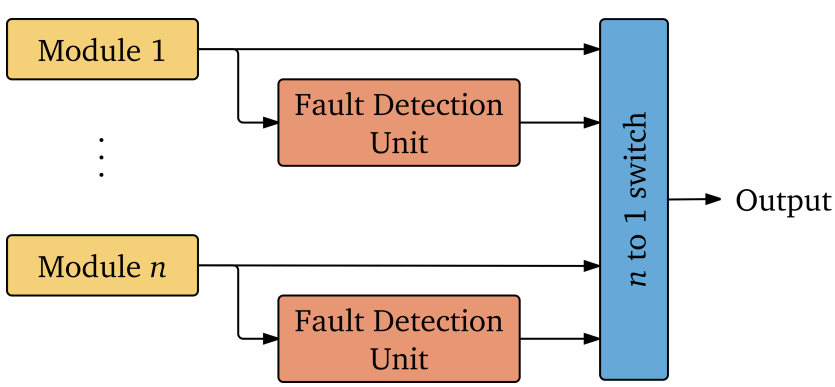

Figure 3.8: Cold standby hardware redundancy. Adapted from [112].

3.6 Conclusions

This Chapter exhibited the core of the theoretical subjects required to comprehend further discourses unfold in the next one. Starting with mathematical relations found in Thermodynamics, a later study of the FEBC introduced the reader to its foundations and distinctive features. Subsequently, a brief outline of instrumentation systems preceded basic DSP theory. Finally, notable reliability concepts and models were reviewed, highlighting cold standby redundancy and its characteristics.

Page intentionally left blank

Chapter 4

Fault-tolerant data acquisition system

Once the theoretical framework needed for the dissertation has been settled, this Chapter concerns the actual implementation of the data logging system, examining each stage of the process. Beginning with the fault-tolerant power supply modules, hardware specifications and software flow is reviewed, before conducting an update on the reliability evaluation of the system. Then, an analysis of the digital filtering carried out is described. Finally, an exhaustive inspection of the algorithm used for calculating thermodynamic properties of the system is discoursed, along with the developed graphical user interface.

4.1 System implementation

In a previous dissertation [58], the theoretical design of the main core of the instrumentation system was outlined, including a first reliability analysis and a preliminary interface based on the modification of a commercial software (PLX–DAQ®). This Section reviews the elements of the fully functional system.

4.1.1 Pressure transducers

After the specifications of the FEBC and the experimental setup, it was concluded that the use of heavy duty pressure sensors with absolute pressure reference offered a wide range of versatility. Honeywell®'s PX2 and PX3 series are designed to meet the requirements of industrial applications offering reliable, cost-effective products. Table 4.1 shows the general specifications for the pressure transducers used, corresponding to PX2 Series.

Table 4.1: Specifications of transducers Honeywell PX2EN1XX100PAAAX. Adapted from [128]

Electrical specifications	
Supply current	5 mA
Operating supply voltage	5 V
Output transfer function	Ratiometric, [0.5, 4.5] V
Performance specifications	
Accuracy	±0.25 % Full Scale Span (FSS)
Compensated temperature range	[-40, 125] °C
Offset error	±1 % FSS
Operating temperature range	[-40, 125] °C
Port type	1/4 - 18 NPT
Pressure range	[0, 100] psi
Pressure reference	Absolute
Response time	< 2 ms
Total error band	±2 % FSS

4.1.2 Temperature sensors

Resistive Temperature Detectors (RTD) were selected as temperature sensors due to their advantages over other temperature measurement devices, such as thermistors or thermocouples [129]. These advantages include accuracy, linearity, long-term stability, repeatability and temperature range. Some downsides include the relatively high response time and cost. Table 4.2 displays the characteristics of the 4-wire RTD used for the FEBC.

Table 4.2: General specifications of temperature sensors USW3577

Lead wires	24 AWG, stranded conductor
Port type	Stainless steel 3/8 in - 16
RTD probe	Platinum
RTD element resistance at 0 °C	2000 Ω ± 0.06%
RTD element acuracy at 0 °C	±0.15 °C
RTD element DIN 43760 accuracy class	A
TCR	3850 ppm/°C
Temperature range	[-50, 180] °C
Wires	4

4.1.3 Fault-tolerant power supply modules

As reviewed in Section 3.5 and Subsection 3.5.2 in Chapter 3, power supplies have been elements of interest for reliability analyses throughout history. To overcome the problems and consequences associated with power supplies for sensors — previously found in preliminary stages of the design [58] —, fault–tolerant modules were assembled for each DC power bus used in the system, corresponding to 5 V for pressure sensors and 3.3 V for RTDs. An additional power bus of 12 V was designed for the purpose of serving LEDs attached to each sensor, but unlike the two previous buses, it was not designed as fault–tolerant, as will be described later.

In relation to faults associated with failures in power supplies or as an after–effect of high temperature environments, electronic devices are frequently incorporated with a set of features enhancing automatic shutdown or reset, being thermal shutdown and brown-out detection some of the most popular. While these features are useful to keep the electronic device safe from harm, they do not solve the problem of instability or outage of power supplies.

The use of a Low–dropout Voltage Regulator (LDO) as power supply diminishes the energy requirements of the overall system by virtue of its high efficiency. The TPS72XX family of micro-power LDOs produced by Texas Instruments (TI) was selected given their exceptional characteristics, reviewed in Table 4.3. These LDOs are complemented with an external Enable Input ($\overline{EN}$) and Power–Good (PG) status output indicator, determinant features for the development of the fault–tolerant power supply modules. Finally, features of the TI TL750L12 12 V LDO used for the 12 V bus is also shown in Table 4.3.

A fault-tolerant Power Supply Module (PSM) will be defined as a set of LDOs, where one is operating continuously and the remaining spare LDOs operate as cold standby redundant units.

Table 4.3: Basic features of TI TPS72XX and TL750L12 LDOs. Adapted from [130], [131].

	TPS7233	TPS7250	TL750L12
Typical output voltage	3.3 V	5.0 V	12.0 V
Maximum Output Current (MOC)	250 mA	250 mA	150 mA
Minimum input voltage @ MOC	3.98 V	5.41 V	13 V
Enable Input	✓	✓	
Power–Good Indicator	✓	✓	
Reverse Voltage Protection (RCP)	✓	✓	✓
Internal Current Limiting (ICL)	✓	✓	✓
Thermal protection	✓	✓	✓

Figure 3.8, displaying the theoretical strategy of cold standby redundancy as previously reviewed in Subsection 3.5.7 is revisited below. Along with it, Figure 4.2 shows the equivalent cold standby concept using actual components. Notice that, in theory, the Fault Detection Unit (FDU) and the switching unit act separately, however, in the equivalent schematic, the Tiva C Series evaluation board executes both the role of the FDU and the enabling unit. The resemblance in colors is kept to aid in the description.

Observe that each LDO output is supervised by the EK-TM4C1294XL board through a PG signal. The first module is the only active once the PSM is powered. If a fault is detected by the evaluation board by means of the PG signal, the faulty LDO is deactivated before activating one of the spare modules through its $\overline{EN}$ input.

Clearly, the developed approach satisfies the eight stages previously described in Subsection 3.5.6, primarily limiting, detecting and isolating faults, as well as reconfiguring and recovering the main process. The Interrupt Service Rutine (ISR) leading the aforementioned process will be illustrated in later Subsection 4.8.5.

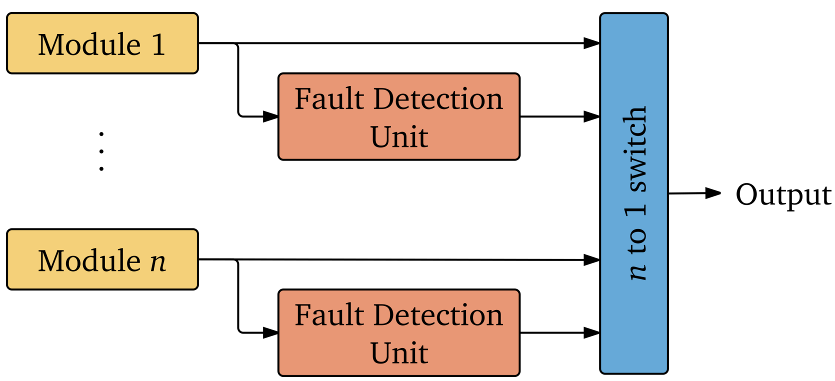

Figure 3.8: Cold standby hardware redundancy. Adapted from [112]. Revisited from page 58.

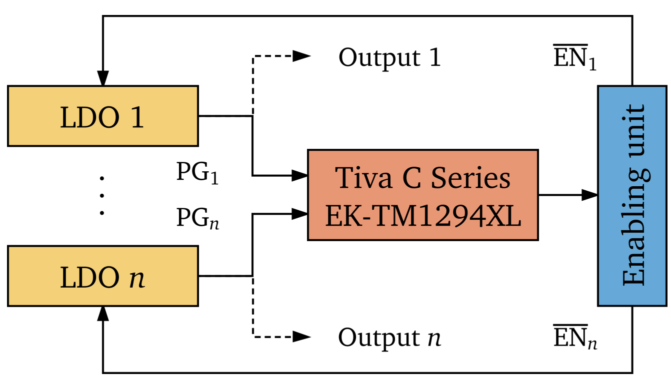

Figure 4.2: Fault-tolerant power supply module

4.1.4 Hardware platform

Over the extensive portfolio of Microcontrollers (MCUs) designed and developed by Texas Instruments, performance MCUs includes 32-bit microcontrollers aimed at control and safety applications. More specifically, the TM4C12x ARM® Cortex®-M4F core-based MCUs, commercially known as the Tiva® C Series, provide a cost-effective solution for industrial applications with outstanding performance and reliability. Table 4.4 displays some essential characteristics of the evaluation board used.

4.1.5 Software platform

An Integrated Development Environment (IDE) is a software tool used for code edition, debugging and compiling. Applications for the evaluation board EK-TM4C1294XL can be developed and debugged in multiple professional software tools, ranging from proprietary tools like Mentor Embedded Sourcery® and IAR® Embedded Workbench, to free, professional IDEs like Keil μVision®. Code Composer Studio® is a professional, industrial–grade free IDE developed and maintained by Texas Instruments®, taking the foundations of the Eclipse® framework and enhancing it with specific features for TI products. With this in mind, CCS was the selected IDE to work with.

4.1.6 Prototype

Testability of the instrumentation system throughout the implementation process was taken into account as a way to keep track of possible faults before its completion and as a recommended element of the design [120]. On the other hand, modularity as a methodology and as a way to improve maintainability was extensively used, proposing a design inspired by those used in CubeSat satellites, where each *floor* contains a dedicated subsystem.

Figure 4.3 depicts the hardware block diagram of the instrumentation system, where each block symbolize a 10 cm x 10 cm PCB while colored arrows represent the connections made between them and the direction of the signals. Notice that signals from the Tiva C Series evaluation board to cold standby modules and LEDs power modules are shown through the connections board. A photograph of the actual prototype is also shown in Figure 4.4.

As already introduced in Subsection 4.1.3, LEDs were attached to each sensor and powered with a single 12 V LDO without fault–tolerance capabilities. Their main purpose is to serve as a visual alarm and localized diagnosis tool at start up, however, given the accompanying Graphical User Interface (GUI), the role of the power supply for LEDs is not considered vital.

Table 4.4: Key specifications of evaluation board EK-TM4C1294XL. Adapted from [132].

Performance features	
Company	Texas Instruments®
Device class	Microcontroller TM4C1294NCPDT
CPU core	32-bit ARM® Cortex^{TM}-M4 with FPU
Performance	120 MHz operation; 150 DMIPS performance
Flash memory	1 MB
SRAM	256 kB
EEPROM	6 kB
Communication interfaces	
CAN bus	Two 2.0 controllers
Ethernet	10/100 MAC + PHY
I2C bus	Ten modules
QSSI	Four modules
UART	Eight modules
USB	2.0 OTG
System integration	
GPIO	15 physical blocks, up to 90 GPIOs
GPTM	Eight 16/32-bit blocks
μDMA	32-channel configurable controller
WDT	Two timers
Advanced Motion Control	
PWM	One module, four blocks, eight outputs
Analog Support	
ADC	Two 12-bit modules, 20 channels, up to 2 MSPS
Analog comparators	Three independent
Digital comparator	Sixteen
Package information	
Current consumption	105.3 mA at 3.3 V, all peripherals on, 120 MHz
Operating range	Industrial [-40, 85] °C

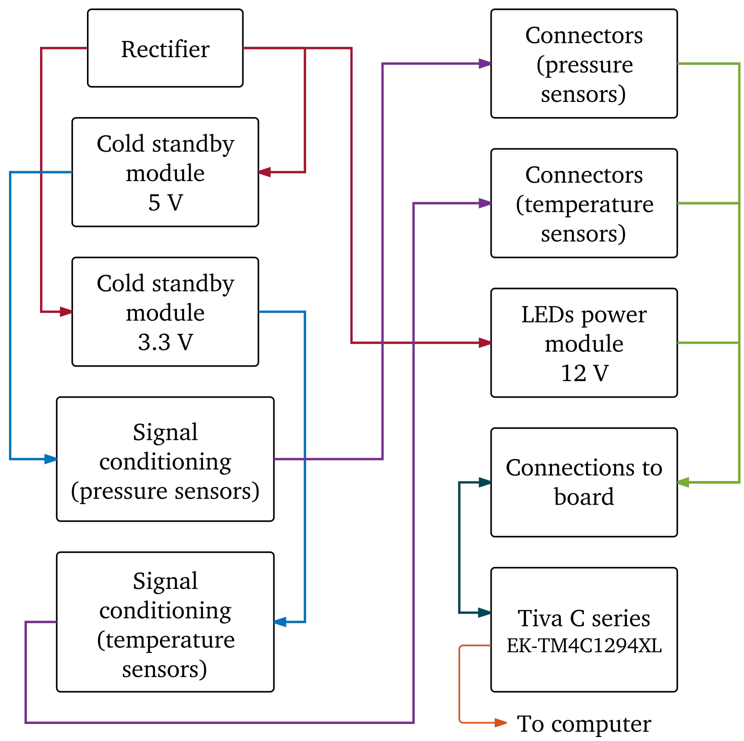

Figure 4.3: Hardware block diagram of instrumentation system prototype

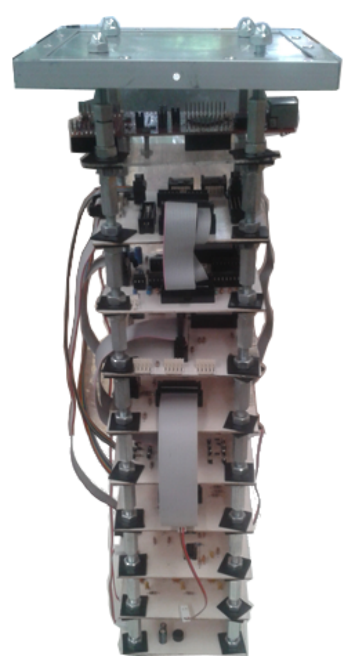

Figure 4.4: Fault-tolerant instrumentation system

4.2 Reliability evaluation

Reliability evaluation of the two PSMs mentioned in Subsection 4.1.3 was performed based on the quantitative technique reviewed in Subsection 3.5.5. Based on this premise, it is important to classify and enumerate the elements involved in each PSM. Only after this preliminary stage the reliability evaluation can be computed.

This Section starts reviewing the reliability of each LDO in their most basic form to establish the groundwork of the reliability objectives. Afterwards, based on established operational conditions several reliability factors will be introduced. Finally, the discussion covers the updated reliability of cold standby redundancy in PSMs.

4.2.1 Assumptions made for reliability analysis

With the purpose of limiting the analysis, some assumptions are made, enlisted below:

1. Failure Rate of each element λ remains constant.
2. Reliability of each component follows the Exponential Failure Law $R(t)$.
3. Components are identical, nonrepairable, and statistically independent.
4. Human interaction is not taken into account as a source of failure.
5. Catastrophic failures are not taken into consideration.

Additionally, based on the former requirements of the instrumentation system, the required function of the modules is described as follows:

1. Steady supply of 5 V and 3.3 V for each power bus
2. FDI capabilities
3. Maximum temperature of operation: 50 °C
4. Mission time t of 10 years (87660 h)

Regarding sensors and Current Limiting Diodes (CLD) used for powering RTDs, extensive screening tests and reliability data was requested to the manufacturers, collecting the received documents in Appendix A. Finally, with regard of the reliability of the EK-TM4C1294XL evaluation board, TI only provides reliability data for the TM4C1294NCPDT microcontroller, without detailing further reliability of the module. Since an additional analysis of the whole board is not part of the dissertation, the reliability analysis is limited to a *perfect switching* cold standby redundant system.

4.2.2 Reliability of Low–dropout Regulators

Figure 4.5 shows the schematic diagram of the TPS7233 LDO while Figure 4.6 illustrates the schematic diagram of TPS7250. In essence, both figures have the same arrangement of elements, with the exception of the added resistor R_2 at the PG output — an open–drain output signal — of the TPS7250 LDO to satisfy the 3.3 V admissible input voltage of the EK-TM4C1294 board.

The first stage of the process deals with the reliability evaluation of each LDO in their most basic form, including additional auxiliary components, without considering soldering or copper paths. Table 4.5 shows the failure rate of each component based on data released by TI and available data from the MIL–HDBK–217F handbook [133], [134]. Lastly, a RBD for each module is shown in Figure 4.7 and 4.8.

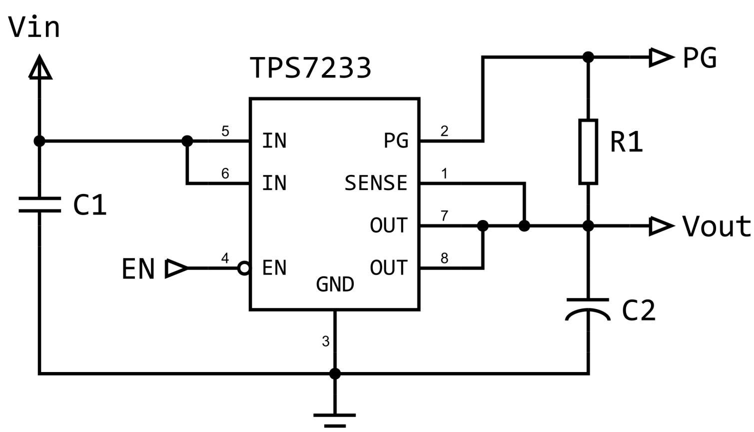

Figure 4.5: TPS7233 Low–dropout Voltage Regulator. Adapted from [130]

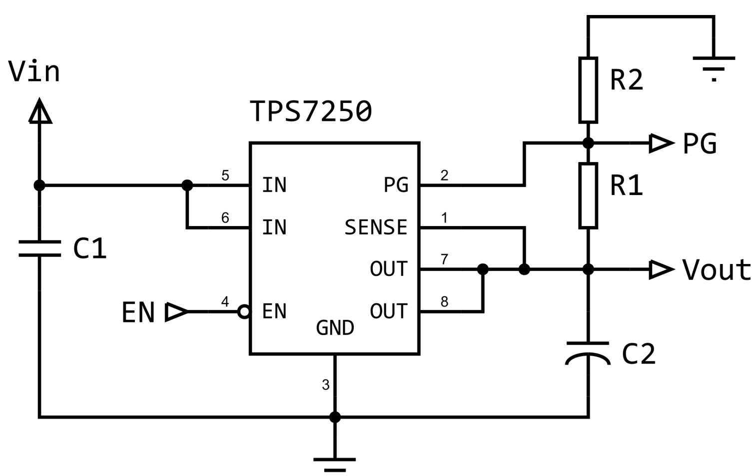

Figure 4.6: TPS7250 Low–dropout Voltage Regulator

Table 4.5: Failure rate of LDOs and auxiliary elements. Adapted from [133], [134].

Device	λ (failures / h)
TPS7233QP	$2.0619\,x10^{-9}$
TPS7250QP	$2.0619\,x10^{-9}$
Capacitor (ceramic)	$9.9\,x10^{-10}$
Capacitor (tantalum)	$4\,x10^{-10}$
Resistor (carbon)	$1.7\,x10^{-9}$

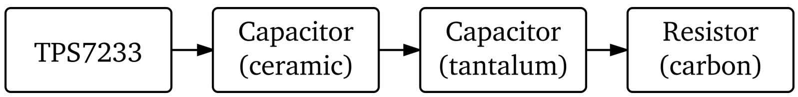

Figure 4.7: Reliability block diagram of 3.3 V PSM

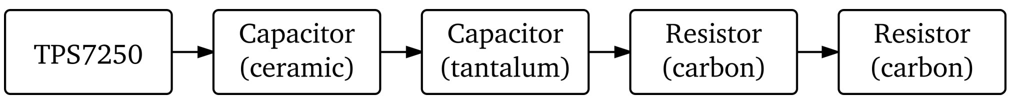

Figure 4.8: Reliability block diagram of 5.0 V PSM

Note that even when the MIL–HDBK–217F corresponds to a Second Generation Handbook [122], it is specifically aimed at electrical and semiconductor devices, making it a widely used source for reliability calculations in electronics. Of course, numerous standards and handbooks have been available recently for intrinsically critical industries — nuclear being an extensively iconic one —, however, they use a more general view including mechanical elements such as springs and bearings.

The military handbook used presents two main ways to calculate the part failure rate for electronic equipment depending on the development stage: Parts Count and Part Stress Analysis. The first, useful in early stages of the development, makes use of part quantities, quality level and application environment; the second requires more details about the equipment used and is commonly used when the hardware is not only being designed but also when it is being built. The latter is the method used for obtaining the part failure rate of capacitors and resistors used in this update.

The basic overall failure rates of PSMs using Equations (3.46) and (3.47b) are shown below:

$$\lambda_{33} = \lambda_{TPS7233} + \lambda_{cc} + \lambda_{tc} + \lambda_r \tag{4.1a}$$

$$\lambda_{50} = \lambda_{TPS7250} + \lambda_{cc} + \lambda_{tc} + 2\lambda_r \tag{4.1b}$$

Where:

λ_{33} Basic overall failure rate of 3.3 V PSM

λ_{50} Basic overall failure rate of 5.0 V PSM

λ_{cc} Failure rate of ceramic capacitor

λ_{tc} Failure rate of tantalum capacitor

λ_{r} Failure rate of carbon resistor

Finally, the basic reliability of each module, for the specified mission time t defined in Subsection 4.2.1 is shown below:

$$R_{33} = e^{-\lambda_{33} \cdot t} = 99.95\% \tag{4.2a}$$

$$R_{50} = e^{-\lambda_{50} \cdot t} = 99.93\% \tag{4.2b}$$

Where:

R_{33} Basic reliability of 3.3 V PSM

R_{50} Basic reliability of 5.0 V PSM

Given the fact that an update is being conducted, part failure rate for capacitors and resistors is now defined in terms of the following two equations, adding different operational factors including temperature, environment and quality, among others:

$$\lambda_{cap} = \lambda_b \pi_C \pi_E \pi_Q \pi_{SR} \pi_T \pi_V \tag{4.3}$$

Where:

λ_{cap} Part Failure Rate of Capacitor

λ_b Base Failure Rate

π_C Capacitance Factor

π_E Environment Factor

π_Q Quality Factor

π_{SR} Series resistance Factor (for tantalum capacitors)

π_T Temperature Factor

π_V Voltage Stress Factor

$$\lambda_{res} = \lambda_b \pi_E \pi_P \pi_Q \pi_S \pi_T \tag{4.4}$$

Where:

λ_{res} Part Failure Rate of Resistor

λ_b Base Failure Rate

π_E Environment Factor

π_P Power Factor

π_Q Quality Factor

π_S Power Stress Factor

π_T Temperature Factor

Used values for the aforementioned factors are briefly discussed in Tables 4.6 and 4.7, which are self explanatory, with the exception of the definitions of Circuit Resistance (CR), Voltage Stress (S_V) and Power Stress (S_P), explained in the following equations:

$$CR = \frac{Resistance\ between\ capacitor\ and\ power\ supply}{Voltage\ applied\ to\ capacitor} \tag{4.5}$$

$$S_V = \frac{Operating\ voltage}{Rated\ voltage} \tag{4.6}$$

$$S_P = \frac{Actual\ power\ dissipation}{Rated\ power} \tag{4.7}$$

Taking the following values:

$$CR = 0.06\,\frac{\Omega}{V} \tag{4.8}$$

$$S_V = 0.3394 \tag{4.9}$$

$$S_P < 0.1 \tag{4.10}$$

Equations (4.3) and (4.4) revealed that some factors do not apply to every component, however, it is easier to display their values and applicability in an overall collection, displayed in Table 4.8.

Table 4.6: Correction factors used for capacitor failure rate

Factor	Description	Value (ceramic) (failures / $10^6 h$)	Value (tantalum) (failures / $10^6 h$)
λ_b	Fixed capacitor, general purpose	0.00099	0.00040
π_C	0.1 μF (ceramic), 8 μF (tantalum)	0.81	1.6
π_E	Ground, mobile. Equipment installed on wheeled vehicles or manually transported	20	
π_Q	Commercial level	10	
π_{SR}	Function of CR	–	3.3
π_T	Temperature of operation (50 °C)	2.9	1.6
π_V	Function of S_V	1.1	1

Table 4.7: Correction factors used for resistor failure rate

Factor	Description	Value (failures / 10^6 h)
λ_b	Fixed resistance	0.0017
π_E	Ground, mobile. Equipment installed on wheeled vehicles or manually transported	16
π_P	Power dissipation	0.17
π_Q	Commercial level	10
π_S	Function of S_P	0.66
π_T	Temperature of operation (50 °C)	1.8

Table 4.8: Correction factors in failures/10^6 h for capacitors and resistors

Element	λ_b	π_C	π_E	π_P	π_Q	π_S	π_{SR}	π_T	π_V
Carbon resistor	0.0017	–	16	0.17	10	0.66	–	1.8	–
Ceramic capacitor	0.00099	0.81	20	–	10	–	–	2.9	1.1
Tantalum capacitor	0.0004	1.6	20	–	10	–	3.3	1.6	1

Now that failure rates of capacitors and resistors have been modified through correction factors, the updated failure rates of PSMs, denoted with an asterisk (*), are shown below:

$$\lambda_{33}^* = \lambda_{TPS7233} + \lambda_{cc}^* + \lambda_{tc}^* + \lambda_r^* \tag{4.11a}$$

$$\lambda_{50}^* = \lambda_{TPS7250} + \lambda_{cc}^* + \lambda_{tc}^* + 2\lambda_r^* \tag{4.11b}$$

Thus, the updated reliability is computed:

$$R_{33}^* = e^{-\lambda_{33}^* \cdot t} = 89.44\% \tag{4.12a}$$

$$R_{50}^* = e^{-\lambda_{50}^* \cdot t} = 88.79\% \tag{4.12b}$$

4.2.3 Reliability of power supply modules

Figure 4.9 displays a plot of the attained reliability in terms of the number of modules n and the product λt using Equation (3.48), with up to six elements. Notice that for a fixed value of λt, spare cold standby modules notably improve the overall reliability of the system. Even when this process can be extended *ad infinitum*, the more modules are added, the more expensive it becomes, with a decrease in the reliability improvement rate.

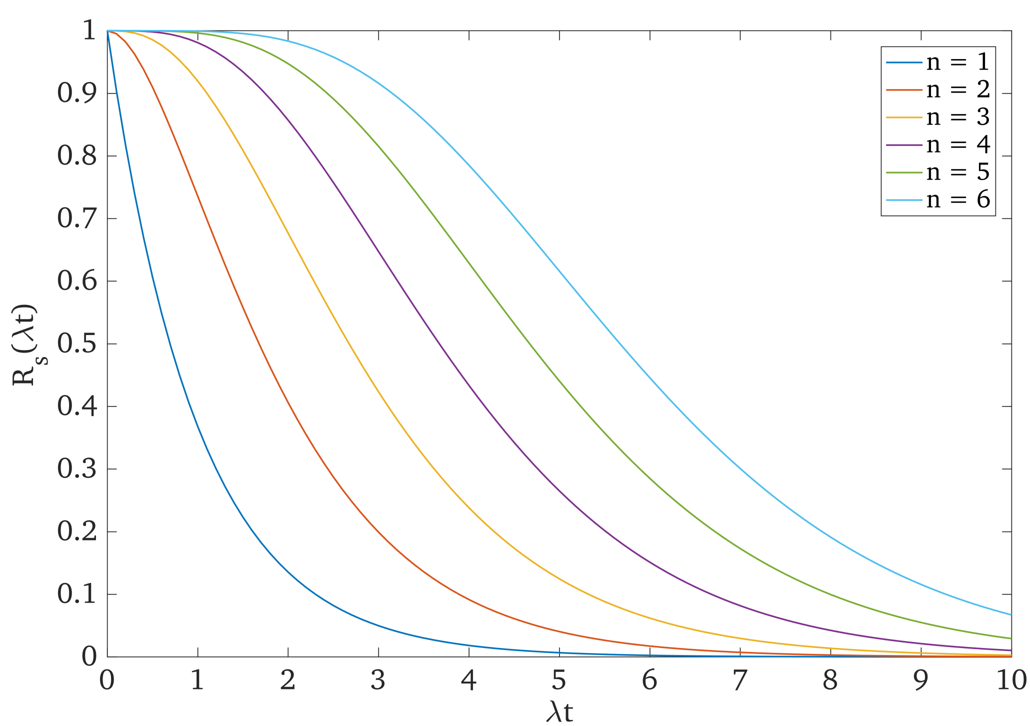

Figure 4.9: Reliability of cold standby modules for n modules

Table 4.9: Reliability of PSMs using cold standby redundancy

Number of modules n	3.3 V PSM	5.0 V PSM
1	89.443%	88.792%
2	99.422%	99.347%
3	99.978%	99.974%

Table 4.10: Final reliability of power modules

PSM	Basic reliability	Corrected reliability	Cold standby redundancy reliability
3.3 V	99.95%	89.44%	99.97%
5.0 V	99.93%	88.79%	99.97%

Using the updated failure rates λ_{33}^{*} and λ_{50}^{*}, along with the cold standby techniques discussed, a new reliability was acquired, reaching up to 99% when three LDOs are used. Table 4.9 displays the results of each computation using Equation (3.48). Finally, the final results gathered in this Section can be found in Table 4.10.

4.3 Digital filtering

The relevance of digital filters is remarkable, offering versatility in its employment in numerous applications, as incorporated in Subsection 3.4.2. The main goal of using digital filters in this platform has to do with their time–domain applications, specifically, smoothing signals.

During early stages of the experimental steam generation unit, the equipment was set up in a noisy environment, where high voltage wires, pumps and motors were also installed. At that time preliminary PCBs had been deployed, thus, going backwards to design intermediate stages of analog filters was not a feasible option. As a result, the examination of digital filters presented in this section was conducted.

To test the performance of Equations (3.38) and (3.39), a known signal with added random noise was generated using MATLAB®, with a maximum of 200 samples. Then, different values of M were used for both MAFs and applied to the same signal. Figures 4.10 and 4.11 display the performance of one–sided and symmetric MAFs, respectively.

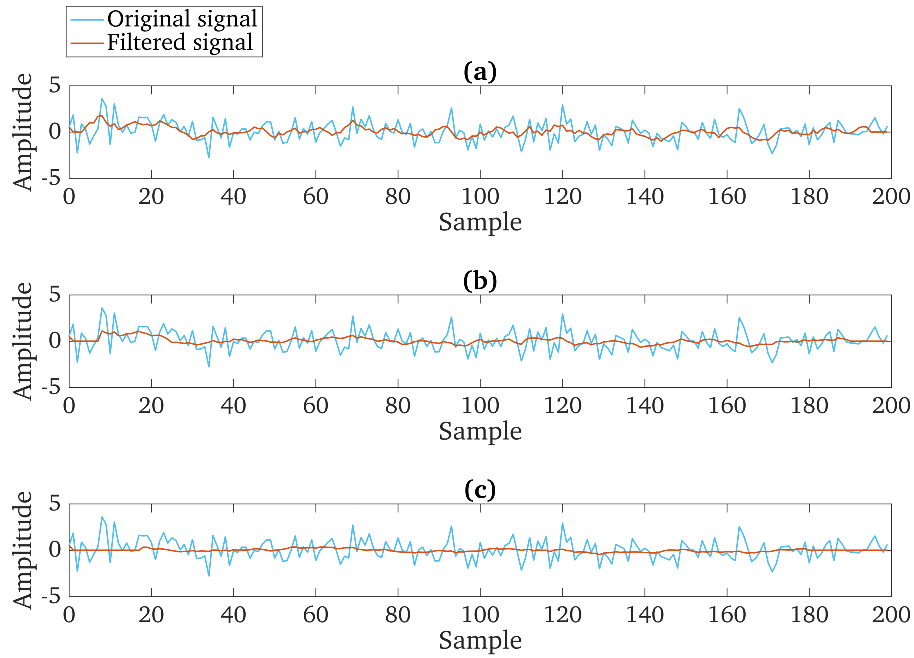

Figure 4.10: One–sided Moving Average Filter (a) $M = 5$, (b) $M = 10$, (c) $M = 20$

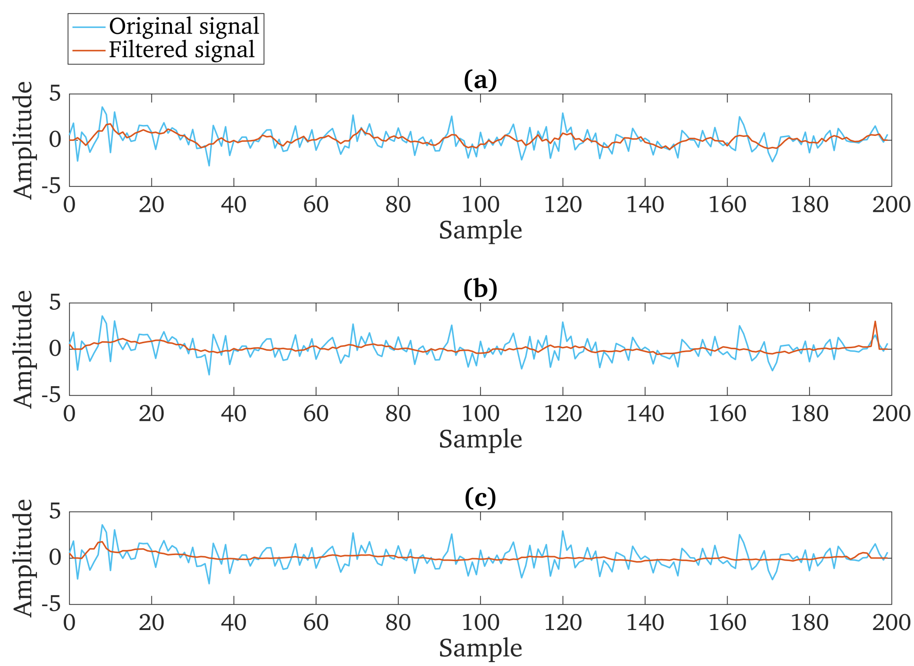

Figure 4.11: Symmetric Moving Average Filter (a) $M = 5$, (b) $M = 11$, (c) $M = 21$

4.4 Implementation of IAPWS–IF97

In previous studies involving the thermodynamic analysis of the FEBC, the Reference Fluid Thermodynamic and Transport Properties Database (REFPROP), developed by the National Institute of Standards and Technology (NIST) has been extensively used [135]. The advantages associated with the use of this software are many, however, one of its primary downsides relates to the cost of purchasing and updating it. Subsequently, given the use of water as a working fluid, an extensive database like REFPROP — which includes organic and inorganic fluids — exceeds the requirements of the project.

Fortunately, properties of water have been exhaustively studied and information related to their mathematical modeling has been available through the years. The International Association for the Properties of Water and Steam (IAPWS) is a decentralized non-profit organization whose central objectives deal with the development of formulations for thermodynamic properties of steam and water and technical counseling for steam power cycles [136].

There are two main formulations for the thermodynamic properties of steam and water published by the IAPWS. The first formulation, originally issued in 1995 and known as IAPWS–95, describes the models for general and scientific use, which, according to the IAPWS itself, is the most accurate formulation, specially for scientific applications. Even when the use of this publication is recommended for most uses, as previously mentioned, the IAPWS has a strong interest in the use of its formulation in the industry, which naturally, has different needs than those of academia, exchanging accuracy for speed in computation and long-term stability over continuous updates [137]. The answer to these needs was accomplished in the publication of the IAPWS–IF97 industrial formulation, adopted in 1997.

The relevance of the work conducted by the IAPWS — specially that in relation to the IAPWS–95 and IAPWS–IF97 formulations — is notorious. Proof of it is the abundant number of printed steam tables and both commercial and open-source software implementations (including online calculators, software for pocket calculators and smart phones) of thermodynamic properties of steam and water using them as a foundation [138].

Additionally, institutions like the NIST, the Ruhr-Universität Bochum (RUB), the Moscow Power Engineering Institute (MPEI), the Hochschule Zittau/Görlitz University of Applied Sciences (HSZG), the American Society of Mechanical Engineers (ASME) and Springer-Verlag GmbH have used these standards [139]–[150].

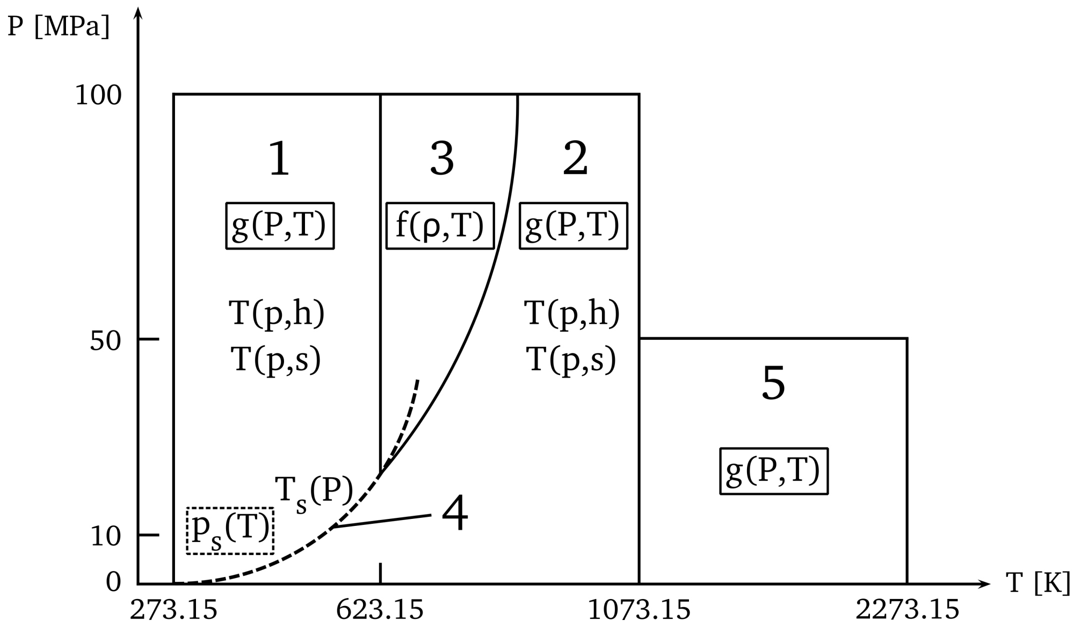

Figure 4.12: P – T diagram describing the regions used in IAPWS–IF97. Adapted from [97].

Unlike IAPWS–IF97, which has five regions and discontinuities between them, the IAPWS–95 formulation is capable of computing thermodynamic properties with the sole use of one region — the Helmholtz free energy equation. Figure 4.12 shows the five regions in which IAPWS–IF97 divides the thermodynamic specter. Notice that the lower the temperature, the higher is the pressure range, and vice versa. Regions 1, 2, 3 and 5 are defined by a unique fundamental equation — the specific Gibbs free energy g or the specific Helmholtz free energy a — in terms of two of the following variables: pressure (P), temperature (T) and density (ρ). Region 4 is defined by either a saturation-pressure or a saturation-temperature equation, while the boundary between regions 2 and 3 is defined with an equation known as B23.

Formerly discussed, the main purpose of the IAPWS–IF97standard is the calculation of thermodynamic properties at high speeds at the cost of simplicity in some of the models. This led to a new set of equations for regions 1, 2 and 4, known as *backwards equations* – $T(\cdot)$ for regions 1 and 2, $T_s(\cdot)$ for region 4 – in terms of the following variables: pressure, enthalpy (h) and entropy (s). According to the IAPWS–IF97 standard, calculations are on average five times faster than the ones using the *old* IAPWS–95 standard.

After the theoretical conditions of the FEBC discussed in Subsection 3.2.4 and observing Figure 4.12, one can notice that the thermodynamic properties of interest lie within regions 1 to 4. This is specially relevant for the algorithm used in the process of finding the thermodynamic properties of states 7 and 8 in the throttling process.

4.5 Dimensionless Gibbs free energy equation for Region 1

In Section 3.1.5, a preliminary discussion of the dimensionless Gibbs free energy was conducted. It can be rewritten numerically in terms of two dimensionless terms known as *reduced pressure* and *inverse reduced temperature*, as follows [97]:

$$\frac{g(P,T)}{RT} = \gamma(\pi,\tau) = \sum_{i=1}^{34} n_i (7.1-\pi)^{I_i} (\tau - 1.222)^{J_i} \tag{4.13}$$

Where:

g Specific free Gibbs energy

P Pressure

R Specific gas constant of water, defined in Equation (3.32)

T Temperature

$\gamma(\pi,\tau)$ Dimensionless Gibbs free energy

π Reduced pressure

τ Inverse reduced temperature

Reduced pressure and inverse reduced temperature are defined by the equations shown below. Table 4.11 shows the values for the reducing quantities used in Equations (4.14) and (4.15). Finally, Table B.1, found in Appendix B, displays the values of coefficients n_i and exponents I_i and J_i.

$$\pi = \frac{P}{P^*} \tag{4.14}$$

$$\tau = \frac{T^*}{T} \tag{4.15}$$

Table 4.11: Reducing quantities for Equation (4.13). Adapted from [97].

Reducing quantity	Value
P^*	16.53 MPa
T^*	1386 K

4.5.1 Enthalpy

As already discussed in Section 3.1.4, every thermodynamic property can be obtained based on the specific Gibbs free energy (dimensionless or not) as a function of pressure and temperature. To find the specific enthalpy, recall its definition and dimensionless form, shown below:

$$h = g(P,T) - T\left(\frac{\partial g}{\partial T}\right)_P \tag{3.31 revisited}$$

$$\frac{h}{RT} = -T\left(\frac{\partial\left(\frac{G}{RT}\right)}{\partial T}\right)_P \tag{3.36b revisited}$$

Which in terms of Equation (4.13) and its derivative can be written as follows [97]:

$$\frac{h(\pi,\tau)}{RT} = \tau\gamma_\tau \tag{4.16}$$

Where:

$$\gamma_\tau = \left(\frac{\partial\gamma}{\partial\tau}\right)_\pi = \sum_{i=1}^{34} n_i(7.1-\pi)^{I_i}\, J_i(\tau-1.222)^{J_i-1} \tag{4.17}$$

4.5.2 Entropy

With regard to the expression of entropy founded on the dimensionless specific Gibbs free energy for Region 1, let us evoke its definition, revisited below:

$$s = -\left(\frac{\partial g}{\partial T}\right)_P \tag{3.30 revisited}$$

Which, in terms of Equation (4.13) can be written in the following manner [97]:

$$\frac{s(\pi,\tau)}{R} = \tau\gamma_\tau - \gamma \tag{4.18}$$

4.5.3 Validation

The IAPWS–IF97 suggests to verify the performance of the generated code using specific input values provided by the standard itself and comparing the calculated results with the reference ones. The advice also includes the use of 8-byte real values, equivalent to a 64-bit floating point value. Given the characteristics of the evaluation board previously discussed in Subsection 4.1.4, a native 32-bit Floating Point Unit (FPU) was used. Tables 4.12 and 4.13 reveal the comparison between the reference (h_{IF97}, s_{IF97}) and calculated values (h_{cal}, s_{cal}) using the EK-TM4C1294XL board.

Table 4.12: Specific enthalpy for suggested values of T and P calculated from Equation (4.16)

	$h_{IF97}\left[\frac{kJ}{kg}\right]$	$h_{cal}\left[\frac{kJ}{kg}\right]$	Absolute Error
$T = 300$ K $P = 3$ MPa	115.331273	115.3312	0.000073
$T = 300$ K $P = 80$ MPa	184.142828	184.142761	0.000067
$T = 500$ K $P = 3$ MPa	975.542239	975.542236	0.000003

Table 4.13: Specific entropy for suggested values of T and P calculated from Equation (4.18)

	$s_{IF97}\left[\frac{kJ}{kg\,K}\right]$	$s_{cal}\left[\frac{kJ}{kg\,K}\right]$	Absolute Error
$T = 300$ K $P = 3$ MPa	0.392294792	0.392294645	0.000000147
$T = 300$ K $P = 80$ MPa	0.368563852	0.368563712	0.00000014
$T = 500$ K $P = 3$ MPa	2.58041912	2.58041906	0.00000006

4.5.4 Range of validity

Equation (4.13) is valid for the range of pressure and temperature shown in Table 4.14, where:

$P_{sat}(T)$ Saturation pressure as a function of temperature, defined in Equation (4.29). Region 4, Subsection 4.7.1.

Table 4.14: Range of validity for dimensionless Gibbs free energy in Region 1. Adapted from [97].

Property	Range
P	$[P_{sat}(T), 100]\, MPa$
T	$[273.15, 623.15]\, K$

4.6 Dimensionless Gibbs free energy equation for Region 2

Although the basic equation defining Region 2 is also based on a dimensionless form of the specific Gibbs free energy, is a modified version of Equation (4.13) in terms of the ideal-gas part and the residual part, as discussed in Subsection 3.1.6, shown below [97]:

$$\frac{g(P,T)}{RT} = \gamma(\pi,\tau) = \gamma^{o}(\pi,\tau) + \gamma^{r}(\pi,\tau) \tag{4.19}$$

Where:

γ^{o} Ideal-gas part of specific Gibbs free energy

γ^{r} Residual part of specific Gibbs free energy

Defined by the following equations:

$$\gamma^{o} = \ln\pi + \sum_{i=1}^{9} n_i^{o}\tau^{J_i^{o}} \tag{4.20a}$$

$$\gamma^{r} = \sum_{i=1}^{43} n_i \pi^{I_i}(\tau - 0.5)^{J_i} \tag{4.20b}$$

Tables 4.15 show the value of reducing quantities. Values of coefficients n_i^{o} and exponents J^{o} can be found in Table B.2. Finally, Table B.3 comprises coefficients n_i and exponents I_i and J_i.

4.6.1 Enthalpy

As with the discussion conducted in Section 4.5 regarding Equation 4.13, thermodynamic properties of Region 2 can be gathered after the derivatives of Equation (4.19). Recalling Equation (3.31), it can be rewritten in terms of the dimensionless Gibbs free energy, as follows:

$$h = g(P,T) - T\left(\frac{\partial g}{\partial T}\right)_P \tag{3.31 revisited}$$

$$\frac{h(\pi,\tau)}{RT} = \tau\left(\gamma_{\tau}^{o} + \gamma_{\tau}^{r}\right) \tag{4.21}$$

Table 4.15: Reducing quantities for Equation (4.19). Adapted from [97].

Reducing quantity	Value
P^{*}	1 MPa
T^{*}	540 K

Where:

$$\gamma_\tau^{\mathrm{o}} = \left(\frac{\partial \gamma^{\mathrm{o}}}{\partial \tau}\right)_\pi \tag{4.22a}$$

$$\gamma_\tau^{r} = \left(\frac{\partial \gamma^{r}}{\partial \tau}\right)_\pi \tag{4.22b}$$

Defined by the following equations:

$$\gamma_\tau^{\mathrm{o}} = \sum_{i=1}^{9} n_i^o J_i^o \tau^{J_i^o - 1} \tag{4.23a}$$

$$\gamma_\tau^{\mathrm{r}} = \sum_{i=1}^{43} n_i \pi^{I_i} J_i (\tau - 0.5)^{J_i - 1} \tag{4.23b}$$

4.6.2 Entropy

Similarly to the discussion of Entropy in terms of the dimensionless specific Gibbs free energy for Region 1 in Subsection 4.5.2, let us revisit the definition of entropy:

$$s = -\left(\frac{\partial g}{\partial T}\right)_P \tag{3.30 revisited}$$

Which, in terms of the dimensionless Gibbs free energy for Region 2, can be rewritten in terms of ideal and residual parts, shown below [97]:

$$\frac{s(\pi, \tau)}{R} = \tau(\gamma_\tau^{\mathrm{o}} + \gamma_\tau^{\mathrm{r}}) - (\gamma^{\mathrm{o}} + \gamma^{r}) \tag{4.24}$$

4.6.3 Validation

As mentioned in Subsection 4.5.3, validation of computed results using reference values is part of the IAPWS–IF97. Comparison between reference and calculated values for Region 2 are shown in Tables 4.16 and 4.17.

Table 4.16: Specific enthalpy for suggested values of T and P calculated from Equation (4.21)

	$h_{IF97}\left[\frac{kJ}{kg}\right]$	$h_{cal}\left[\frac{kJ}{kg}\right]$	Absolute Error
$T = 300$ K $P = 0.0035$ MPa	2549.91145	2549.91162	0.00017
$T = 700$ K $P = 0.0035$ MPa	3335.68375	3335.68359	0.00016
$T = 700$ K $P = 30$ MPa	2631.49474	2631.49414	0.0006

Table 4.17: Specific entropy for suggested values of T and P calculated from Equation (4.24)

	$s_{IF97}\left[\frac{kJ}{kg\,K}\right]$	$s_{cal}\left[\frac{kJ}{kg\,K}\right]$	Absolute Error
$T = 300$ K $P = 3$ MPa	8.52238967	8.52239037	0.0000007
$T = 300$ K $P = 80$ MPa	10.1749996	10.1750002	0.0000006
$T = 500$ K $P = 3$ MPa	5.17540298	5.17540264	0.00000034

4.6.4 Range of validity

Table 4.18 shows the valid range of pressure and temperature of Equation (4.19), where

$P_{sat}(T)$ Saturation pressure as a function of temperature, defined in Equation (4.29). Region 4, Subsection 4.7.1.

$\pi(\theta)$ Equation B23, auxiliary equation for the boundary between Regions 2 and 3.

Table 4.18: Range of validity for dimensionless Gibbs free energy in Region 1. Adapted from [97].

Range	Pressure [MPa]	Temperature [K]
1	$(0, P_{sat}(T)]$	$[273.15, 623.15]$
2	$(0, \pi(\tau)]$	$(623.15, 863.15]$
3	$(0, 100]$	$(863.15, 1073.15]$

Table 4.19: Coefficients for Equation B23 (Equation (4.25). Adapted from [97].

Coefficient	Value
n_1	$3.4805185628969\,x10^{2}$
n_2	1.1671859879975
n_3	$1.0192970039326',x10^{-3}$

Table 4.20: Reducing quantities for Equation B23 (Equation (4.25)). Adapted from [97].

Reducing quantity	Value
P^*	1 MPa
T^*	1 K

Equation B23 is defined below:

$$\pi(\theta) = n_1 + n_2\theta + n_3\theta^2 \tag{4.25}$$

Where θ, the reduced temperature, is defined by the following equation:

$$\theta = \frac{1}{\tau} \tag{4.26}$$

Finally, Tables 4.19 and 4.20 show the values of coefficients n_1 to n_3 and the reducing quantities for Equation (4.25).

4.7 Saturation-pressure and Saturation-temperature equations for Region 4

As declared in Section 4.4, regions 1 to 4 are of special interest because of the thermodynamic range they cover. Region 4 is a prominent one, describing the saturation line, described by an implicit quadratic equation in terms of the saturation pressure (P_{sat}) and saturation temperature (T_{sat}) [97], as described by the following equation:

$$\beta^2\vartheta^2 + n_1\beta^2\vartheta + n_2\beta^2 + n_3\beta\vartheta^2 + n_4\beta\vartheta + n_5\beta + n_6\vartheta^2 + n_7\vartheta + n_8 = 0 \tag{4.27}$$

Where:

β Transformed pressure

ϑ Transformed temperature

Table 4.21: Values of reducing quantities (Equations 4.28a and 4.28b). Adapted from [97].

Reducing quantity	Value
P^*	1 MPa
T^*	1 K

Defined by the following equations:

$$\beta = \left(\frac{P_{sat}}{P^*}\right)^{\frac{1}{4}} \tag{4.28a}$$

$$\vartheta = \frac{T_{sat}}{T^*} + \frac{n_9}{\left(\frac{T_{sat}}{T^*}\right) - n_{10}} \tag{4.28b}$$

Table B.4 describe the values used for coefficients n_1 to n_{10}. On the other hand, Table 4.21 displays the reducing quantities P^* and T^*, respectively.

Equation 4.27 can be solved with regard to P_{sat} or T_{sat}. These solutions are described in the following subsections.

4.7.1 Saturation–pressure equation

The solution of Equation 4.27 for saturation pressure is the following:

$$\frac{P_{sat}}{P^*} = \left[\frac{2C}{-B + \sqrt{B^2 - 4AC}}\right]^4 \tag{4.29}$$

Where:

$$A = \vartheta^2 + n_1\vartheta + n_2 \tag{4.30a}$$

$$B = n_3\vartheta^2 + n4\vartheta + n_5 \tag{4.30b}$$

$$C = n_6\vartheta^2 + n_7\vartheta + n_8 \tag{4.30c}$$

Table 4.22: Saturation pressures for selected values of T

T [K]	P_{IF97} [MPa]	P_{cal} [MPa]	Absolute Error
300	0.00353658941	0.00353658712	0.00000000229
500	2.63889776	2.63889861	0.00000085
600	12.3443146	12.3443089	0.0000057

Table 4.23: Saturation temperatures for selected values of P

P [MPa]	T_{IF97} [K]	T_{cal} [K]	Absolute Error
0.1	372.755919	372.7559181	0.000001
1	453.035632	453.035675	0.000018
10	584.149488	584.149719	0.000048

4.7.2 Saturation–temperature equation

The solution of Equation 4.27 for saturation pressure is shown below:

$$\frac{T_{sat}}{T^*} = \frac{n_{10} + D - \sqrt{(n_{10})^2 - 4(n_9 + n_{10}D)}}{2} \tag{4.31}$$

Where:

$$D = \frac{2G}{F - \sqrt{F^2 - 4EG}} \tag{4.32a}$$

$$E = \beta^2 + n_3\beta + n_6 \tag{4.32b}$$

$$F = n_1\beta^2 + n_4\beta + n_7 \tag{4.32c}$$

$$G = n_2\beta^2 + n_5\beta + n_8 \tag{4.32d}$$

4.7.3 Validation

Following the validation of enthalpy and entropy for Regions 1 and 2, formerly examined in Subsections 4.5.3 and 4.6.3, reference values (P_{IF97}, T_{IF97}) are compared with the calculated ones (P_{cal}, T_{cal}) for Region 4, shown in Tables 4.22 and 4.23.

Table 4.24: Range of validity for dimensionless Gibbs free energy in Region 2. Adapted from [97].

Equation	Range
Saturation–pressure	$[273.15, 647.096]$ K
Saturation–temperature	$[611.213, 22.064]$ MPa

4.7.4 Range of validity

Equations (4.29) and (4.31) are valid for the range of pressure and temperature shown in Table 4.24.

4.8 Throttling process

Figure 4.13 illustrates the orifice-plate/throttle-valve before the separator, where the thermodynamic properties of interest — both upstream and downstream — are shown. Table 4.25 describes each property, where an asterisk (*) indicates the properties directly measured.

After the measured properties, it is possible to determine the missing ones following the implementation of the IAPWS–IF97, which will be described in the following subsections. The first two subsections involve the upstream stage, while the last two analyze the downstream stage. An auxiliary flowchart of the algorithm, demonstrated in Figure 4.16, is shown in Subsection 4.8.5.

4.8.1 Finding saturation temperature given upstream pressure

Once the initialization of variables is finished and the measured properties previously described in Section 4.8 are acquired, the first step is finding out if the upstream state is saturated liquid or not. To attain this result, saturation temperature at upstream pressure ($T_{sat}@P_u$), is found using Equation (4.31), from Region 4. Then, three alternatives will arise:

1. $T_u < T_{sat}@P_u$, then upstream state is compressed liquid.
2. $T_u = T_{sat}@P_u$, the state is saturated liquid.
3. $T_u > T_{sat}@P_u$, then the state is overheated steam

The first two cases discussed in Subsection can be joint ($T_u \leq T_{sat}@P_u$) because overheated steam is the only state wanted to be discarded.

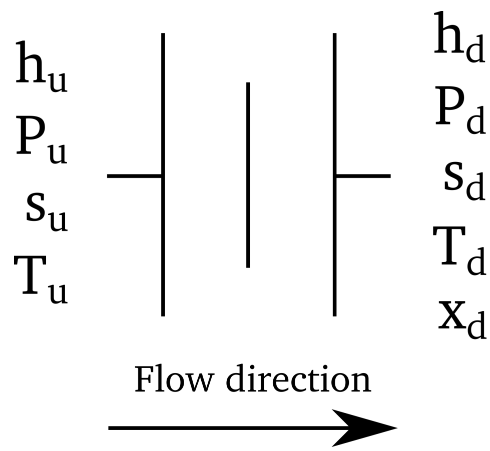

Figure 4.13: Thermodynamic properties of interest in orifice plate

Table 4.25: Thermodynamic properties of interest in orifice plate

	Upstream properties		Downstream properties
h_u	Specific upstream enthalpy	h_d	Specific downstream enthalpy
s_u	Specific upstream entropy	s_d	Specific downstream entropy
P_u	Upstream pressure*	P_d	Downstream pressure*
T_u	Upstream temperature*	T_d	Downstream temperature*
		x_d	Downstream vapor fraction

4.8.2 Finding specific enthalpy and entropy at upstream pressure and temperature

Upstream enthalpy (h_u) and entropy (s_u) can be computed using Equations (4.16) and (4.18) respectively, both part of Region 1. As per the previous review in Subsection 3.2.3, throttling process is modeled as an isenthalpic process, therefore, downstream and upstream enthalpy are the same:

$$h_d = h_u = h \tag{4.33}$$

4.8.3 Finding downstream steam fraction

To find downstream steam fraction, preparatory properties must be attained, including the following:

$T_{sat}@P_d$ Saturation temperature at downstream pressure

$h_f@P_u, T_{sat}$ Specific enthalpy of saturated liquid at upstream pressure and saturation temperature

$h_g@P_d, T_{sat}$ Specific enthalpy of saturated vapor at upstream pressure and saturation temperature

Table 4.26: Auxiliary properties for finding downstream steam fraction

Property	Equation	Region
$T_{sat}@P_d$	(4.31)	4
$h_f@P_u, T_{sat}$	(4.16)	1
$h_g@P_d, T_{sat}$	(4.21)	2

Table 4.26 displays the equations used for each of the aforementioned properties, including the regions in which they are located. Notice that $T_{sat}@P_d$ is necessary to compute the calculation of $h_f@P_u, T_{sat}$ and $h_g@P_d, T_{sat}$. Later, calculation of downstream steam fraction x_d is directly calculated using the following expression:

$$x_d = \left[\frac{h_u - hf}{h_g - h_f}\right] \cdot 100 \tag{4.34}$$

4.8.4 Finding downstream entropy

As the final step, the following two auxiliary properties are calculated:

$h_f@P_d, T_{sat}$ Specific entropy of saturated liquid at upstream pressure and saturation temperature

$h_g@P_u, T_{sat}$ Specific entropy of saturated vapor at upstream pressure and saturation temperature

Equation (4.18), part of Region 1, is used to determine $h_f@P_d, T_{sat}$; on the other hand, $h_g@P_u, T_{sat}$ is found using Equation (4.24), part of Region 2. Finally, downstream entropy is found using the following expression:

$$s_d = s_f + \left(\frac{x}{100}\right)(s_g - s_f) \tag{4.35}$$

4.8.5 Software structure and flow

Software developed for the Tiva C Series evaluation board can be divided in 4five modules, briefly described below:

1. Initialization of variables and software modules
2. Monitoring of pressure and temperature
3. FDI Interrupt Service Rutine (ISR)
4. Computing of thermodynamic properties through IAPWS–IF97 functions
5. Graphical User Interface (GUI)

Figure 4.14 displays a data flow graph of the overall instrumentation system in its most basic nature (i.e. omitting redundancy) including Application-specific Integrated Circuitry (ASIC) part of the pressure sensors. Additionally, Figure 4.15 displays a basic flowchart of the main program along with the FDI ISR, activating when there is a change of state in the PG outputs, from high to low.

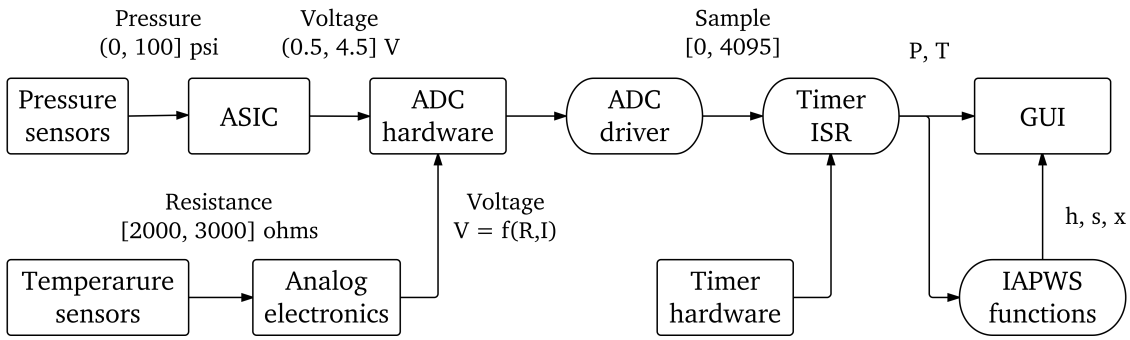

Figure 4.14: Data flow graph, showing hardware (rectangles) and software (ovals)

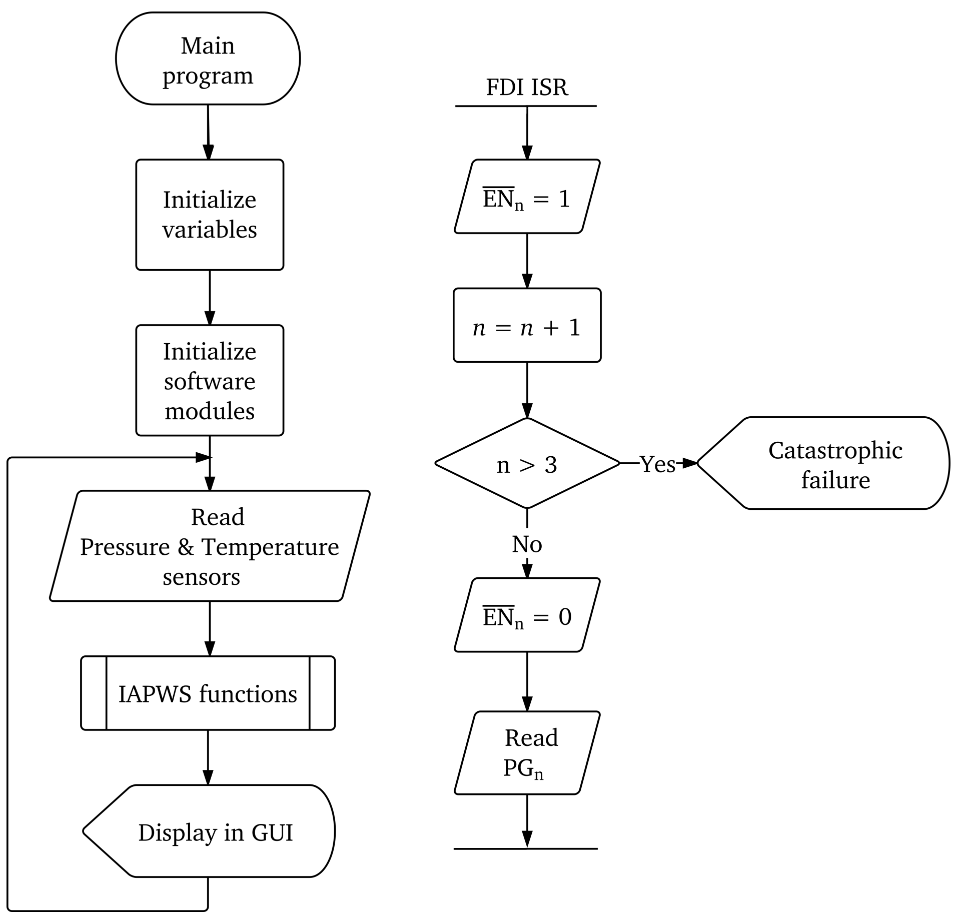

Figure 4.15: Data flow of main program and ISR

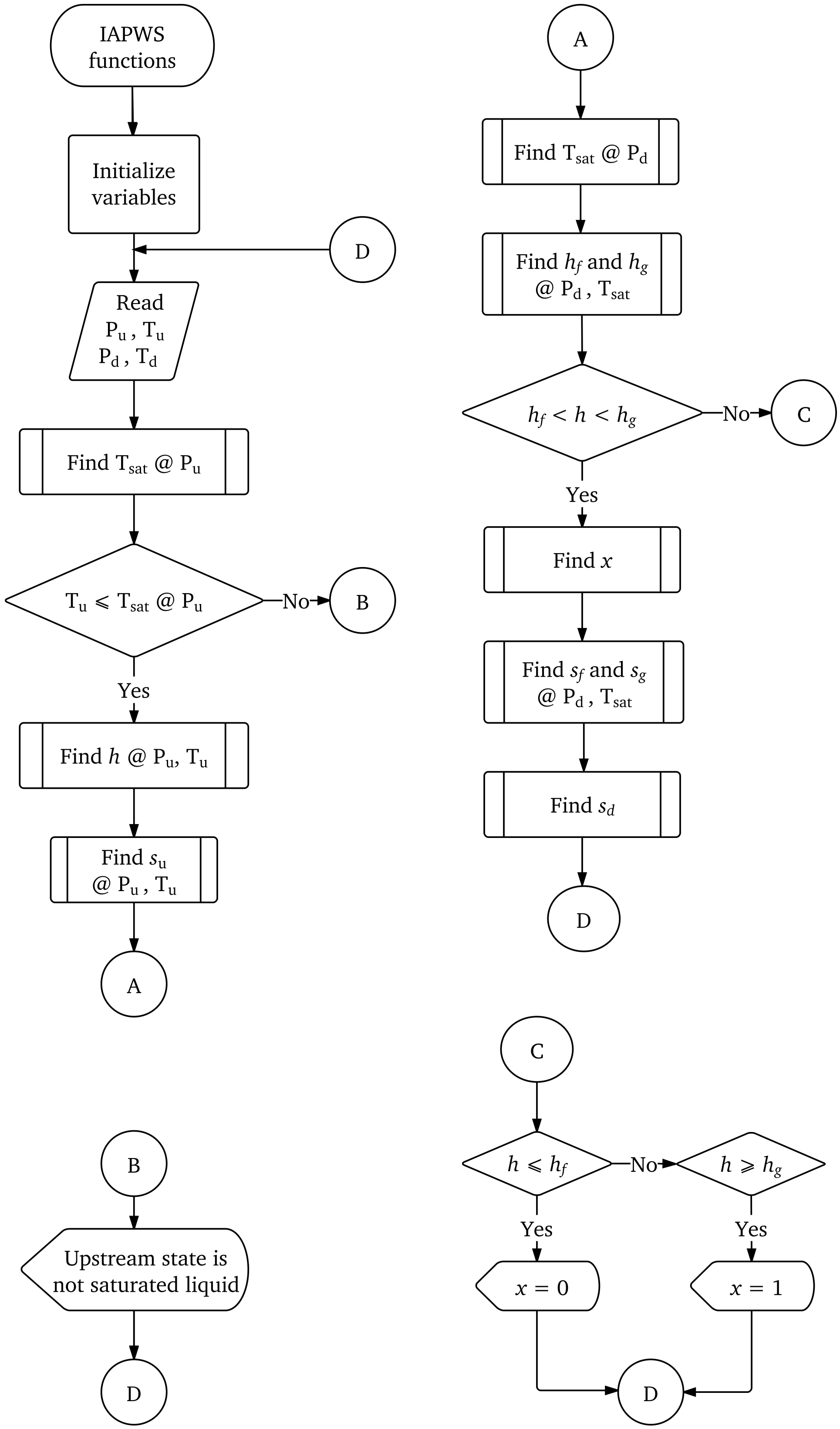

Figure 4.16: Flow chart of computation of thermodynamic properties

4.9 Graphical User Interface

According to the previous review found in Subsection 4.1.5 concerning the software platform used, Code Composer Studio® was used given its superior features, free availability and guaranteed compatibility with the Tiva C Series platform. Besides the preceding arguments, the utilized version of the IDE was complemented with GUI Composer, a powerful open–source editor for creating GUIs, based on a modification of the Maqetta application, run by International Business Machines (IBM).

The following subsections examine the different sections of the developed GUI for the experimental setup. Even when processing sample time is shorter, to be able to visualize data in a comfortable manner, refresh rate of every GUI is fixed to 1 s. Table 4.27 displays the localization of the sensors used in the experimental steam generation setup; in addition to the known states, two reference sensors measuring ambient temperature and atmospheric pressure were used.

4.9.1 ADC values

Early phases of the development required an agile interface to test correct wiring of sensors and acquire preliminary readouts. Figures 4.17 and 4.18 display ADC readouts for pressure and temperature sensors, respectively. One important feature of the shown plots — and the next ones in the following subsections — is that the generated data can be exported in CSV format, ready to be used in MATLAB® or Microsoft® Excel, for latter processing.

Table 4.27: Localization of sensors in steam generation experimental setup

Device	State	Pressure	Temperature
Heat exchanger	B	✓	✓
	C		✓
Radiator	U		✓
	V		✓
Orifice plate	7	✓	✓
	8	✓	✓
Separator	5	✓	✓
Reference		✓	✓

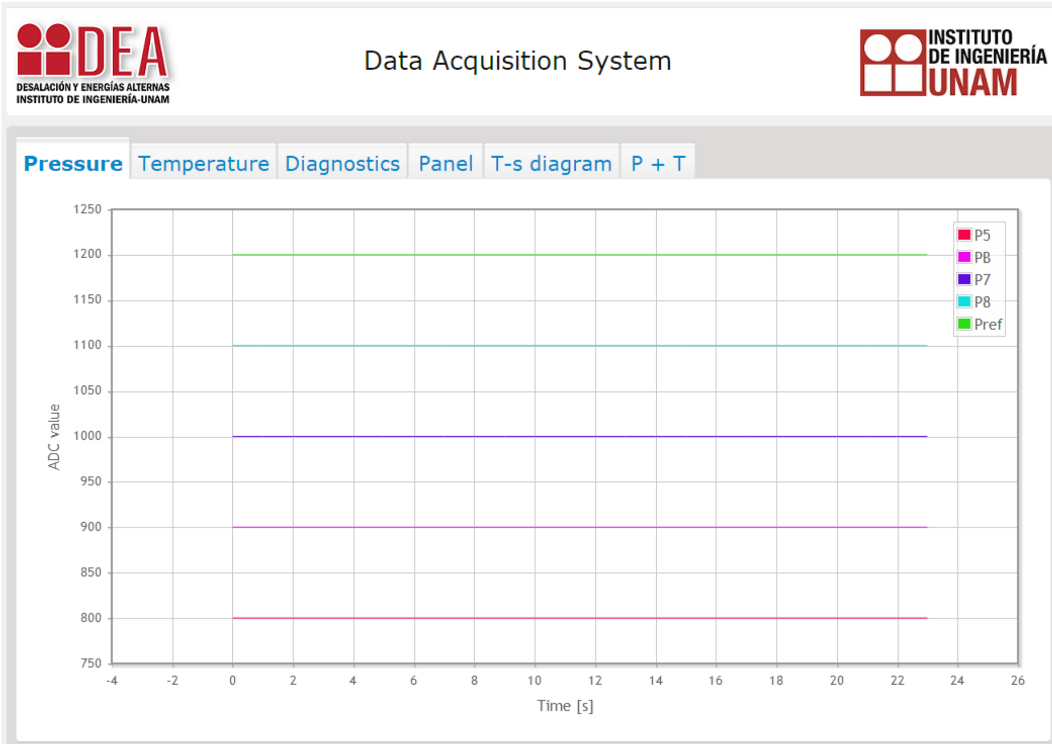

Figure 4.17: ADC values of pressure sensors (simulated values)

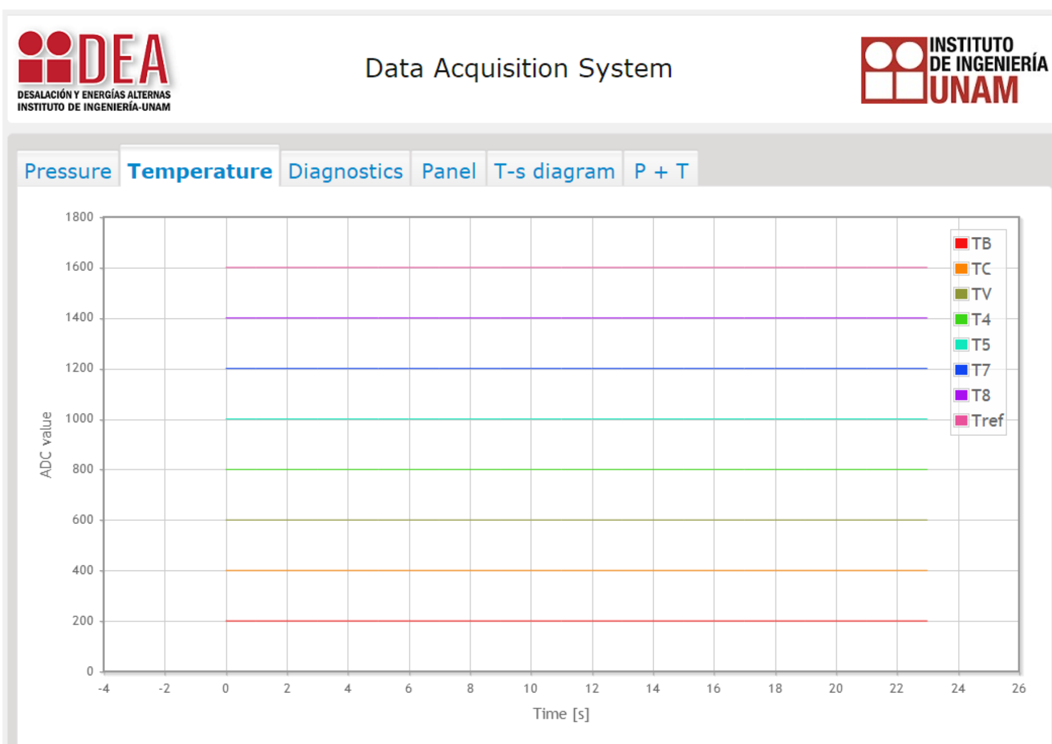

Figure 4.18: ADC values of temperature sensors (simulated values)

4.9.2 Diagnostics

Subsection 4.1.3 dealt with the operation of the fault–tolerant PSMs, generally describing its additional capabilities of fault detection and isolation. Figure 4.20 shows the diagnostics panel, displaying the state of the PG and $\overline{EN}$ signals, as well as an overall online indicator, specifying the availability of the system. In case of a catastrophic failure or faults in the complete set of LDOs contained in PSM, this indicator would reveal them.

4.9.3 Main panel

The main panel shown in Figure 4.19 contains two inner tabs in which individual gauges for each sensor are displayed. In the event of a variable reaching a previously set threshold, a red indicator would be turned on, alerting the operator.

4.9.4 T – s diagram

One of the essential features of this tab, shown in Figure 4.22, is a T – s diagram where upstream and downstream states of the orifice plate are shown. Visualization of these states is meant to be used just as a guide, since the exact downstream steam fraction x_d and specific enthalpy h_d are also displayed.

4.9.5 Simultaneous data logging

The last tab of the GUI displays two plots where simultaneous plots for pressure and temperature are displayed. As already explained in Section 4.9, displayed data can be exported immediately, providing the opportunity to export data for both variables simultaneously.

4.10 Performance evaluation

Subsection 3.5.6, part of the theoretical framework introduced in Chapter 3 and Subsection 4.1.3, part of this Chapter, stressed the multiple advantages and features of the cold standby redundancy for PSMs and their deployment. This section includes the evaluation of the commutation process after the introduction of a fault in one of the 3.3 V PSMs.

On the other hand, one way to assess the performance of the generated code is code profiling, a dynamic tool commonly used by developers to identify specific characteristics of the code, such as memory usage, time of execution, frequency and duration of function calls [151]. The availability of this data may be crucial for future improvements or optimization of execution.

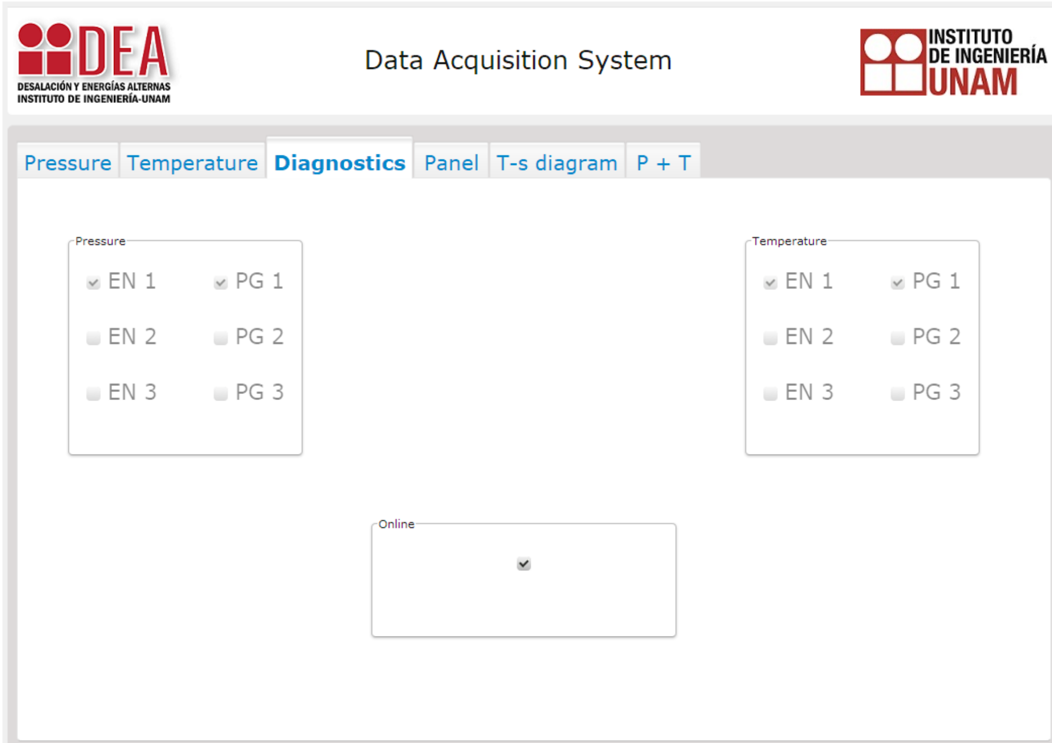

Figure 4.19: Diagnostics panel for standby power modules

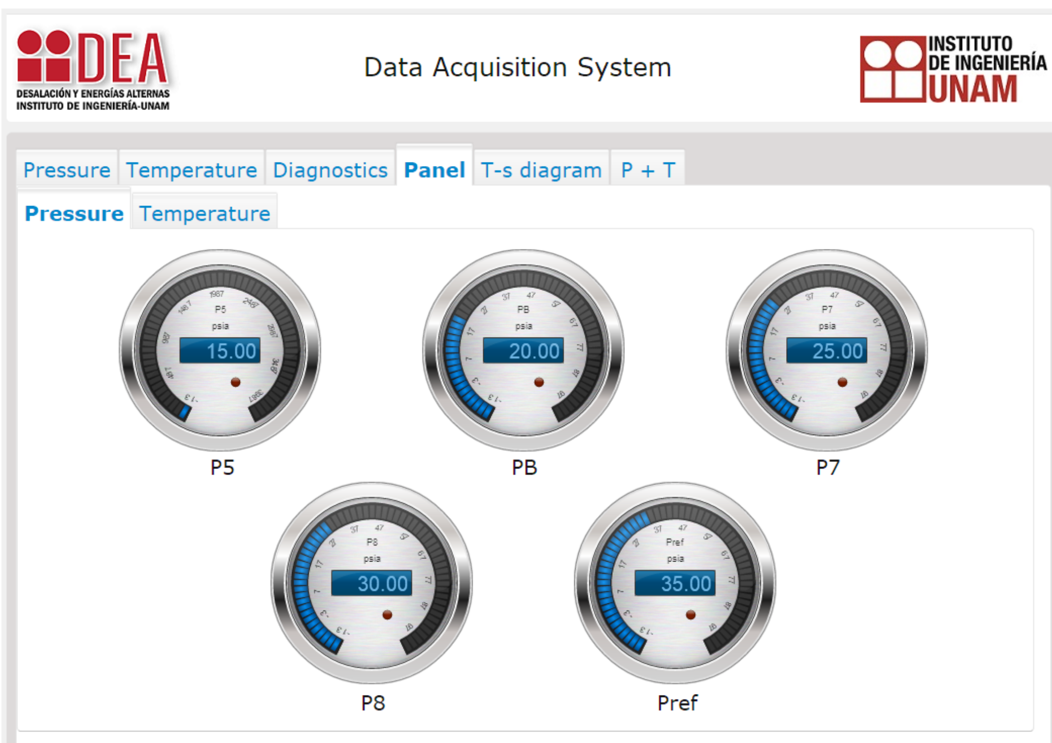

Figure 4.20: Panel for pressure readouts (simulated values)

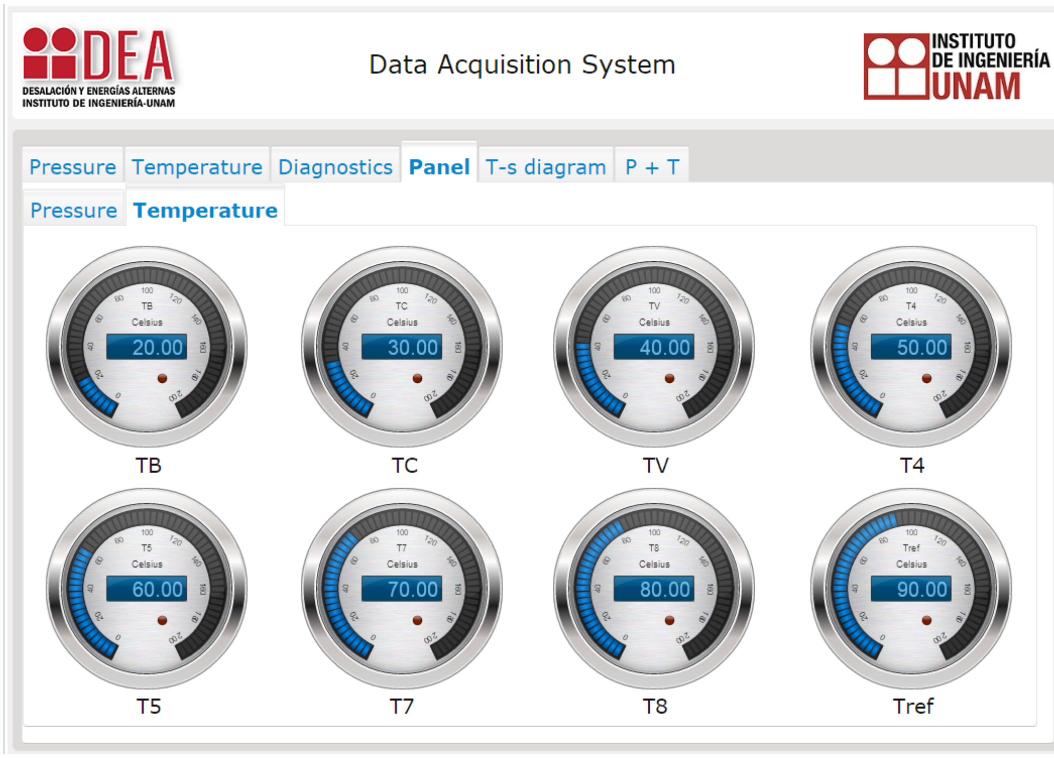

Figure 4.21: Panel for temperature readouts (simulated values)

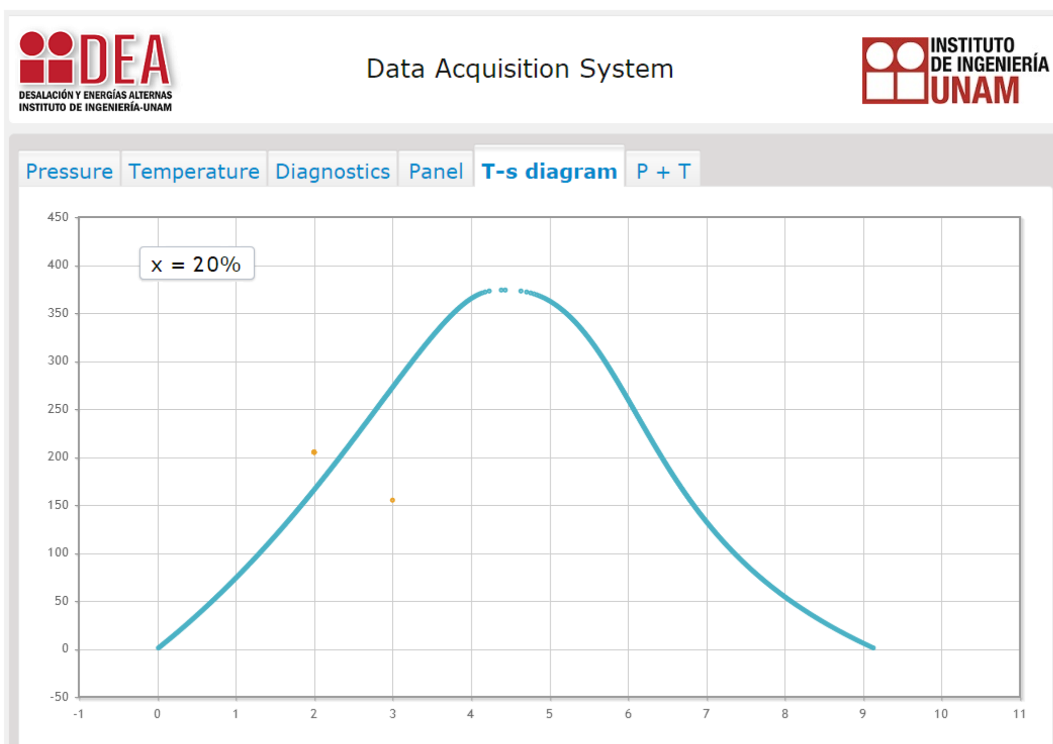

Figure 4.22: Online T-s diagram (simulated values)

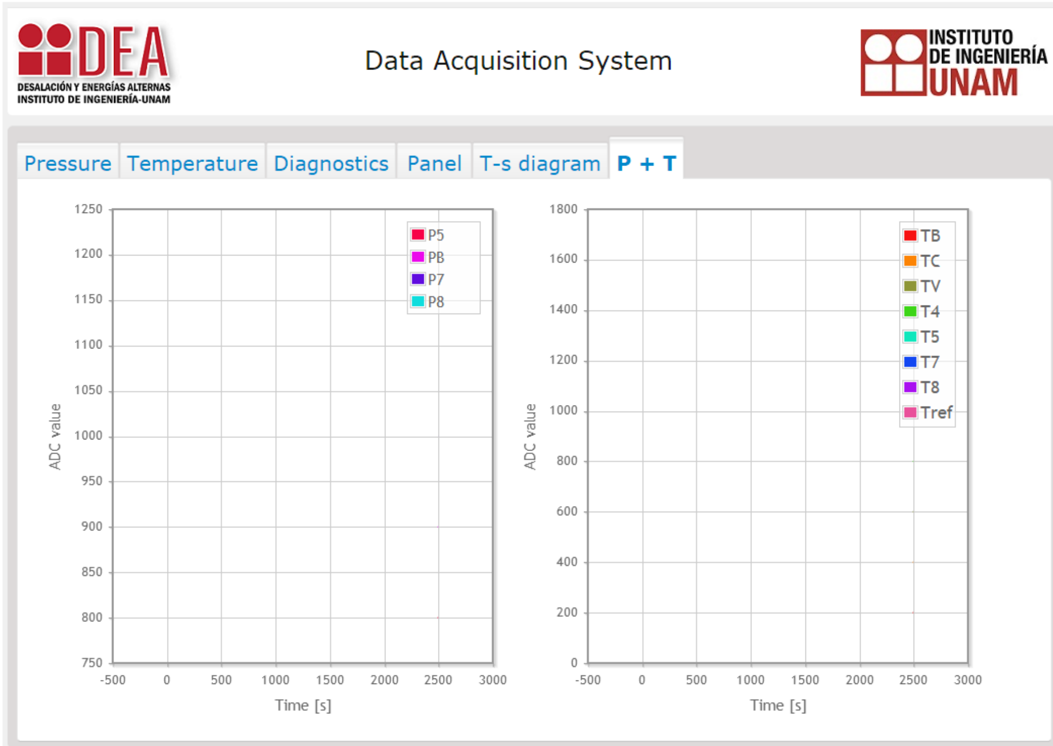

Figure 4.23: Pressure and temperature readouts (simulated values)

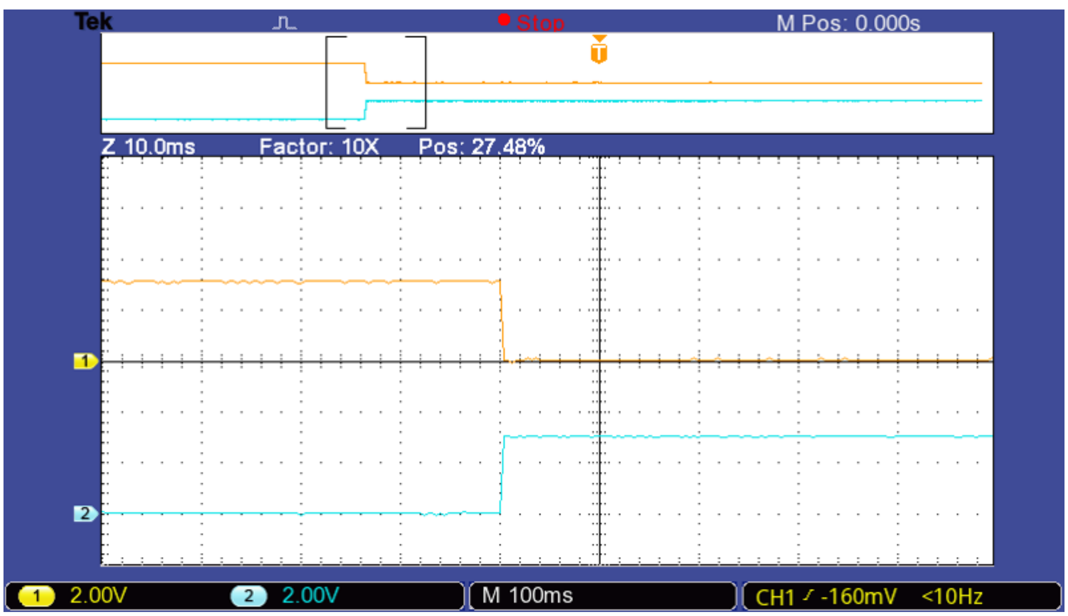

Figure 4.24: Commutation of cold standby redundant power supplies

Table 4.28: Execution times for embedded operations at 120 MHz

Operation	Number of cycles	Time of execution
Overall initialization	1,754,835	14.6 ms
FPU initialization	36	0.3 μs
Data logging	99,162	0.82 ms
IAPWS functions	3,252,806	27.1 ms

4.10.1 Cold-standby redundant module commutation

The test explained in Section 4.10 is illustrated in Figure 4.24. Channel 1 displays the main LDO, while Channel 2 represents one of the spare cold standby units. It can be noticed that the time scale is set to 100 ms per division, with an additional zoom of 10x, resulting in a scale of 10 ms per division. Commutation process involving FDI and reconfiguration takes less than 1 ms.

4.10.2 Code profiling

Execution time becomes crucial in software development when a considerable number of computations are performed in real time. Based on the capabilities of the IDE used, execution times for the most important operations were computed, shown in Table 4.28.

4.11 Conclusions

Arrangement of the actual instrumentation system was deployed taking special care of modularity and reproducibility using available commercial components, satisfying the cold standby redundancy theory. It must be noted that even when a reliability update was deliberated, it serves as an improvement of a previous analysis, and it does not represent a final or exhaustive analysis since other elements like connectors, wiring and soldering — not considered — may affect the overall reliability of each PSM.

When environmental and operational aspects are added to the discussion, offering a more realistic approach, a decrease in the overall reliability is notorious. Once the cold standby redundancy techniques are applied, the updated reliability even surpasses the original basic reliability, reaching up to 99% for a 10-year mission period. One downside of the proposed fault-tolerant arrangement is that LDOs part of each PSM rely on the same input voltage before regulation, making it a common-mode failure. In this dissertation, reliability analysis focused on the reliability of the PSM regardless of the aforementioned risk.

On the processing stage, both MAFs demonstrate a superior performance even at lower values of M, satisfactorily displaying the essential outline of the original signal. Finally, contrary to the symmetric MAFs, in one-sided MAFs the delay is drastically more evident as the value of M increases. Also, at higher values of M, the smoothing behavior is enhanced, as expected. One downside of symmetric MAFs is that, computationally, using recursion, they need two nested for-loops, slowing down the process.

Computation of thermodynamic properties using the IAPWS–IF97 standard was validated throughout the entire process using values provided by the formulation itself and the X–steam MATLAB® function.

Finally, results of code profiling show that even when the computing is not optimized, execution times are satisfactory for the requirements of the system. Furthermore, it can be eventually minimized, moving floating point operations to SRAM as these are processing/power intensive, as advised by the Code Composer Studio® Optimizer Assistant.

Results and discussion

Introduction

As previously mentioned in Subsection 1.2.2 of Chapter 1, one of the most relevant modifications of the setup, in comparison to previous incarnations of the system, is the replacement of two gas boilers connected in series for a single electric boiler. While safety and the constant purchase of gas was a crucial reason for the substitution, the electric boiler allowed members of the iiDEA® group to modify it and reach constant temperatures through a control system. Regarding instrumentation, a temperature sensor part of the aforementioned control system was set at state C, measuring the outlet temperature of the *hot side* of the heat exchanger. Finally, both sides of the heat exchanger were pumped by 120 W Grundfos® pumps. Figure 3.4 displays a revisited schematic diagram of the setup.

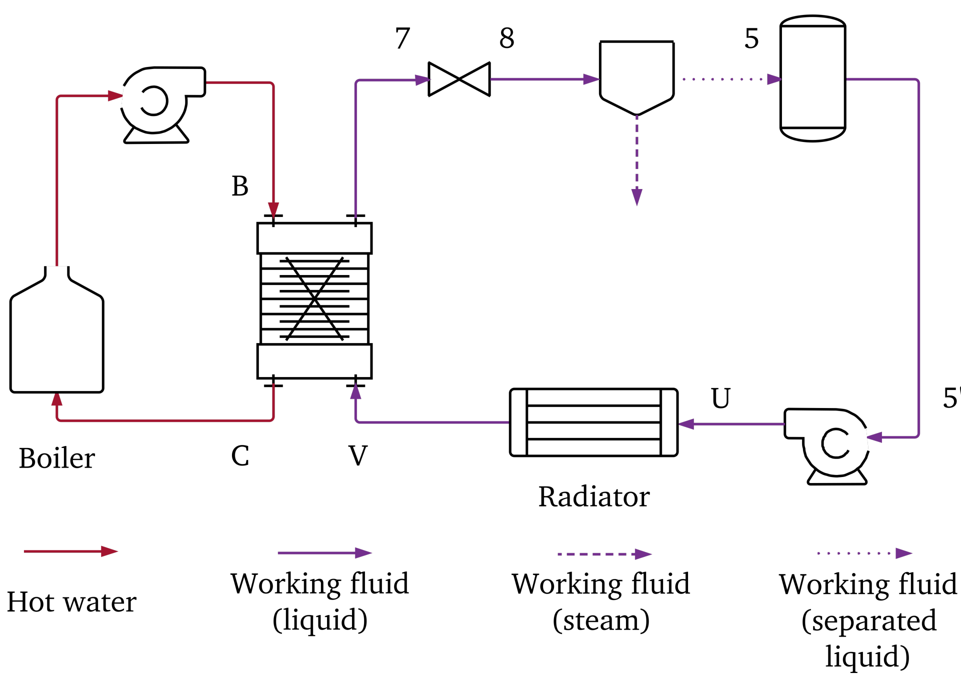

Figure 3.4: Steam generation experimental unit. Revisited from page 46.

Procedure

Once the proposed instrumentation system in this dissertation was finished and each subsystem was thoroughly tested, a series of online tests were performed on the experimental setup. Given the availability at the time of the experiment, a resistor of 2,000 W was used in the boiler, maintaining an average steady temperature of 82 °C at state C with the pump in the *hot* side running.

Once the maximum temperature was reached, the pump in the *cold* side of the heat exchanger was turned on. After completing the stabilization period, a manual throttling valve was used to change the downstream pressure drop. Figure 4.26 shows the obtained results for both upstream/downstream pressure and temperature. Additionally, basic statistical measures (mean $\bar{x}$ and standard deviation σ) are displayed in Table 4.29.

As already dissected in Subsection 4.3 of Chapter 4, MAFs were used for the purpose of smoothing signals in the time-domain. Figures 4.27 and 4.28 display the filtered pressure data for different values of M. Likewise, Figures 4.29 and 4.30 show corresponding filtered temperature data. Delay periods have been omitted to demonstrate the usefulness of the filtered data. In the same way, statistical measures were obtained for each new set of filtered data, shown in Tables 4.31 and 4.32.

Notice that even when these results display the largest pressure drop acquired during the experiment, steam generation could not be achieved. In previous dissertations [152], which conducted experiments using the previous heating setup (gas boilers in series), larger pressures and temperatures were achieved with a 2 mm-diameter orifice plate and a steady temperature of 120 °C at state B, as shown in Table 4.30.

Table 4.29: Raw data analysis

Measure	P_u kPa	P_d kPa	T_u °C	T_d °C
Mean	148.775	76.987	81.352	80.389
Standard deviation	0.4652	0.4400	0.3681	0.3378

Table 4.30: Historical experimental data from previous setup. Adapted from [152].

P_u kPa	P_d kPa	T_u °C	P_d °C
160	100	110	105

Table 4.31: Summary statistics of P_u and P_d data after MAF

Data	$M = 5$		$M = 11$		$M = 21$	
	$\bar{x}$	σ	$\bar{x}$	σ	$\bar{x}$	σ
P_u [kPa]	148.7683	0.2408	148.7644	0.1818	148.7637	0.1411
P_d [kPa]	76.9898	0.2237	76.9930	0.2209	77	0.1116

Table 4.32: Summary statistics of T_u and T_d data after MAF

Data	$M = 5$		$M = 11$		$M = 21$	
	$\bar{x}$	σ	$\bar{x}$	σ	$\bar{x}$	σ
T_u [°C]	81.354	0.2601	81.356	0.2222	81.3587	0.1966
T_d [°C]	80.3842	0.1874	80.382	0.1812	80.386	0.1234

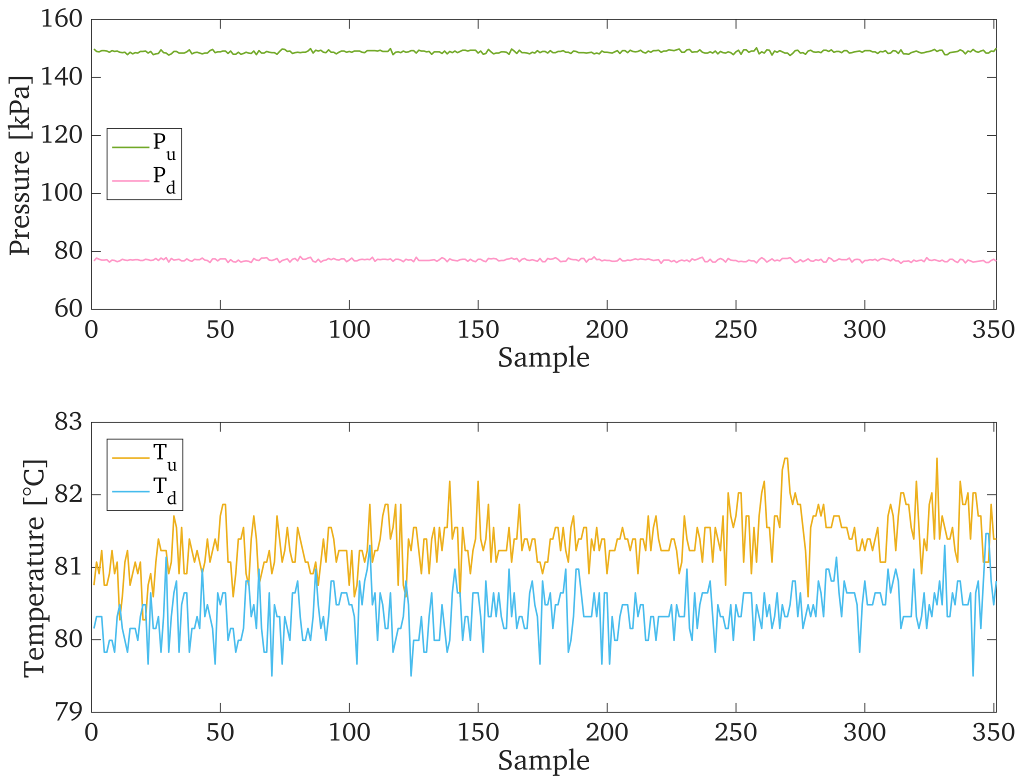

Figure 4.26: Raw data of pressure and temperature readouts

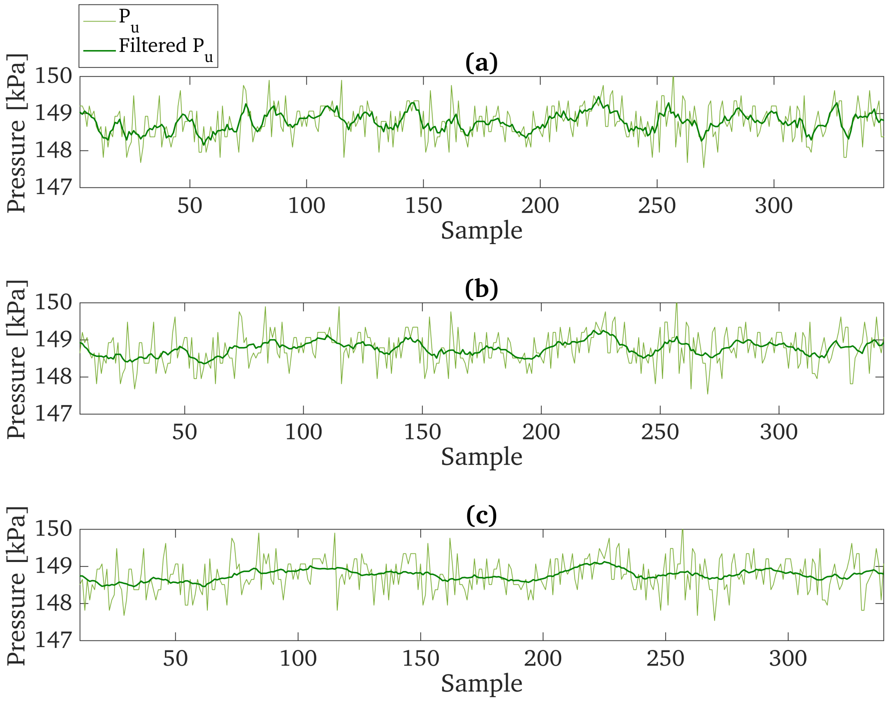

Figure 4.27: Filtered P_u data for different values of M. (a) M = 5 (b) M = 11 (c) M = 21

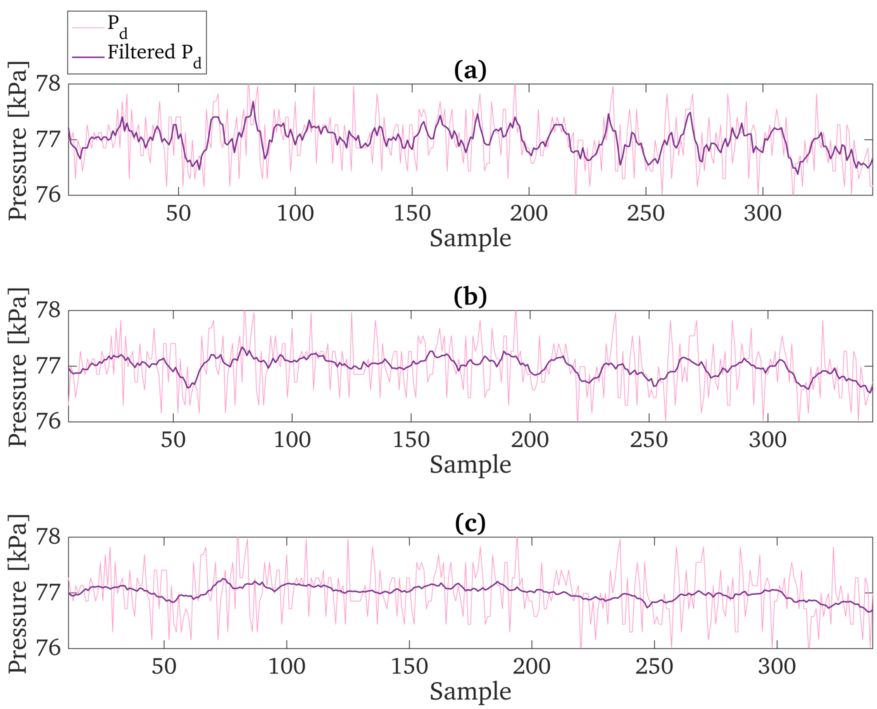

Figure 4.28: Filtered P_d data for different values of M. (a) M = 5 (b) M = 11 (c) M = 21

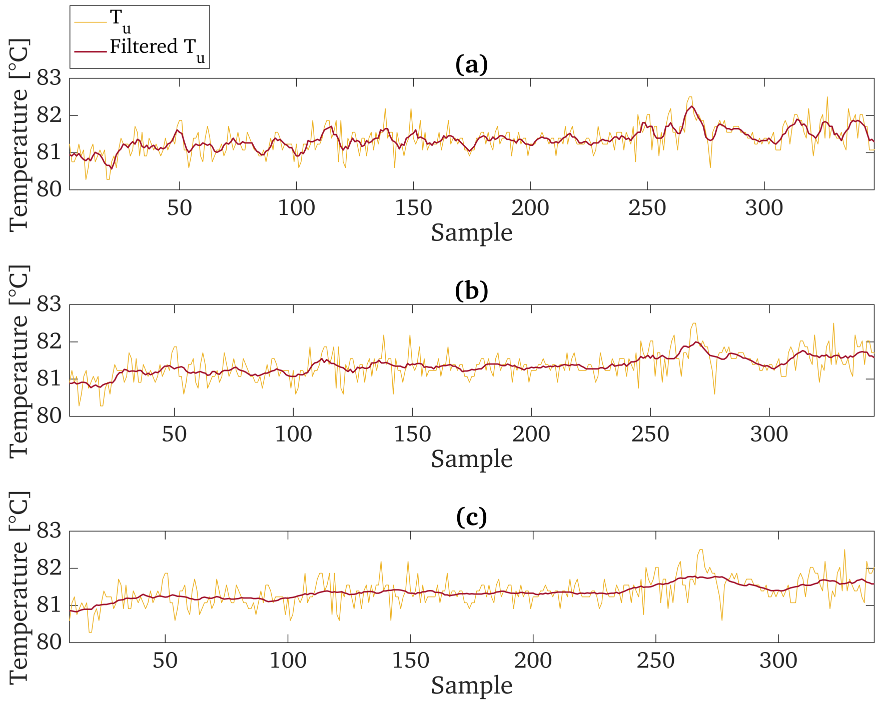

Figure 4.29: Filtered T_u data for different values of M. (a) M = 5 (b) M = 11 (c) M = 21

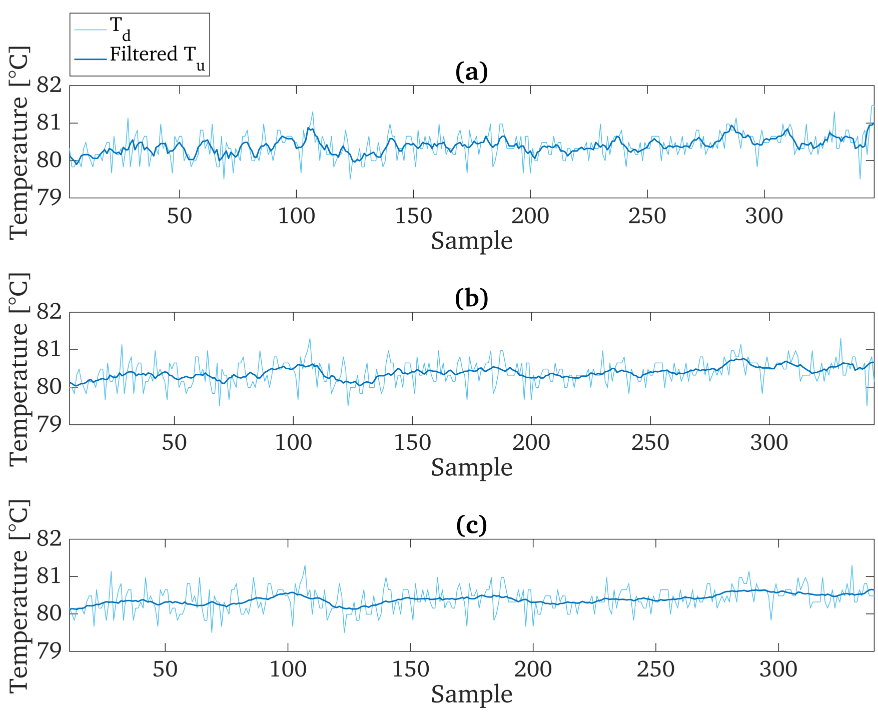

Figure 4.30: Filtered T_d data for different values of M. (a) M = 5 (b) M = 11 (c) M = 21

Table 4.33: Needed downstream pressures for different hypothetical values of steam fraction

Hypothetical steam fraction %	Downstream pressure kPa
1	40
2	31
3	24
4	19
5	14

Taking upstream pressure and temperature data with the largest value of M ($P_u = 148.7637$ kPa, $T_u = 81.3587$ °C), already presented in Tables 4.31 and 4.32, the resulting enthalpy is the following:

$$h = 340.7\,\frac{kJ}{kg} \tag{4.36}$$

Since the throttling process is isenthalpic, downstream enthalpy remains constant, as previously reviewed in Subsection 3.2.3, Chapter 3. To attain a flash evaporation process with a hypothetical steam fraction of 1%, based on the previous conditions, a downstream pressure of 40 kPa should be achieved. Table 4.33 demonstrate the needed downstream pressures for different hypothetical values of steam fraction based on the conditions of the experiment (i.e. keeping the values of P_u, T_u and T_d constant).

Summary and conclusions

Summary

This thesis demonstrated the creation of a fully functional fault-tolerant instrumentation system designed to serve a steam generation unit part of an experimental geothermal power cycle developed by the iiDEA® group. It covered the foundations of geothermal energy as a way to stress the potential and usefulness of geothermal energy, outlining the current trends and policies on the subject. After the review, several topics constituting the needed theoretical framework were introduced, focusing on the features of the Flash Evaporation Binary Cycle along with thermodynamic relations, fundamentals of digital signal processing and reliability evaluation. Finally, the hardware and software platform was exhaustively documented, including an updated reliability evaluation, an open-source GUI and the implementation of the IAPWS–IF97 formulation.

Conclusions

After the dissertation, several conclusions can be made, compiled below:

1. The development of a fully functional data acquisition system was accomplished, being able to display and record values of pressure and temperature at five and eight states, respectively. Additionally, at the throttling valve, upstream/downstream enthalpy and entropy is computed. Finally, downstream steam fraction is also calculated for the purpose of verifying a flash evaporation process.

2. A reliability update on the PSMs for a mission time of 10 years — considering environmental and operational conditions — was conducted, achieving an overall reliability of 99.978% for the 3.3 V PSM and 99.974% for the 5.0 V PSM.

3. An open-source stand-alone GUI was developed, providing the thermodynamic properties already discussed, with a sample time of 1 s. At the same time provides diagnostics on the state of active and cold standby redundant PSMs.

4. Demonstration of MAFs for smoothing signals was proved using real data acquired during the experiment in a noisy environment.

5. Due to constrains in the water heating equipment used and modifications in the pipelines of the experimental setup, steam generation could not be accomplished. For the upstream pressure and temperature registered at the throttling valve, a downstream pressure of 40 kPa would be needed to accomplish a 1% steam fraction.

Suggested future research

Unfortunately, the Maqetta plattform — in which TI GUI Composer was based on — stopped its active development in 2013 and ceased offering free hosting for existing projects in 2014 [153], limiting the GUI developed in this dissertation for local platforms. As an alternative, TI responded in 2016 with a self hosted cloud service in the next version of its software [154], known as GUI Composer 2.0, which could be used in the future for integrating the system to the cloud. Lastly, an upgrade of the algorithm could be developed introducing known models for refrigerants, diversifying the applications of the proposed platform.

Bibliography

[1] J. W. Valvano, *Embedded Systems: Introduction to ARM Cortex-M Microcontrollers*. CreateSpace, 2017.

[2] Software Engineering Center, Information-Technology Promotion Agency, *Embedded System Development - Process Reference Guide*, 2012.

[3] K. Sierra Doroteo, “Diseño y construcción de un separador de flujos para un ciclo de generación geotermoeléctrica”, iiDEA Group, Undergraduate thesis, Faculty of Engineering, National Autonomous University of Mexico, 2014.

[4] L. A. Herrera Bonilla, “Análisis y evaluación de dispositivos de estrangulamiento para la evaporación instantánea en un ciclo de generación geotermoeléctrica”, iiDEA Group, Undergraduate thesis, Faculty of Engineering, National Autonomous University of Mexico, 2015.

[5] D. García García, “Análisis del acoplamiento de los elementos del ciclo cbei”, iiDEA Group, Undergraduate thesis, Faculty of Engineering, National Autonomous University of Mexico, 2015.

[6] National Aeronautics and Space Administration. (2017). Technology Readiness Level Definitions, [Online]. Available: `https://www.nasa.gov/pdf/458490main_TRL_Definitions.pdf` (visited on 02/15/2017).

[7] R. J. Geerts, B. Gremmen, J. Jacobs, and G. Ruivenkamp, “Towards a philosophy of energy”, *Scientiae Studia*, vol. 12, pp. 105 –127, 2014.

[8] L. Mumford, *Technics and civilization*. The University of Chicago Press, 2010.

[9] World Energy council. (2016). Energy resources: Geothermal, [Online]. Available: `https://www.worldenergy.org/data/resources/resource/geothermal` (visited on 10/18/2016).

[10] C. J. Cleveland and C. Morris, “Geothermal”, in *Handbook of Energy: Chronologies, Top Ten Lists and Word Clouds*. Elsevier, 2014, vol. 2.

[11] E. Rodríguez Arias, “Geothermal energy in the framework of international environmental law”, in *Geothermal Power Generation*, R. DiPippo, Ed. Elsevier, 2016, pp. 763–786.

[12] P. Birkle, “Development of geothermal energy in Mexico and its energetic potential for the future”, in *Towards a Cleaner Planet*, J. Klapp, J. L. Cervantes-Cota, and J. F. C. Alcalá, Eds. Springer, 2007.

[13] M. H. Dickson and M. Fanelli, *Geothermal Energy: Utilization and Technology*, United Nations Educational, Scientific and Cultural Organization, Ed. John Wiley & Sons, 2003.

[14] M. Kaltschmitt, W. Streicher, and A. Wiese, *Renewable energy: Technology, Economics and Enviroment*. Springer, 2007.

[15] Geothermal Communities. (2016). Geothermal systems and technologies, [Online]. Available: http://geothermalcommunities.eu/assets/presentation/5.Course_GT.pdf.

[16] A. Watson, *Geothermal Engineering: Fundamentals and Applications*. Springer, 2013.

[17] R. DiPippo, *Geothermal Power Plants: Principles, Applications, Case Studies and Environmental Impact*, 4th ed. Elsevier, 2016.

[18] B. Lunis, "Geopressured-Geothermal Direct Use Potentials are Significant", *GHC Bulletin*, 1990.

[19] B. Matek, "2014 Annual U.S. & Global Geothermal Power Production Report", Geothermal Energy Association, Report, 2014.

[20] F. Pearce. (2016). Iceland drills hottest hole to tap into energy of molten magma, [Online]. Available: https://www.newscientist.com/article/2109872-iceland-drills-hottest-hole-to-tap-into-energy-of-molten-magma/ (visited on 02/03/2017).

[21] L. Rybach, "Classification of geothermal resources by potential", *Geothermal Energy Science*, 2015.

[22] P. Muffler and R. Cataldi, "Methods for regional assessment of geothermal resources", *Geothermics*, vol. 7, pp. 53–89, 1978.

[23] M. P. Hochstein, "Classification and assessment of geothermal resources," Small geothermal resources, UNITAR/UNDP Centre for Small Energy Resources, Report, 1990.

[24] G. C. Benderitter, "Possible approach to geothermal research and relative cost estimate", Small Geothermal Resources, UNITAR/UNDP Centre for Small Energy Resources, Report, 1990.

[25] R. Haenel, L. Rybach, and L. Stegena, "Fundamentals of geothermics", in *Handbook of Terrestrial Heat-Flow Density Determination*, R. Haenel, L. Rybach, and L. Stegena, Eds. Springer, 1988.

[26] K. C. Lee, "Classification of geothermal resources by exergy", *Geothermics*, vol. 30, no. 4, pp. 431–442, 2001.

[27] S. K. Sanyal, "Classification of Geothermal Systems - A possible Scheme", *Thirtieth Workshop on Geothermal Reservoir Engineering Stanford University*, 2005.

[28] REN21, "The First Decade: 2004-2014, 10 Years of Renewable Energy Progress", 2014.

[29] United Nations Framework Convention on Climate Change. (2015). The Paris Agreement, [Online]. Available: http://unfccc.int/paris_agreement/items/9485.php (visited on 10/18/2016).

[30] K. Gawell, M. Reed, and M. Wright, *Preliminary Report: Geothermal Energy, The Potential for Clean Power from the Earth*. Geothermal Energy Association, 1999.

[31] "2016 Annual U.S. & Global Geothermal Power Production Report", Geothermal Energy Association, Report, 2016.

[32] R. Bertani, “Geothermal Energy: an Overview”, *International Geothermal Days*, 2009.

[33] ——, “Geothermal power generation in the world: 2010-2014 update report”, *Geothermics*, vol. 60, pp. 31–43, 2016.

[34] World Energy Council, *World energy resources 2016*, 2016.

[35] *The Future of Geothermal Energy*. Massachusetts Institute of Technology, 2006.

[36] L. Y. Bronicki, “Introduction to geothermal power generation”, in *Geothermal Power Generation*, R. DiPippo, Ed. Elsevier, 2016, pp. 1–3.

[37] “Renewables 2016: Global Status Report”, REN 21. Renewable Energy Policy Network for the 21st Century, Report.

[38] H. Gupta and S. Roy, *Geothermal Energy: An Alternative Resource for the 21 Century*. Elsevier, 2006.

[39] Dewhurst Group, LLC. (2017). What is the Geothermal Development Facility for Latin America, [Online]. Available: `https://www.youtube.com/watch?v=wfxxTDP9ewE` (visited on 01/27/2017).

[40] E. Barbier, “Geothermal energy technology and current status: An overview”, *Renewable and Sustainable Energy Reviews*, vol. 6, pp. 3–65, 2002.

[41] International Energy Agency, Ed., *World Energy Outlook 2013 Factsheet*, 2014.

[42] New Energy Events, *Geothermal Congress for Latin America and the Caribbean*, 2015.

[43] Geothermal Development Facility for Latin America. (2016). GDF - About, [Online]. Available: `http://gdflac.com/about` (visited on 10/30/2016).

[44] D. Chandrasekharam and J. Bundschuh, *Geothermal Energy Resources for Developing Countries*, D. Chandrasekharam and J. Bundschuh, Eds. 2002, vol. 10, pp. 129–147.

[45] United Nations University - Geothermal Training Program. (2016). Current status, [Online]. Available: `http://www.unugtp.is/en/organization/about-the-unu-gtp/status` (visited on 10/30/2016).

[46] H. Aaheim and J. Bundschuh, “The value of geothermal energy for developing countries”, in *Geothermal Energy Resources for Developing Countries*, D. Chandrasekharam and J. Bundschuh, Eds. A.A. Balkema Publishers, 2002, pp. 37–51.

[47] E. Portale and J. de Wit, *Tracking Progress Towards Sustainable Energy for All in the Middle East and North Africa*, World Bank Group, 2015.

[48] International Energy Agency. (2016). World Energy Outlook 2016 Energy Access, [Online]. Available: `http://www.worldenergyoutlook.org/resources/energydevelopment/energyaccessdatabase/` (visited on 04/27/2016).

[49] ——, (2016). Mexico Energy Outlook 2016, [Online]. Available: `https://www.iea.org/publications/freepublications/publication/MexicoEnergyOutlook.pdf` (visited on 04/27/2016).

[50] Cámara de Diputados del H. Congreso de la Unión, Diario Oficial de la Federación, México, *Ley de Transición Energética*, 2015.

[51] United Nations, Department of Economic and Social Affairs, Population Division, *World Population Prospects: The 2015 Revision, Key Findings and Advance Tables*. 2015.

[52] J. Lund, D. Freestone, and T. Boyd, “Direct utilisation of geothermal energy: 2010 worldwide review”, *Geothermics*, vol. 40, pp. 159–180, 2015.

[53] M. F. Armenta, L. Gutiérrez-Negrín, and D. Nieva, “International energy agency - geothermal implementing agreement: Mexico”, International Energy Agency Geothermal, Country Report, 2014.

[54] L. C. Gutiérrez-Negrín, “Mexico: Update of the Country Update, and IRENA’s REmap”, *Newsletter of the International Geothermal Association*, no. 100, 2015.

[55] L Gutiérrez-Negrín, R Maya-González, and J Quijano-León, “Present situation and perspectives of geothermal in Mexico”, *Proceedings World geothermal Congress*, pp. 1–10, 2015.

[56] Y. Morita, K. Kawahara, and S. Saito, “MHPS Axial Flow Turbine & Direct Contact Condenser, and Recent Projects in Mexico”, *GRC Transactions*, vol. 40, pp. 863 –866, 2016.

[57] Francisco Rojas. (2016). Grupo Dragon to commission 25.5 MW Unit 3 at Domo de San Pedro in Mexico, [Online]. Available: `http://www.thinkgeoenergy.com/grupo-dragon-to-commission-25-5-mw-unit-3-at-domo-de-san-pedro-in-mexico/` (visited on 10/18/2016).

[58] M. A. Benítez Torreblanca, “Instrumentación electrónica tolerante a fallas para Ciclo Binario de Evaporación Instantánea CBEI-iiDEA”, iiDEA Group, Undergraduate thesis, Faculty of Engineering, National Autonomous University of Mexico, 2015.

[59] L. Gutiérrez Negrín and M. Lippmann, “Mexico: Thirty-three years of production in the Los Azufres geothermal field”, *Geothermal Power Generation*, pp. 717–742, 2016.

[60] GreenPower, *Mexican International Renewable Energy Congress - Infographics*, 2015.

[61] J. Entingh, D. McLarty, and E. Easwaran, “Small Geothermal Electric Systems for Remote Powering”, in *Geothermal Resources Council Transactions*, vol. 18, 1994, pp. 39–46.

[62] J. W. Pritchett, “Electrical generating capacities of geothermal slim holes”, *Proceedings of the World Geothermal Congress*, 2000.

[63] V. T. Radja and E. Saragih, “Utilization of small scale geothermal power plants for rural electrification in Indonesia”, *Proceedings of the World Geothermal Congress*, vol. 3, pp. 2103–2107, 1995.

[64] N. Farquharson, A. Schubert, and U. Steiner, “Geothermal Energy in Munich (and Beyond). A Geothermal City Case Study”, *GRC Transactions*, vol. 40, pp. 189 –196, 2016.

[65] J. Weber, B. Ganz, R. Schellschmidt, S. Burkhard, and R. Schulz, “Geothermal Energy Use in Germany”, *World Geothermal Congress*, pp. 427–432, 2015.

[66] Bundesministerium für Umwelt, Naturschutz und Reaktorsicherheit (BMU), “Innovation through research”, Bundesministerium für Umwelt, Naturschutz und Reaktorsicherheit, 2011 Annual Report on Research Funding in the Renewable Energies Sector, 2012.

[67] N. Andritsos, P. Dalabakis, G. Karydakis, N. Kolios, and M. Fytikas, “Characteristics of low-enthalpy geothermal applications in Greece”, *Renewable Energy*, vol. 36, no. 4, pp. 1298–1305, 2011.

[68] H. Gutiérrez and S. Espíndola, “Using Low Enthalpy Geothermal Resources to Desalinate Seawater and Electricity Production on Desert Areas in Mexico”, *Proceedings of the World Geothermal Congress*, 2000.

[69] I. R. Torres, "Experience with low enthalpy geothermal projects in Mexico", *Geotermia*, vol. 27, no. 2, pp. 13–21, 2014.

[70] British Petroleum. (2016). Geothermal power, [Online]. Available: `http://www.bp.com/en/global/corporate/energy-economics/statistical-review-of-world-energy/renewable-energy/geothermal-power.html` (visited on 11/15/2016).

[71] C. Donnellan, *Energy alternatives: A Comparative Analysis*. The Science and Public Policy Program, University of Oklahoma, 1994, p. 720.

[72] U.S. Energy Information Administration, *Levelized Cost and Levelized Avoided Cost of New Generation Resources in the Annual Energy Outlook 2016*, 2016.

[73] Lazard, *Lazard's Levelized Cost of Energy analysis 10.0*, 2016.

[74] E. B. González, "Feasibility Study of Geothermal Utilization of Remoteness Areas: Design and Optimization of a Small Standard Power Plant", Master's thesis, School for Renewable Energy Science, Iceland, 2011.

[75] European Commission's Joint Research Centre, *New World Bank and European Commission map shows that 95% of the world's population lives on 10% of the land*, 2015. [Online]. Available: `https://ec.europa.eu/jrc/sites/jrcsh/files/jrc_081217_newsrelease_travel_times_en.pdf` (visited on 06/11/2015).

[76] Electratherm. (2016). Geothermal hot springs, [Online]. Available: `https://electratherm.com/applications/geothermal/hot-springs/` (visited on 11/12/2016).

[77] Infinity Turbine LCC. (2016). About Infinity Turbine LLC, [Online]. Available: `http://www.infinityturbine.com/about.html` (visited on 11/12/2016).

[78] Electratherm. (2016). FAQ, [Online]. Available: `https://electratherm.com/products/faqs/` (visited on 11/12/2016).

[79] International Energy Agency, Ed., *World Energy Outlook - Executive Summary*, 2016.

[80] *Energy vision update 2009 - Thirsty Energy: Water and Energy in the 21st Century*, 2009.

[81] International Energy Agency, "Water for Energy: Is energy becoming a thirstier resource?", *World Energy Outlook*, pp. 1–33, 2012.

[82] M. Richards, Ed., *Finding Geothermal Energy in Texas*, Southern Methodist University, 2008.

[83] L. E. Capuano, "Geothermal well drilling", in *Geothermal Power Generation*, R. DiPippo, Ed. Elsevier, 2016, pp. 107–139.

[84] K. Baumann, "Some recent developments in large steam turbine practice", *Journal of Instrumentation and Electrical Engineering*, vol. 302, pp. 565–623, 1921.

[85] W. Harvey and K. Wallace, "Flash steam geothermal energy conversion systems", in *Geothermal Power Generation*, R. DiPippo, Ed. Elsevier, 2016, pp. 249–290.

[86] H. M. Aviña Jiménez, *Tipos de centrales geotermoeléctricas convencionales*, 2013.

[87] D. E. White, "Characteristics of geothermal resources", in *Geothermal energy: resources, production, stimulation*, P. Kruger and C. Otte, Eds. Stanford University Press, 1973, pp. 69–94.

[88] Geothermal Communities. (2016). Production of electricity from geothermal energy, [Online]. Available: www.geothermalcommunities.eu/assets/elearning/7.2.Power_from_GE.pdf.

[89] K. Phair, “Direct steam geothermal energy conversion systems: dry steam and superheated steam plants”, in *Geothermal Power Generation*, R. DiPippo, Ed. Elsevier Ltd, 2016, pp. 291–319.

[90] R. DiPippo, “Geothermal power plants: Evolution and performance assessments”, *Geothermics*, vol. 53, pp. 291–307, 2015.

[91] H. M. Sadiq J. Zarrouk, “Efficiency of geothermal power plants: A worldwide review”, *Geothermics*, vol. 51, pp. 142–153, 2014.

[92] Y. A. Çengel, *Thermodynamics: an Engineering Approach*. McGraw-Hill, 2015.

[93] K. Wark, *Advanced Thermodynamics for Engineers*. McGraw-Hill, 1994.

[94] W. C. Carter. (2017). The Gibbs Free Energy and Helmholtz Free Energy, [Online]. Available: http://pruffle.mit.edu/3.00/Lecture_02_web/node16.html (visited on 02/04/2017).

[95] K. A. Nelson and M. Bawendi. (2017). Thermodynamics and Kinetics - The Gibbs Free Energy, [Online]. Available: https://ocw.mit.edu/courses/chemistry/5-60-thermodynamics-kinetics-spring-2008/lecture-notes/5_60_lecture13.pdf (visited on 02/04/2017).

[96] C. W. Myles. (2017). Thermodynamic Properties of Fluids, [Online]. Available: www.phys.ttu.edu/~cmyles/Phys5305/Lectures/1.%20Fluids%201.ppt (visited on 02/04/2017).

[97] The International Association for the Properties of Water and Steam, *Revised Release on the IAPWS Industrial Formulation 1997 for the Thermodynamic Properties of Water and Steam*, The International Association for the Properties of Water and Steam, 2007.

[98] National Programme on Technology Enhanced Learning. (2017). Thermodynamic properties of real fluids, [Online]. Available: http://nptel.ac.in/courses/103101004/downloads/chapter-5.pdf (visited on 02/04/2017).

[99] C. O. Méndez, M. F. Armenta, and G. R. Silva, “Potencial geotérmico de la República Mexicana”, *Geotermia*, vol. 24, no. 1, pp. 50–58, 2011.

[100] C. A. Galván, R. P. Ledesma, and M. A. T. Vera, “Geothermal prospects in the Baja California Peninsula”, *Geothermics*, vol. 55, pp. 39–57, 2015.

[101] H. M. Aviña Jiménez, G. León de los Santos, and M. Á. Benítez Torreblanca, “Comparison of the energetic performance of a binary cycle and a flash evaporation binary cycle, using low-enthalpy geothermal energy”, *International Journal of Sustainable Engineering*, vol. 10, no. 2, pp. 90–98, 2017.

[102] M. R. Neuman. (2015). Basic instrumentation systems, [Online]. Available: http://www.biomed.mtu.edu/~osoykan/classes/be3600/note2003/basicins.pdf (visited on 10/15/2015).

[103] R. J. Hansman, “Characteristics of instrumentation”, in *The Measurement, Instrumentation and Sensors Handbook*, J. G. Webster and H. Eren, Eds. CRC Press, 1999.

[104] John Fluke Manufacturing Company, *Metrology solutions*, 1991.

[105] R. Palás-Areny, "Amplifiers and signal conditioners", in *The Measurement, Instrumentation and Sensors Handbook*. CRC Press, 1999.

[106] S. W. Smith, *The Scientist & Engineer's Guide to Digital Signal Processing*. California Technical Publishers, 1997.

[107] MathWorks. (2017). Signal Smoothing, [Online]. Available: `https://www.mathworks.com/help/signal/examples/signal-smoothing.html` (visited on 02/04/2017).

[108] International Standards Organization, *ISO 9000-2005: Quality Management Systems - Fundamentals and Vocabulary*, 2005.

[109] J. Strutt and D. Bowden, *Reliability Engineering and Risk Management Overview*, in *Risk and Reliability Management*, Cranfield University School of Water Sciences, Ed., 1999.

[110] B. S. Dhillon, *Design Reliability: Fundamentals and Applications*. CRC Press LLC, 1999.

[111] R. Isermann, "Trends in the application of model-based fault detection and diagnosis of technical processes", *Control Engineering Practice*, vol. 5, pp. 709–719, 1997.

[112] E. Dubrova, *Fault-Tolerant Design*. Springer, 2013.

[113] R. Isermann, *Fault-Diagnosis Systems: An Introduction from Fault Detection to Fault Tolerance*. Springer-Verlag, 2006.

[114] J. Strutt, *System reliability analysis*, in *Risk and Reliability Management*, Cranfield University School of Water Sciences, Ed., 1999.

[115] J. F. Prada, "The Value of Reliability in Power Systems: Pricing Operating Reserves", *Massachusetts Institute of Technology, Energy Laboratory*, no. June, 1999.

[116] H. Alwi, C. Edwards, and C. P. Tan, *Fault Detection and Fault-Tolerant Control Using Sliding Modes*. Springer, 2011.

[117] J. Yiu, *The Definitive Guide to ARM Cortex - M3 and Cortex - M4 Processors*. Elsevier, 2014.

[118] Renesas Electronics, *Semiconductor Reliability Handbook*, 2017. [Online]. Available: `https://www.renesas.com/zh-tw/doc/products/others/r51zz0001ej0250.pdf`.

[119] J. Gray, "A Census of Tandem Systems Availability Between 1985 and 1990", *IEEE Transactions on Reliability*, vol. 39, no. 4, pp. 409–418, 1990.

[120] C. Olofsson, *Instrumentation and Control Systems Important to Safety in Nuclear Power Plants*. International Atomic Energy Agency, 2002.

[121] M. Holmgren. (1999). X steam, thermodynamic properties of water and steam, [Online]. Available: `https://www.mathworks.com/matlabcentral/fileexchange/9817-x-steam--thermodynamic-properties-of-water-and-steam` (visited on 02/15/2017).

[122] M. Lazzaroni, L. Cristaldi, L. Peretto, P. Rinaldi, and M. Catelani, *Reliability Engineering: Basic Concepts and Applications in ICT*. Springer-Verlag Berlin Heidelberg, 2011.

[123] B. S. Dhillon, *Applied Reliability and Quality: Fundamentals, Methods and Procedures*. Springer, 2007.

[124] D. P. Siewiorek and R. S. Swarz, *Reliable Computer Systems: Design and Evaluation*, 3rd. A K Peters Ltd., 1998.

[125] R. Isermann, *Fault-Diagnosis Systems: An Introduction from Fault Detection to Fault Tolerance*. Springer-Verlag, 2006.

[126] ——, *Fault-Diagnosis Applications - Model-based condition monitoring: Actuators, drives, machinery, plants, sensors, and fault-tolerant systems*. Springer-Verlag, 2011.

[127] W. Kuo and M. J. Zuo, *Optimal Reliability Modeling: Principles and Applications*. John Wiley & Sons, Inc., 2003.

[128] Honeywell, *PX2 Series Heavy Duty Pressure Transducers*, 2014.

[129] William C. Dunn, *Fundamentals of Instrumentation and Process Control*. McGraw-Hill, 2005.

[130] Texas Instruments, "*Micropower low-dropout (LDO) voltage regulators*" *TPS72X datasheet*, 2000.

[131] ——, "*Low-dropout voltage regulators*" *TL75XL datasheet*, 2009.

[132] ——, *Tiva TM4C1294NCPDT Microcontroller datasheet*, 2014.

[133] ——, (2016). DPPM/FIT/MTBF estimator, [Online]. Available: `http://www.ti.com/quality/docs/estimator.tsp` (visited on 08/27/2016).

[134] United States Department of Defense, *Reliability Prediction of Electronic Equipment MIL-HDBK-217F Notice 2*. 1991.

[135] H. M. Aviña Jiménez, G. León de los Santos, D. Sauceda Carbajal, F. García Torres, and M. Á. Benítez Torreblanca, “Alternatives for vacuum generation in unconventional seawater desalination systems”, *Desalination and Water Treatment*, vol. 57, no. 56, pp. 27 085–27 095, 2016.

[136] The International Association for the Properties of Water and Steam. (2017). Index, [Online]. Available: `http://www.iapws.org/index.html` (visited on 01/27/2017).

[137] The International association for the Properties of Water and Steam. (2017). What is the difference between the IAPWS-95 formulation "for general and scientific use" and the IAPWS-IF97 "industrial" formulation?, [Online]. Available: `http://www.iapws.org/faq2/twoform.html` (visited on 01/27/2017).

[138] ——, (2017). Main IAPWS Thermodynamic Property Formulations, [Online]. Available: `http://www.iapws.org/newform.html` (visited on 01/27/2017).

[139] Moscow Power Engineering Institute. (2017). Thermodynamic Properties of Ordinary Water Substance for General and Scientific Use, [Online]. Available: `http://twt.mpei.ac.ru/mcs/worksheets/iapws/IAPWS95.xmcd` (visited on 01/27/2017).

[140] ——, (2017). Water and Steam Tables for Industrial Use – Interactive reference book, [Online]. Available: `http://twt.mpei.ac.ru/ochkov/WSPHB/Engindex.html` (visited on 01/27/2017).

[141] American Society of Mechanical Engineers. (2017). Steam Properties for Industrial Use Based on IAPWS–IF97 Professional Version, [Online]. Available: `https://www.asme.org/products/books/steam-properties-industrial-use-based-iapwsif97` (visited on 01/27/2017).

[142] ——, (2017). International Steam Tables for Industrial Use, Third Edition (CRTD-Volume 58), [Online]. Available: `http://www.asme.org/products/books/international-steam-tables-industrial-use-third` (visited on 01/27/2017).

[143] National Institute of Standards and Technology. (2017). NIST/ASME Steam Properties Database: Version 3.0 - The Latest IAPWS Standard Formulation, [Online]. Available: https://www.nist.gov/srd/nist10 (visited on 01/27/2017).

[144] A. H. Harvey, "Thermodynamic Properties of Water: Tabulation from the IAPWS Formulation 1995 for the Thermodynamic Properties of Ordinary Water Substance for General and Scientific Use ", *NIST Internal/Interagency Reports*, vol. 5078, 1998. [Online]. Available: https://www.nist.gov/sites/default/files/documents/srd/NISTIR5078.htm (visited on 01/27/2017).

[145] Ruhr-Universität Bochum. (2017). Software for the IAPWS-95 Formulation, [Online]. Available: http://www.thermo.ruhr-uni-bochum.de/en/prof-w-wagner/software/54-wagner/wagner/165--software-fuer-die-iapws-95-formulation-h2o.html (visited on 01/27/2017).

[146] ——, (2017). Software for the Industrial Formulation IAPWS-IF97 for Water and Steam, [Online]. Available: http://www.thermo.ruhr-uni-bochum.de/en/prof-w-wagner/software/iapws-if97.html (visited on 01/27/2017).

[147] Hochschule Zittau/Görlitz University of Applied Sciences. (2017). Zittau's Fluid Property Calculator, [Online]. Available: https://web1.hszg.de/thermo_fpc/index.php (visited on 01/27/2017).

[148] ——, (2017). Property Libraries for Pocket Calculators, [Online]. Available: http://f-m.hszg.de/index.php?id=7573&L=4 (visited on 01/27/2017).

[149] ——, (2017). Property Libraries, [Online]. Available: http://f-m.hszg.de/index.php?id=6529&L=4 (visited on 01/27/2017).

[150] W. Wagner and H. J. Kretzschmar, *International Steam Tables Properties of Water and Steam – Based on the Industrial Formulation IAPWS-IF97*. Springer, 2008.

[151] Microsoft Developer Network. (2017). Beginners Guide to Performance Profiling, [Online]. Available: https://docs.microsoft.com/en-us/visualstudio/profiling/beginners-guide-to-performance-profiling (visited on 03/18/2017).

[152] K. Sierra Doroteo and L. A. Herrera Bonilla, "Reporte de datos experimentales - Última etapa de experimentación", Engineering Institute, National Autonomous University of Mexico, iiDEA Group, Report, 2015.

[153] Maqetta. (2012). Project Summary, [Online]. Available: http://maqetta.org/overview/summary.html (visited on 11/12/2016).

[154] Texas Instruments. (2016). Download CCS, [Online]. Available: http://processors.wiki.ti.com/index.php/Download_CCS (visited on 11/12/2016).

Page intentionally left blank

Appendix A

Reliability and screening data

The following documents are provided:

1. Reliability tests results of Current Limiting Diodes (1N5283 – 1N5314 series)
2. Screening conditions of Current Limiting Diodes (1N5283 – 1N5314 series)
3. US Sensor® RTD aging chart
4. Evaluation testing of Honeywell® PX2 series pressure transducers

Reliability Test Results

TESTS :	HTRB LIFE	PERIOD :	ENDING 12/31/07
FAMILY :	Current Limiting Diode, DO35CLD	CASE :	DO-35
PART NUMBERS INCLUDED :	1N5283 – 1N5314 SERIES, CCL0035 – CCL5750 SERIES, CCLH080 – CCLH150 SERIES		
TEST CONDITIONS :	T_A=150°C, V_T=25V		

Statistical Data

CONFIDENCE LEVEL :	60%
ACTIVATION ENERGY :	0.7 eV
ACCELERATION FACTOR :	270
FAILURE RATE AT OPER. TEMP. (55°C) :	2.30 FITS
MTTF :	4.3×10^8 Hours

REPORT DATE :	February 5, 2008
PREPARED BY :	CG
APPROVED BY :	JR

Reliability Engineering Department
Central Semiconductor Corp.

cc-478C

Reliability Test Results

TESTS : ENVIRONMENTAL PERIOD : ENDING 12/31/03

FAMILY : Current Limiting Diode, DO35CLD CASE : DO-35

PART NUMBERS INCLUDED : 1N5283 – 1N5314 SERIES, CCL0035 – CCL5750 SERIES, CCLH080 – CCLH150 SERIES

NO.	TEST ITEM	TEST CONDITION	FAILURE RATE
1	HIGH TEMP.	T_A=150°C, t=1000 HOURS	0/2400
2	LOW TEMP.	T_A=-65°C, t=1000 HOURS	0/2400
3	HUMIDITY	T_A=85°C, RH=85%, t=1000 HOURS	0/2400
4	TEMPERATURE CYCLING	150°C/25°C/-55°C 15MIN/<1MIN/15MIN 10 CYCLES	0/2400
5	THERMAL SHOCK	LIQUID TO LIQUID 0°C/100°C 10 CYCLES	0/2400
6	PRESSURE COOKER	T_A=121°C, p=15 PSIG t=168 HOURS	0/2400
7	SOLDERABILITY	$T_{(SOLDER)}$=245°C, t=5 SEC	0/600
8	SOLDER DIP	TOTAL IMMERSION, 265°C, 10 SEC	0/240

REPORT DATE : February 5, 2008

PREPARED BY : CG

APPROVED BY : JR

Reliability Engineering Department
Central Semiconductor Corp.

cc-478B

U.S. Sensor Corp. Aging Chart
Platinum RTD Element (3,850ppm)
U:\EXCEL\CURVES\AGE-RTD-60C

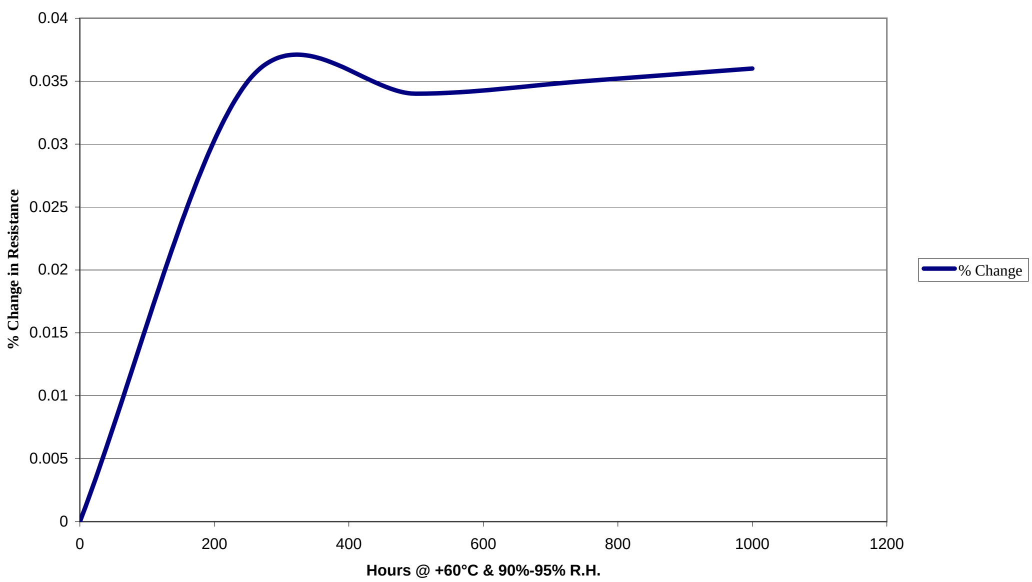

Evaluation Testing - Results Summary
PX2 Ratiometric Output (AA - AD)

1 Scope

This test report summarizes the results of evaluation testing performed on PX2 Pressure Sensor listings which are directly related to the Ratiometric Output configuration. All testing was performed by the Honeywell Evaluation Engineering group at Honeywell's Freeport, Illinois, USA, site.

2 Ratiometric Output (AA - AD) Configurations Applicable

Series	Connector Type	Port Type	Pressure Range (A=Absolute, S=Sealed Gage)
PX2	A = Packard Metripak 150 B = Micro M12 IEC 61076-2 C = DIN EN 175301-803C D = Deutsch DTM04-3P E = Cable 1 meter	N1 = NPT 1/4 - 18 N2 = NPT 1/8 - 27 S1 = 9/16-18 UNF SAE J1926-3 S2 = 7/16-20 UNF SAE J1926-3 F1 = 45° Flare (Schrader) SAE J512 M1 = M12 X 1.5 ISO 6149-3 G1 = G1/4 ISO 1179-3 G2= G1/8 ISO 1179-3	100P=100 psi 150P=150 psi 010B= 10 bar 001G=1 MPa 200P = 200 psi 250P = 250 psi 016B = 16 bar 1.6 =1.6 MPa 300P = 300 psi 025B = 25 bar 2.5G =2.5 MPa 500P = 500 psi 040B = 40 bar 4.0G=4.0 MPa 600P = 600 psi 667P = 667 psi 046B = 46 bar

3 Test Summary and Conditions

SAMPLES TESTED:

Three pressure ranges were tested to validate the entire range from 100P to 500P →100PA, 300PA, 500PA
All connectors and ports were qualified.
Some configurations validated by similarity using Current, Regulated electrical outputs.

ACCEPTANCE CRITERIA:

The PX2 Ratiometric Output Pressure Transducer samples must successfully pass all specified criteria as defined in the product specification. All test samples were characterized in an automated characterization test setup prior to and after every test. The general test summary is tabulated in Table C.

The test results are summarized in Tables C1, C2 and C3 below.

TEST PERFORMED	TEST CONDITIONS	QTY Tested	PASS (Y/N)	COMMENTS
TEMPERATURE / PRESSURE CHARACTERIZATION	Temperature(s): 25,-40,-20,25,85,125,25°C Pressure(s): (2,5,10,15,20,25,50,75,100,50,2)%FSS Supply Voltage: 5.0 VDC Soak time: 60 Minutes	240	Y	Full Scale Span (FSS), Full scale defined as the output of a device with maximum operational pressure applied.
SERIAL LEG: The following tests were performed in series. The durations are shorter than their stand alone equivalent tests, but the same sample set was exposed to multiple environments.				
SUPPLY VOLTAGE CHECK	All test samples were characterized at the minimum, nominal and maximum rated supply voltage in an automated characterization test setup. Supply Voltage: 4.5, 4.75, 5.0, 5.25, and 5.5 VDC	20	Y	
FULL SCALE DRIFT	Test Temperature: 25°C Supply Voltage: 5.0 VDC Sampling Time: 10 Minutes Pressure: Full scale Duration: 1000 Hours Monitoring: Yes	20	Y	Full scale defined as the output of a device with maximum operational pressure applied. Only performed on 500psi configuration.
MECHANICAL SHOCK MIL-STD-202F Method 213B Cond. F	Shock Pulse Profile: Half-Sine wave Shock Pulse Amplitude: 100 Gs Shock Pulse Duration: 6 Milliseconds Shock Pulse per Axis: 3 Number of Axis Tested: 6 Total Number of Shock Pulses: 18	20	Y	
VIBRATION – SINE SWEEP	Amplitudes (sine): 20G's Frequency Range: Sweep from 10Hz, 2000, 10Hz Axis Tested: 3 Sweeps per Axis: 3 Sweep Time: 20 Minutes Time per Axis: 1 Hour Total Time: 3 Hours	20	Y	
DROP TEST	Samples were dropped on a concrete floor from a height of 1 meter. Six drops per part were recorded.	5	Y	
FITTING TORQUE TEST	Torque was applied continuously and increased until torque reading reached 100 ft/lbs.	5	Y	Performed on all port configurations.
WARM UP STABILITY (24 HOURS)	Test Temperature: 25°C Supply Voltage: 5.0 VDC Supply Cycle Time: 4 Hrs on; 20 Hrs off, 4 Hrs on; 20 Hrs off, 4 Hrs on Sampling Time: 10 Seconds Monitoring: Yes	20	Y	
NULL DRIFT	Test Temperature: 25°C	20	Y	Only performed on 100psi configuration.

TEST PERFORMED	TEST CONDITIONS	QTY Tested	PASS (Y/N)	COMMENTS
	Supply Voltage: 5.0 VDC Sampling Rate: 10 Minutes Pressure: Ambient Pressure (0 PSIG)/Uncontrolled Duration: 500 Hours Monitoring: Yes			
LOW TEMPERATURE DRIFT	Test Temperature: -40°C Supply Voltage: 5.0 VDC Test Duration: 1,000 Hours Turn On Dwell: 4 Hours powered/monitored prior Cold Exposure Sampling Rate: 10 Minutes Monitoring: Yes	20	Y	Only performed on 100psi configuration.
OVER PRESSURE TEST	Test Temperature: 25°C Pressure: 3x FSS @ 100 / 300 psi, 2x FSS @500 psi Number of Cycles: 5	20	Y	
BURST TEST	Test Temperature: 25°C Pressure: 5x FSS @ 100 / 300 psi, 3x FSS @500 psi Duration at Each Pressure Range: 1 minute	20	Y	Test to fail – all met requirements
REVERSE VOLTAGE TEST	Apply +12.0VDC ±0.25VDC to DUT, measure output voltage. Apply -16.0VDC ±0.1VDC to DUT for 15 minutes and remove. Apply +12.0VDC ±0.25VDC to DUT, measure output voltage.	10	Y	
OVERVOLTAGE TEST	Apply +12.0VDC ±0.25 VDC to DUT, measure output voltage. Apply 30.0VDC ±0.1 VDC to DUT for 15 minutes and remove. Apply +12.0VDC ±0.25 VDC to DUT, measure output voltage.	10	Y	
ELECTROSTATIC DISCHARGE (ESD) IEC 61000-4-2	Contact Discharge, +/- 4kV Air Discharge, +/- 8kV	2	Y	Criterion B
IEC RADIATED IMMUNITY (RI) IEC 61000-4-3	10 V/m (80-1000 MHz) 3 V/m (1.4-2.0 GHz) 1 V/m (2.0-2.7 GHz)	2	Y	Criterion A
FAST TRANSIENT BURST IEC 61000-4-4	+/- 1000V	2	Y	Criterion B
IMMUNITY TO CONDUCTED DISTURBANCES IEC 61000-4-6	3V	2	Y	Criterion A
RADIATED EMISSIONS CISPR 11	Group 1, Class A Limits	2	Y	
ISO 11452-2 RADIATED (ALSE) IMMUNITY	100 V/m (200MHz – 2GHz)	2	Y	Compliant
THERMAL SHOCK 1000 CYCLES (AIR TO AIR)	Cold Chamber Temperature: -40°C Hot Chamber Temperature: 125°C Turn On Dwell: 4 hours powered/monitored Dwell Time at each Temp. Level: 30 Minutes Transfer Time from Cold to Hot: < 5 Seconds	20	Y	

TEST PERFORMED	TEST CONDITIONS	QTY Tested	PASS (Y/N)	COMMENTS
	Total Time for Cold-Hot Cycle: 1 Hour Total Number of Cold-Hot Cycles: 1,000 Cycles Sampling Rate: 10 Minutes Power Supply: 5.0 VDC Monitoring: Yes			
HIGH TEMPERATURE / HUMIDITY WITH BIAS (1000 HOURS)	Temperature: 85°C Humidity: 85% R.H. Total Number of Hours: 1,000 Hours Supply Voltage: 5.0 VDC Pressure: Null Sampling Rate: 10 minutes Monitoring: Yes	20	Y	
PRESSURE /TEMPERATURE CYCLING (4 MILLION CYCLES)	Total Pressure Cycles: 4 Million Pressure Cycling Range: 0 to 2x FSS Pressure Cycle Rate: 5 Hz Test medium: Mobil DTE 25 Temperature Cycling Range: -40°C to 125°C Total Length: 10 days	20	Y	Performed on all port configurations.
OVER PRESSURE CYCLING (10 MILLION CYCLES)	Temperature: 25°C Total Pressure Cycles: 10 Million Pressure Applied: 0 to 2x FSS Monitored: No Duty Cycle: 50% Frequency: 5Hz	20	Y	
BURN-IN MAX TEMPERATURE / VOLTAGE	Test Temperature: 125°C Supply Voltage: 5.5 VDC Test Duration: 500 Hours Sampling Rate: 10 minutes Monitoring: Yes	20	Y	
SERIAL LEG: The following tests were performed in series. The durations are shorter than their stand alone equivalent tests, but the same sample set was exposed to multiple environments.				
THERMAL SHOCK 100 CYCLES (AIR TO AIR)	Cold Chamber Temperature: -40°C Hot Chamber Temperature: 125°C Dwell Time at each Temp. Level: 30 Minutes Transfer Time from Cold to Hot: < 5 Seconds Total Time for Cold-Hot Cycle: 1 Hour Total Number of Cold-Hot Cycles: 100 Cycles	20	Y	
HUMIDITY HEAT CYCLING (168 CYCLES)	The test samples were subjected to the temperature and humidity sequence stated below: 1) Pre-condition samples at a chamber temperature of 50°C for 24 hours. 2) Raise chamber temperature to 80°C and relative humidity to 92.5% in 2 hours. 3) Soak at these levels for 6 hours. 4) Lower chamber temperature to 35°C and relative humidity to 85% in 16 hours. 5) The above steps constitutes one 24-hour cycle. Repeat the cycle 7 times for a 168 hour 7 day test.	20	Y	

TEST PERFORMED	TEST CONDITIONS	QTY Tested	PASS (Y/N)	COMMENTS
VIBRATION – SINE SWEEP	Amplitudes (sine): 20G's Frequency Range: Sweep from 10Hz, 2000, 10Hz Axis Tested: 3 Sweeps per Axis: 3 Sweep Time: 20 Minutes Time per Axis: 1 Hour Total Time: 3 Hours	20	Y	
SUBMERSION (5 DUNKS 125°C TO 0°C)	Sample Soak Temperature: 125°C Temperature Soak Duration: 30 Minutes Submersion Depth: Connector 76mm below water surface Submersion Time: 30 Minutes Water Temperature: 0°C – 4°C Total Number of Cycles: 5 Cycles	20	Y	
CONNECTOR STRENGTH TEST	The sample was mounted to mounting plate. A connector was plugged into the test sample and the mounting plate was secured in a vise. A 10 pound weight was attached to connector wires (bundled together) and suspended from them for 1 minute in a parallel direction to the sample housing and 1 minute in a perpendicular direction to the sample housing.	20	Y	
SERIAL LEG: The following tests were performed in series. The durations are shorter than their stand alone equivalent tests, but the same sample set was exposed to multiple environments.				
HIGH TEMPERATURE / HUMIDITY WITH BIAS (168 HOURS)	Temperature: 85°C Humidity: 85% R.H. Total Number of Hours: 168 Hours Supply Voltage: 5.0 VDC Pressure: Null	20	Y	
THERMAL SHOCK 200 CYCLES (AIR TO AIR)	Cold Chamber Temperature: -40°C Hot Chamber Temperature: 125°C Dwell Time at each Temp. Level: 30 Minutes Transfer Time from Cold to Hot: < 5 Seconds Total Time for Cold-Hot Cycle: 1 Hour Total Number of Cold-Hot Cycles: 200 Cycles	20	Y	
OVER PRESSURE CYCLING (1 MILLION CYCLES)	Temperature: 25°C Total Pressure Cycles: 1 Million Pressure Applied: 0 to 2x FSS Monitored: No Duty Cycle: 50% Frequency: 5Hz	20	Y	

Table C1 Durability

TEST PERFORMED	TEST CONDITIONS	QTY Tested	PASS (Y/N)	COMMENTS
IP69K HIGH PRESSURE WASHDOWN	Temperature: 80 ± 5°C Equipment: Washdown Tester Water Pressure: 1160-1450 PSI Flow Rate: 190 ± 5 gallons / hour Angle: 90°, 60°, 30°, 0° Distance: 100-150 mm Spray Duration: 30 Seconds Spray Frequency: 60 Seconds Number of cycles: 5 Per Sample Basket Rotation Speed: 3.3 RPM	5	Y	Applicable for Deutsch and Cable Harness connectors
IP67 SUBMERSION TEST	Submersion Depth: 1 Meter (3.281 feet) Test Duration: 30 Minutes	5	Y	Applicable for Deutsch, Cable Harness, Packard, DIN and M12 connectors
IP6x DUST TEST	Agitate Duration: 10 Seconds Agitate Interval: 20 Seconds Exposure Time: 8 Hours Amount of Dust: 6Kg/m^3 ± 5% Coarse Dust	5	Y	Applicable for all connector options
SALT FOG TEST	The test samples were subjected to the Salt Fog test in accordance with ASTM B 117-95 Standard Practice for Operating Salt Spray (Fog) Apparatus. The test samples were positioned to insure uniform exposure to the salt spray. The samples were exposed to the salt fog continuously for 96 hours. The salt solution percentage was 5 % and the temperature of the exposure zone was 35°C. The compressed air supply to the nozzles in the chamber was maintained to be between 12 and 15 psi. The samples were so positioned in the chamber so that there was no condensed salt solution falling on them. At the end of the exposure period, the test samples were washed in running water not warmer than 38°C and then immediately dried.	5	Y	Applicable for all connector options

Table C2 Environmental

TEST PERFORMED	TEST CONDITIONS	QTY Tested	PASS (Y/N)	COMMENTS
MEDIA TESTING per Non-Standard Chemical Exposure based on Modified ASHRAE 97 Specification	Samples of each adhesive were mounted onto a stainless steel manifold. The manifolds were filled with the challenge chemical and placed into ovens at the requested temperature condition. Exposure Chemical / Exposure Temperature / Duration Engine Oil 10W30 / 125C / 18 days Brake Fluid DOT3 / 125C / 18 days Tap Water / 90C / 18 days R134A Refrigerant / 90C / 18 days	20	Y	

Table C3 Media

Appendix B

Auxiliary data for IAPWS–IF97

B.1 Reference constants of IAPWS–IF97

In Section 3.1.5, the value of the specific gas constant of water R was first introduced. This section deals with supplementary key parameters used by the IAPWS–IF97 standard to establish the different fundamental equations of each region.

B.1.1 Critical parameters of water

$$P_c = 22.064\, MPa \tag{B.1a}$$

$$T_c = 647.096\, K \tag{B.1b}$$

$$\rho_c = 322\, \frac{kg}{m^3} \tag{B.1c}$$

Where:

P_c Critical pressure

T_c Critical temperature

ρ_c Critical density

B.1.2 Conditions at the triple point

$$P^t = 611.657\, Pa \tag{B.2a}$$

$$T^t = 273.16\, K \tag{B.2b}$$

Where:

P^t Pressure of the triple point

T^t Temperature of the triple point

B.1.3 Critical parameters of water

$$P_c = 22.064\, MPa \tag{B.3a}$$

$$T_c = 647.096\, K \tag{B.3b}$$

$$\rho_c = 322\, \frac{kg}{m^3} \tag{B.3c}$$

Where:

P_c Critical pressure

T_c Critical temperature

ρ_c Critical density

B.1.4 Saturated liquid properties of water at the triple point

$$h^t_{sat} = 0.611783\, \frac{J}{kg} \tag{B.4a}$$

$$s^t_{sat} = 0\, \frac{kJ}{kg\, K} \tag{B.4b}$$

$$u^t_{sat} = 0\, \frac{kJ}{kg} \tag{B.4c}$$

Where:

h^t_{sat} Specific enthalpy of saturated liquid at the triple point

s^t_{sat} Specific internal entropy of saturated liquid at the triple point

u^t_{sat} Specific internal energy of saturated liquid at the triple point

B.2 Coefficients for Region 1

Table B.1: Coefficients n_i and exponents I_i and J_i for Equation (4.13). Adapted from [97].

i	I_i	J_i	n_i	i	I_i	J_i	n_i
1	0	-2	$1.4632971213167\,x10^{-1}$	18	2	3	$-4.4141845330846\,x10^{-6}$
2	0	-1	$-8.4548187169114\,x10^{-1}$	19	2	17	$-7.2694996297594\,x10^{-16}$
3	0	0	-3.756360367204	20	3	-4	$-3.1679644845054\,x10^{-5}$
4	0	1	3.3855169168385	21	3	0	$-2.8270797985312\,x10^{-6}$
5	0	2	$-9.5791963387872\,x10^{-1}$	22	3	6	$-8.5205128120103\,x10^{-10}$
6	0	3	$1.5772038513228\,x10^{-1}$	23	4	-5	$-2.2425281908\,x10^{-6}$
7	0	4	$-1.6616417199501\,x10^{-2}$	24	4	-2	$-6.5171222895601\,x10^{-7}$
8	0	5	$8.1214629983568\,x10^{-4}$	25	4	10	$-1.4341729937924\,x10^{-13}$
9	1	-9	$2.8319080123804\,x10^{-4}$	26	5	-8	$-4.0516996860117\,x10^{-07}$
10	1	-7	$-6.0706301565874\,x10^{-4}$	27	8	-11	$-1.2734301741641\,x10^{-09}$
11	1	-1	$-1.8990068218419\,x10^{-2}$	28	8	-6	$-1.7424871230634\,x10^{-10}$
12	1	0	$-3.2529748770505\,x10^{-2}$	29	21	-29	$-6.8762131295531\,x10^{-19}$
13	1	1	$-2.1841717175414\,x10^{-2}$	30	23	-31	$1.4478307828521\,x10^{-20}$
14	1	3	$-5.283835796993\,x10^{-5}$	31	29	-38	$2.6335781662795\,x10^{-23}$
15	2	-3	$-4.7184321073267\,x10^{-4}$	32	30	-39	$-1.1947622640071\,x10^{-23}$
16	2	0	$-3.0001780793026\,x10^{-4}$	33	31	-40	$1.8228094581404\,x10^{-24}$
17	2	1	$4.7661393906987\,x10^{-5}$	34	32	-41	$-9.3537087292458\,x10^{-26}$

B.3 Coefficients for Region 2

Table B.2: Values of coefficients n_i^o and exponents J_i^o for Equation (4.19). Adapted from [97].

i	J_i^o	n_i^o	i	J_i^o	n_i^o
1	0	-9.6927686500217	6	-2	1.4240819171444
2	1	$1.0086655968018\,x10^{1}$	7	-1	-4.383951131945
3	-5	$-5.608791128302\,x10^{-3}$	8	2	$-2.8408632460772\,x10^{-1}$
4	-4	$7.1452738081455\,x10^{-2}$	9	3	$2.1268463753307\,x10^{-2}$
5	-3	$-4.0710498223928\,x10^{-1}$			

Table B.3: Values of coefficients n_i and exponents I_i and J_i for Equation (4.19). Adapted from [97].

i	I_i	J_i	n_i	i	I_i	J_i	n_i
1	1	0	$-1.7731742473213\,x10^{-3}$	23	7	0	$-5.905956432427\,x10^{-18}$
2	1	1	$-1.7834862292358\,x10^{-2}$	24	7	11	$-1.2621808899101\,x10^{-6}$
3	1	2	$-4.5996013696365\,x10^{-2}$	25	7	25	$-3.8946842435739\,x10^{-2}$
4	1	3	$-5.7581259083432\,x10^{-2}$	26	8	8	$1.1256211360459\,x10^{-11}$
5	1	6	$-5.032527872793\,x10^{-2}$	27	8	36	$-8.2311340897998\,x10^{0}$
6	2	1	$-3.3032641670203\,x10^{-5}$	28	9	13	$1.9809712802088\,x10^{-8}$
7	2	2	$-1.8948987516315\,x10^{-4}$	29	10	4	$1.0406965210174\,x10^{-19}$
8	2	4	$-3.9392777243355\,x10^{-3}$	30	10	10	$-1.0234747095929\,x10^{-13}$
9	2	7	$-4.3797295650573\,x10^{-2}$	31	10	14	$-1.0018179379511\,x10^{-9}$
10	2	36	$-2.6674547914087\,x10^{-5}$	32	16	29	$-8.0882908646985\,x10^{-11}$
11	3	0	$2.0481737692309\,x10^{-8}$	33	16	50	$1.0693031879409\,x10^{-1}$
12	3	1	$4.3870667284435\,x10^{-7}$	34	18	57	$-3.3662250574171\,x10^{-1}$
13	3	3	$-3.227767723857\,x10^{-5}$	35	20	20	$8.9185845355421\,x10^{-25}$
14	3	6	$-1.5033924542148\,x10^{-3}$	36	20	35	$3.0629316876232\,x10^{-13}$
15	3	35	$-4.0668253562649\,x10^{-2}$	37	20	48	$-4.2002467698208\,x10^{-6}$
16	4	1	$-7.8847309559367\,x10^{-10}$	38	21	21	$-5.9056029685639\,x10^{-26}$
17	4	2	$1.2790717852285\,x10^{-8}$	39	22	53	$3.7826947613457\,x10^{-6}$
18	4	3	$4.8225372718507\,x10^{-7}$	40	23	39	$-1.2768608934681\,x10^{-15}$
19	5	7	$2.2922076337661\,x10^{-6}$	41	24	26	$7.3087610595061\,x10^{-29}$
20	6	3	$-1.6714766451061\,x10^{-11}$	42	24	40	$5.5414715350778\,x10^{-17}$
21	6	16	$-2.1171472321355\,x10^{-3}$	43	24	58	$-9.436970724121\,x10^{-7}$
22	6	35	$-2.3895741934104\,x10^{1}$				

B.4 Coefficients for Region 4

Table B.4: Coefficients for saturation equations in Region 4 (Equations 4.27, 4.28a and 4.28b). Adapted from [97].

Coefficient	Value
n_1	1167.0521452767
n_2	−724213.16703206
n_3	−17.073846940092
n_4	12020.82470247
n_5	−3232555.0322333
n_6	14.91510861353
n_7	−4823.2657361591
n_8	405113.40542057
n_9	−0.23855557567849
n_{10}	650.17534844798